الجمهورية الجزائرية الديمقراطية الشعبية
People's **D**emocratic **R**epublic of **A**lgeria
وزارة التعليم العالي والبحث العلمي
Ministry of **H**igher **E**ducation and **S**cientific **R**esearch
تبسة _جامعة الشهيد الشيخ العربي التبسي
Echahid **C**heikh **L**arbi **T**ebessi **U**niversity_**T**ebessa
كليه العلوم والتكنولوجيا
Faculty of **S**ciences and **T**echnology
قسم الهندسة الكهربائية
Electrical **E**ngineering **D**epartment

THESIS

With a view to obtaining the LMD 3rd cycle doctoral degree
Option: Automatic, Speciality: Industrial Electrotechnics
LABGET Laboratory

Presented by: AOUN Sakina

Theme

Contribution To Advanced Faults Diagnosis in Renewable Energy Conversion Chain

Publicly supported on: 09/01/2025 before the jury composed of:

Jury members	Grade	Designation	University
Pr.Youcef SOUFI	Professor	Chairman	Echahid Cheikh Larbi Tebessi University- Tebessa
Pr.Tahar BAHI	Professor	Examiner	Badji Mokhtar Annaba University- Annaba
Pr.Djalal DIB	Professor	Examiner	Echahid Cheikh Larbi Tebessi University- Tebessa
Pr. Yahia KOURD	Professor	Examiner	Mohamed-Cherif Messaadia University-Souk Ahras
Dr.Abdelhakim BENDAKIR	MCA	Examiner	Echahid Cheikh Larbi Tebessi University- Tebessa
Pr.Aziz BOUKADOUM	Professor	Supervisor	Echahid Cheikh Larbi Tebessi University- Tebessa
Dr.Laatra YOUSFI	MCA	Co-supervisor	Echahid Cheikh Larbi Tebessi University- Tebessa

University Year 2024-2025


بسم الله الرحمن الرحيم

Acknowledgment

In the Name of Allah, the Most Merciful, the Most Compassionate. All praise be to Allah, the Lord of the worlds, and prayers and peace be upon Muhammad, His servant and messenger.

First and foremost, I must acknowledge my limitless thanks to Allah, the Ever- Magnicent; the Ever-Thankful, for His help and blessings. I am sure that this work would have never become the truth, without His guidance.

I am profoundly grateful to my thesis advisors, Professor Aziz Boukadoum and Dr. Laatra Yousfi, for their guidance, support, and patience throughout the entire process of researching and writing this thesis. Their insightful feedback and encouragement were invaluable in making this work possible.

I also wish to thank my committee members for agreeing to review and evaluate this work.

Lastly, my heartfelt appreciation goes to my family and friends for their unwavering support and encouragement throughout my academic journey. Their love and care have been a constant source of strength and motivation.

ABSTRACT

Wind energy plays an increasingly crucial role in electricity production, requiring proactive involvement of wind farms in managing the electrical grid. Additionally, diagnosing potential faults in the wind energy chain and detecting failures are major priorities for both industry and research. This thesis aims to enhance the energy quality of variable-speed wind turbines using a doubly-fed induction generator (DFIG) by developing a comprehensive control method. The primary objective is to regulate active and reactive power through field-oriented control (FOC) to meet the requirements of the wind farm control system. To achieve this, three types of controllers were investigated: proportional-integral (PI) controller, fuzzy logic controller (FLC), and neural network-based controller (NNC). Simulations have shown the superiority of NNC in terms of dynamic responsiveness and precise tracking of power reference values. Simultaneously, a diagnostic method using fuzzy logic was devised to monitor and detect ITSC and open-phase circuits in the stator windings of the DFIG within the wind system. This method solely utilizes phase currents to detect and locate faults in real-time. Furthermore, to address converter failure issues, a fault detection technique for pulse width modulation (PWM) inverters was studied. This technique combines fuzzy logic and neural networks to accurately identify short-circuit and open-circuit faults in the wind generator inverter.

Keywords:

Wind energy; Doubly-fed induction generator (DFIG); Field-oriented control (FOC); Proportional-integral (PI) controller; Fuzzy logic controller (FLC); Neural network-based controller (NNC); Faults; Diagnostic; inter-turn short circuits; open-phase circuits; short-circuit; open-circuit; PWM inverters.

RÉSUMÉ

L'énergie éolienne joue un rôle de plus en plus crucial dans la production d'électricité, nécessitant une implication proactive des parcs éoliens dans la gestion du réseau électrique. De plus, le diagnostic des défauts potentiels dans la chaîne d'énergie éolienne et la détection des pannes sont des priorités majeures pour l'industrie et la recherche. Cette thèse se concentre sur l'amélioration de la qualité énergétique des éoliennes à vitesse variable à base d'un générateur asynchrone à double alimentation (GADA) et en développant une méthode de contrôle globale. L'objectif principal est de réguler l'énergie active et réactive en utilisant un contrôle à flux orienté pour répondre aux exigences du système de contrôle du parc éolien. Pour atteindre cet objectif, trois types de contrôleurs ont été explorés : le contrôleur proportionnel-intégral (PI), le contrôleur logique flou (FLC) et un contrôleur basé sur les réseaux neuronaux (NNC). Les simulations ont démontré la supériorité du NNC en termes de réactivité dynamique et de capacité à suivre précisément les valeurs de référence de puissance. En parallèle, une approche de diagnostic basée sur la logique floue a été développée pour surveiller et détecter les courts-circuits inter-spires et les circuits à phase ouverte dans les enroulements statoriques de la GADA dans le système éolien. Cette méthode utilise uniquement les courants de phase pour détecter et localiser les défauts en temps réel. De manière complémentaire, pour résoudre le problème des pannes de convertisseurs, une technique de détection de défauts pour un onduleur à modulation de largeur d'impulsion (MLI) a été étudiée. Cette technique combine la logique floue et les réseaux neuronaux pour identifier avec précision les défauts de court-circuit et de circuit ouvert dans l'onduleur de génération éolienne.

Mots clés :

Énergie éolienne ; Générateur asynchrone à double alimentation (GADA) ; Contrôle à flux orienté ; Contrôleur proportionnel-intégral (PI) ; Contrôleur logique flou (FLC) ; Contrôleur basé sur les réseaux neuronaux (NNC) ; Défauts ; Diagnostic ; Courts-circuits inter-spires ; Circuits à phase ouverte ; Court-circuit ; Circuit ouvert ; Onduleur à MLI.

ملخص

تلعب طاقة الرياح دورًا متزايد الأهمية في إنتاج الكهرباء، مما يتطلب مشاركة استباقية لمزارع الرياح في إدارة الشبكة الكهربائية. بالإضافة إلى ذلك، يعد تشخيص الأعطال المحتملة في سلسلة طاقة الرياح واكتشاف حالات الفشل من الأولويات الرئيسية لكل من الصناعة والبحث .تركز هذه الأطروحة على تحسين جودة الطاقة لتوربينات الرياح متغيرة السرعة باستخدام مولد تحريضي مزدوج التغذية وتطوير طريقة تحكم شاملة .الهدف الأساسي هو تنظيم الطاقة النشطة والمتفاعلة من خلال استخدام التحكم الموجه ميدانيًا لتلبية متطلبات نظام التحكم في مزرعة الرياح .ولتحقيق هذا الهدف، تم استكشاف ثلاثة أنواع من وحدات التحكم :وحدة التحكم التناسبية المتكاملة، وحدة التحكم المنطقية المضببة، ووحدة التحكم المعتمدة على الشبكة العصبية .أظهرت عمليات المحاكاة تفوق وحدة التحكم المعتمدة على الشبكة العصبية من حيث الاستجابة الديناميكية والتتبع الدقيق للقيم المرجعية للطاقة بالتوازي، تم تطوير نهج تشخيصي يعتمد على المنطق الغامض لرصد واكتشاف الدوائر القصيرة بين المنعطفات والدوائر مفتوحة الطور في ملفات الجزء الثابت للمولد التعريفي مزدوج التغذية في نظام الرياح .تستخدم هذه الطريقة فقط تيارات الطور لاكتشاف الأخطاء وتحديد موقعها في الوقت الفعلي .علاوة على ذلك ، لمعالجة مشاكل فشل المحول ، تمت دراسة تقنية اكتشاف الأخطاء لمحولات تعديل عرض النبضة .تجمع هذه التقنية بين المنطق الغامض والشبكات العصبية لتحديد أعطال الدارة القصيرة والدارة المفتوحة بدقة فيعاكس مولد الرياح.

الكلمات الدالة:

طاقة الرياح ؛ مولد تحريضي مزدوج التغذية ؛ التحكم الموجه ميدانيًا ؛ وحدة التحكم التناسبية المتكاملة؛ وحدة التحكم المنطقية المضببة ؛وحدة التحكم المعتمدة على الشبكة العصبية؛ الأعطال؛ تشخيص؛ الدوائر القصيرة بين المنعطفات؛ الدوائر مفتوحة الطور؛ الدارة القصيرة ؛ الدارة المفتوحة

GLOSSARY

AI	: Artificial Intelligence
WECS	: Wind Energy Conversion System
VAWT	: Vertical -Axis Wind Turbines
HAWT	: Horizontal-Axis Wind Turbines
FL	: Fuzzy Logic
FLS	: Fuzzy Logic Systems
FLC	: Fuzzy Logic Controller
QTA	: Qualitative Trend Analysis
PCA	: Principal Component Analysis
ANN	: Artificial Neural Network
DFIG	: Doubly-Fed Induction Generator
DFIM	: Doubly-Fed Induction Machine
IGBT	: Insulated Gate Bipolar Transistor
PWM	: Pulse Width Modulation
RSC	: Rotor-Side Converter
GSC	: Grid-Side Converter
MPPT	: Maximum Power Point Tracking Control
IFOC	: Indirect Field-Oriented Control
PI	: Proportional-Integral
NNC	: Neural Network Controller
SC	: Short-Circuit
OC	: Open Circuits
ITSC	: Inter Turn Short Circuit
MMC	: Modular Multilevel Converters
2L-BTB	: 2-Level Back-To-Back
3L-NPC BTB	: 3-Level Neutral-Point-Clamped Back-To-Back
PCB	: Printed Circuit Boards
FFT	: Fast Fourier Transform
AAVC	: Average Absolute Current Values

LIST OF TABLES

CHAPTER I:

CHAPTER II:

CHAPTER III:

CHAPTER IV:

LIST OF FIGURES

CHAPTER I:

CHAPTER II:

CHAPTER III:

CHAPTER IV:

CONTENTS

SCIENTIFIC PRODUCTION

GENERAL INTRODUCTION

General Introduction

Demographic growth and extensive industrialization across all sectors have significantly increased the demand for electrical energy in recent years. Concurrently, the scarcity of global hydrocarbon resources, the risks associated with nuclear energy such as accidents and pollution and the growing environmental and ecological awareness among populations and governments have made renewable energy sources increasingly attractive for future electricity generation.

Among these renewable energy sources, we find wind energy, which is currently the subject of lively debate and is increasingly attracting interest to meet the ever-growing demand for electrical energy.

Wind energy is an environmentally friendly and non-polluting energy source, as its use does not produce greenhouse gas emissions. Wind turbines convert the kinetic energy of the wind into electrical energy, which can be used to power consumers, stored in batteries, or fed into the electrical grid. However, these turbines are subject to various faults that can affect their operational performance. Therefore, an intensive shutdown of a wind turbine chain inevitably causes immeasurable losses [1].

In order to avoid such shutdowns, it is essential to rigorously monitor wind turbines to ensure optimal energy efficiency. This monitoring must be able to detect, locate, and identify faults in order to determine the necessary maintenance actions. These steps, which form the basis of fault diagnosis, must be carried out as quickly as possible.

The doubly-fed induction machine and power converters play a crucial role in variable-speed wind turbines, offering significant advantages such as precise speed control, efficient conversion of wind energy, optimal power management, and overall improvement in wind energy conversion system efficiency. These components are fundamental for fully utilizing the potential of wind energy.

Despite the robustness of the asynchronous machine, it can still experience failures similar to those of other electrical machines. These failures can result from various internal factors, such as mechanical issues (rotor/stator friction, eccentricity, bearing faults) and electrical issues (broken bars, stator faults, insulation faults). Additionally, external factors such as mechanical stresses (torque pulsation, improper mounting, overload), environmental conditions (temperature, humidity, contamination), and electrical factors (voltage fluctuations, voltage transients, voltage

imbalance) can also contribute to these failures. Therefore, it is essential to equip these machines with reliable diagnostic systems to prevent any damage, no matter how minor.

Regarding power converters, although they are essential for variable-speed wind turbines, they can experience various faults that impact turbine operation and performance. These faults include short-circuits and open-circuits that may occur in the power switches.

In practice, implementing diagnostic strategies for wind turbines is often complex [2]. These approaches can generally be categorized into three main types: the first relies on prior knowledge of the system's behavior, the second is based on pre-established quantitative or qualitative models, and the third involves analyzing received signals using artificial intelligence algorithms.

The advent of AI in recent years has brought about new methods in fault diagnosis. The motivation behind using AI techniques lies in their ability to generalize and adapt to new, unforeseen situations, as well as the increasing availability of data for training purposes.

In this context, the main objective of our thesis work is to develop fault detection and diagnostic methods in the wind conversion chain using advanced techniques, aiming to enhance the performance and profitability of energy production.

To accomplish this objective, this thesis is organized into four chapters, each focusing on a distinct aspect of fault diagnosis in the wind energy conversion chain:

The first chapter presents a historical overview of wind energy conversion systems, detailing the operating principles of wind turbines, the different types of turbines used, and the essential components of wind energy systems. It also introduces the concepts of fault diagnosis and the various methods employed, including the emerging use of AI.

The second chapter focuses on the modeling and control of a variable-speed wind turbine based on a DFIG. It examines in detail the electromechanical components of the energy conversion chain and presents the control laws used to optimize the turbine's operation, including PI, FLC, and NN controllers.

The third chapter explores diagnostic methods for electrical faults encountered in DFIGs used in wind farms. It examines the types of possible faults, their detection methods, and emphasizes on artificial intelligence techniques such as fuzzy logic for accurate detection.

The fourth chapter specifically focuses on the failures of power converters used in wind energy conversion systems. It explores fault diagnostic methods, particularly those based on data, highlighting the use of fuzzy logic and neural networks for fault detection.

By integrating these chapters, this thesis aims to contribute to enhancing the reliability and sustainability of renewable energy conversion systems.

CHAPTER I

General Overview of Wind Energy Conversion System & Fault Diagnosis Methods

I.1 Introduction

Electricity generation using wind energy is booming in most countries, due to its potential to provide a clean and sustainable source of energy. However, the wind energy conversion chain is subject to various faults and anomalies that can compromise its efficiency and sustainability. To ensure the optimal operation of wind power plants, it is essential to develop advanced diagnostic methods to identify, analyze, and correct these faults effectively and proactively [3][4].

This chapter is divided into two parts. The first part provides a historical overview of wind turbine conversion systems, explaining the operating principles of wind turbines, detailing the different types of turbines along with their advantages and disadvantages, and describing the various components that comprise their energy systems. In the second part, we define the terms used in fault diagnosis. We will then classify system faults according to their location, temporal evolution and impact on the performance of the systems to be monitored. We will also classify fault diagnosis methods. In addition, we will mention the emergence of artificial intelligence (AI) in fault diagnosis.

I.2 Historical

For more than 3000 years, humans have been utilizing wind energy, establishing it as one of the oldest energy sources. In ancient Egypt, sailors employed wind power to propel their sailboats, while millers used it to grind grain. These historical examples demonstrate that wind energy is by no means a recent concept. Its utilization dates back millennia, demonstrating its ongoing significance in the evolution of energy technologies. During the Middle Ages, windmills spread widely throughout Europe, finding utility in grinding grain and pumping water. In the late 19th century, specifically during the years 1887-1888, the production of electricity from the wind began. It was in 1887 when the very first windmill capable of generating electricity was erected in Scotland. This remarkable achievement inspired innovative projects in the United States and numerous European countries. Thus, wind energy began its promising journey as a source of electricity during that period. In the latter half of the 20th century, wind turbines as we know them today were developed [5]. According to the Global Wind Energy Council data for the year 2022, China leads as the largest producer of wind energy and the world's biggest market for new installations, followed by the United States and Brazil. Wind energy has the advantage of being considered a renewable and clean source of energy, as it does not run out and does not generate greenhouse gas emissions. This feature makes it all the more interesting for a society increasingly

concerned about environmental issues. However, wind energy faces various challenges, including a still relatively high cost of electricity generation and limited availability in some parts of the world.

I.3 Principle of Wind Energy Conversion

Wind energy is a renewable energy source that captures the power of the wind to turn turbines and generate electricity.

A wind turbine is a machine engineered to convert some of the wind's kinetic energy into mechanical energy through rotation. This rotation then drives a generator that produces electricity [6].

Driven by the wind, the propeller begins to turn, causing its blades to rotate. This mechanical energy is converted into electrical energy through a slow main shaft, a gearbox, and a generator, which then either feeds into the grid, is consumed locally, or is stored in batteries [7].

Figure I.1 depicts the primary components of a conventional wind energy conversion system linked to the electrical grid.

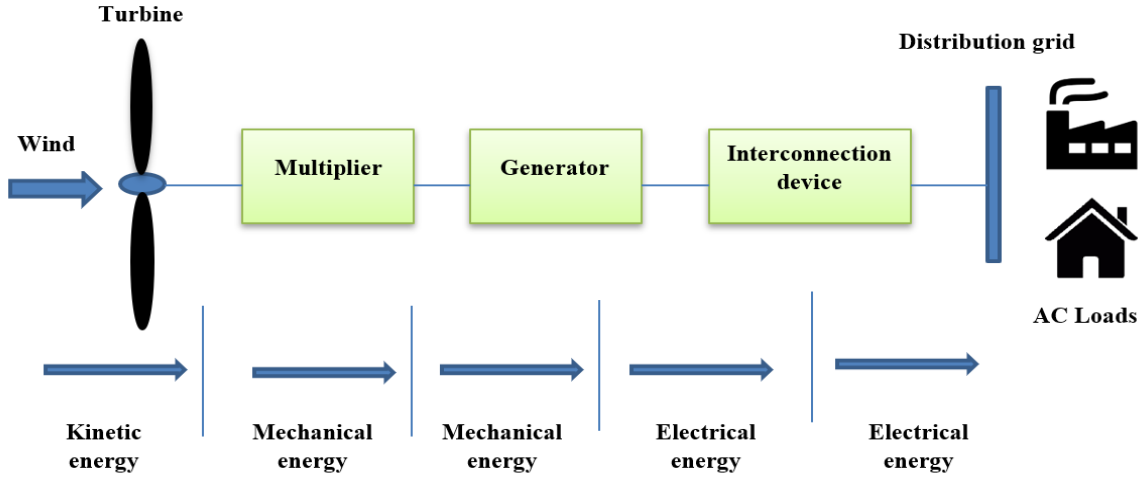

Figure I. 1 Structure of the grid-connected WECS.

I.4 Classification of wind turbine types

Wind turbines can be classified based on several criteria, including:

I.4.1 Depending on the rotation speed

Based on generator speed, wind turbines are categorized into two types: fixed speed and variable speed.

I.4.1.1 Fixed Speed Wind Turbine

Fixed-speed wind turbines were the first to be designed and developed using asynchronous cage machines, as shown in Figure I.2. These turbines are the most commonly used for high-power generation due to their simple design. The asynchronous machines are directly connected to the grid, operating at a fixed rotor speed close to the synchronization speed dictated by the pulsation of currents between the stator and the grid [8].

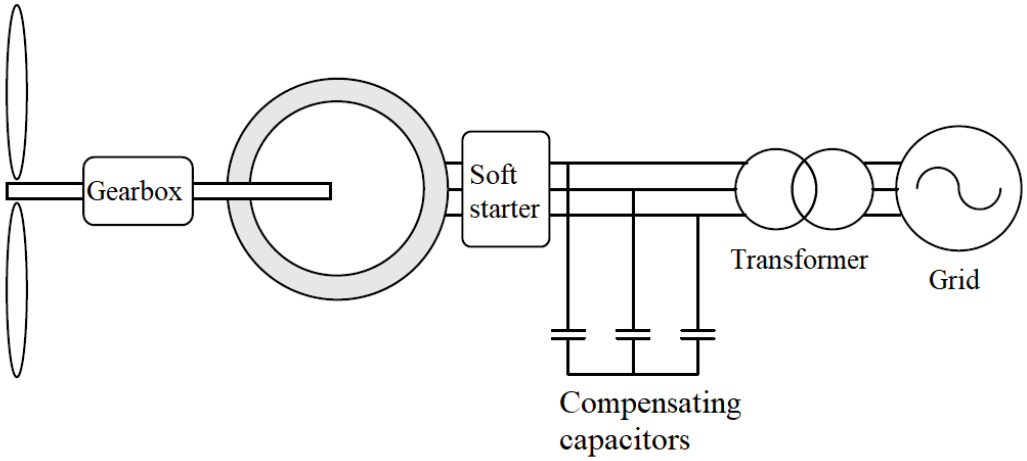

Figure I. 2 Fixed-speed wind turbine.

The advantages and disadvantages of this type can be listed as follows:

A. Advantages of fixed speed wind turbines

- Simple: Fixed-speed wind turbines feature a straightforward mechanism and a basic structure, making them easy to understand and use. This simplicity aids in their manufacture, installation, and maintenance.
- Robust: Fixed speed wind turbines are known for their durability and resilience. They are designed to withstand harsh weather conditions. Their robust construction allows them to continue to operate reliably for long periods without significant damage or breakdowns.
- Economical: fixed-speed wind turbines are cost-effective in several respects. First, their simple design and construction make them less expensive to manufacture and install compared to more complex wind technologies. Second, their robustness reduces the need for frequent repairs and maintenance, resulting in lower operating costs. Finally, constant-speed wind turbines do not require power electronics, further reducing their overall cost.

- Reduced maintenance: Fixed-speed wind turbines require less maintenance than other types of wind turbines. They have fewer moving parts and do not rely on complex control systems. As a result, there is less wear and fewer components that require regular inspection and replacement. This reduces downtime and maintenance costs.
- No need for power electronics: fixed speed wind turbines operate without power electronics. This reduces the complexity and cost of the turbine.

B. Disadvantages of fixed speed wind turbines

- Non-optimized power extraction: fixed-speed wind turbines cannot adjust their rotor speed to suit wind conditions. This means that the power extracted from the wind is not optimized, as the turbine may not operate at maximum efficiency. This can result in lower energy production than with variable-speed turbines.
- Uncontrolled reactive power: In fixed-speed turbines, reactive power is not controlled, which can lead to voltage fluctuations and grid instability, affecting overall power quality.
- Additional capacitor banks: To magnetize the electrical machine of a fixed-speed wind turbine, additional capacitor banks are required. These banks supply the necessary reactive power for the magnetization process. However, incorporating capacitor banks increases the system's complexity and cost.

I.4.1.2. Variable Speed Wind Turbine

Variable speed wind turbines are a modern innovation in wind turbine technology, made feasible by the integration of power electronics. This advancement enables them to operate effectively across a wide range of speeds, thereby improving energy production quality and enhancing overall energy capture efficiency. In addition, variable speed wind turbines can reduce noise and lower mechanical system costs [9][10]. These turbines use different types of generators with power electronics structures [8]. There are two main structures for variable-speed wind turbines, illustrated in Figures I.3 and I.4.

Figures I.3 show the first structure which involves the use of an asynchronous cage generator with a bidirectional (AC/DC/AC) converter.

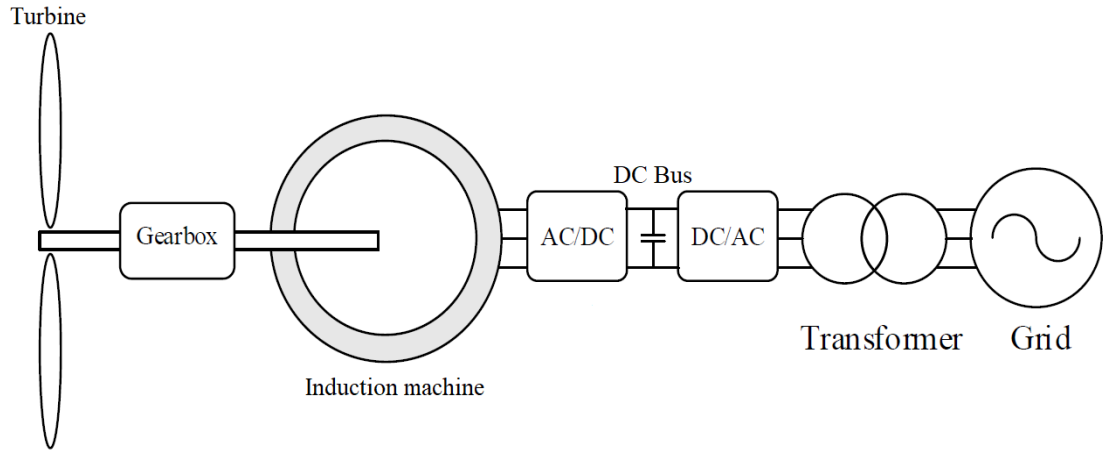

Figure I. 3 Variable-speed wind turbine.

Figure I.4 shows the second structure involving a doubly-fed induction generator (DFIG) which is powered directly to the stator and through a bidirectional converter (AC/DC/AC).

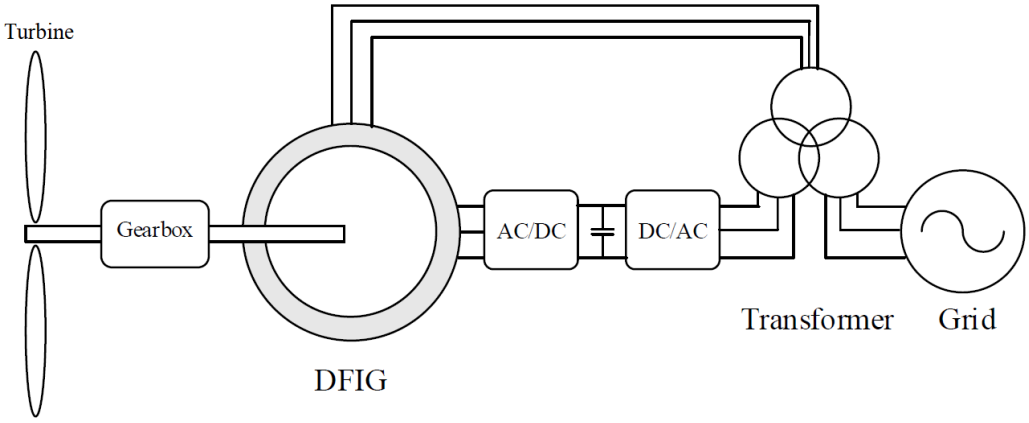

Figure I. 4 Variable-speed wind turbine based DFIG.

A. Advantages of variable speed wind turbines

- Regulation of active and reactive power sent to the grid: Variable-speed wind turbines can manage both active and reactive power, optimizing wind energy production and improving alignment with grid demands.
- Elimination or reduction of the need for speed multipliers: Variable speed turbines can reduce or even completely eliminate the need for a speed multiplier, simplifying design and reducing maintenance costs.

- Increased operating range: Variable-speed wind turbines are able to operate efficiently even at lower wind speeds. This means they can produce energy even when wind conditions are less favorable, increasing uptime and overall energy production.
- Enhanced integration of wind turbines into the power grid: Variable-speed wind turbines facilitate smoother integration into the existing power grid. Their capability to regulate both active and reactive power allows for improved grid coordination, mitigating issues related to wind power stability and intermittency.
- Simplicity of generator speed control thanks to the blade orientation system: Variable-speed wind turbines use a blade orientation system that enables easy control of generator rotation speed. This makes it possible to optimize energy production by adjusting the speed of rotation according to wind conditions.

B. Disadvantages of fixed speed wind turbines

- Complex Control System: Variable-speed wind turbines necessitate a more sophisticated control system compared to fixed-speed turbines. This is because the turbine speed must be adjusted based on wind conditions to optimize power generation. The control system must continuously monitor wind speed and adjust the turbine speed accordingly, which adds to the overall complexity and cost of the turbine.
- High Cost of Power Converters: Variable-speed wind turbines require power converters to transform the variable frequency output of the turbine into a fixed frequency suitable for grid connection. These power converters can be costly, contributing to the higher overall expense of variable-speed turbines compared to fixed-speed turbines.
- The periodic maintenance required for the gearbox and sliding contacts for brush rings.

I.4.2 Depending on the orientation of the axis of rotation

Wind turbines are classified according to the position of their rotor (axis of rotation) into two types: vertical-axis wind turbines (VAWT) and horizontal-axis wind turbines (HAWT) [11].

I.4.2.1 Vertical-Axis Wind Turbines

Figure I.5 illustrates Vertical-Axis Wind Turbines (VAWTs), which convert wind's kinetic energy into electrical energy. These turbines have a vertical axis of rotation perpendicular to the ground, with the generator and gearbox positioned at the tower's base. They can function at low wind speeds and are not dependent on wind direction [12].

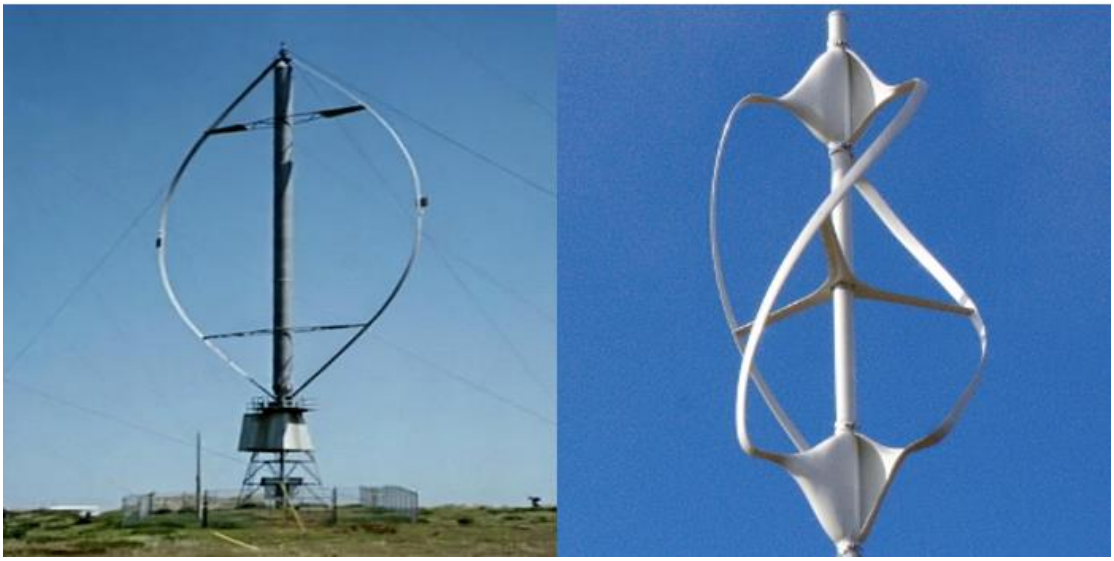

Figure I. 5 Vertical-Axis Wind Turbines (VAWT).

A. Advantages of VAWT

The main advantages of VATW are [8]:

- Simpler design: VAWTs have a simpler design than HAWTs. They do not require complex mechanisms to orientate the rotor according to wind direction. This makes them easier and less costly to manufacture and install.
- Easier installation and maintenance: Key components, including the gearbox, electric generator, and control devices, are located at the base of the turbine on the ground. This setup simplifies access for maintenance and repairs, eliminating the need for technicians to climb to high elevations to perform maintenance tasks.
- Operation in all wind directions: Unlike HAWTs, which require a steering mechanism to face the wind, vertical-axis turbines can operate in all airflow directions. This means they can capture wind energy even when the wind changes direction, increasing their overall efficiency.

B. Disadvantages of VAWT

- Low efficiency with wide power fluctuations: VAWTs are subject to wide power fluctuations, which means that the amount of energy produced can vary considerably depending on wind conditions.

- Complete dismantling of wind turbines for rotor bearing replacement: In the event of rotor bearing failure, it is necessary to completely dismantle the vertical axis wind turbine for replacement. This can lead to significant costs and downtime.
- The need for an auxiliary starting device: VAWT often requires an auxiliary starting device to set them in motion. This can add extra costs and complexity to the installation.
- In VAWT, the high-power generating devices take up a lot of land, so they can't be sited on agricultural sites or other areas where space is limited.

I.4.2.2 Horizontal-Axis Wind Turbines

This type of wind turbine features a rotor mounted on a mast that is perpendicular to the wind. The blades of these turbines drive the generator shaft. Horizontal-axis wind turbines come in various configurations, including single-blade, two-blade, and three-blade designs [13][14].

Single- and two-bladed turbines have the advantage of producing less vibration, but they are also less efficient and generate more noise. Turbines with an even number of blades should be avoided because of their instability. Reducing the number of blades reduces costs while increasing wind energy efficiency. Among the various configurations, the three-blade turbine is the most commonly used because of its excellent efficiency and optimum cost [15].

HAWTs are categorized into two types: "up-wind" and "down-wind", as shown in the Figure I.6. In the "up-wind" configuration, the rotor faces into the wind, allowing the airflow to directly reach the blades. This setup avoids the "tower shadow" effect, where the tower obstructs wind flow to the blades. To ensure optimal performance, an automatic and continuous steering mechanism is crucial. This mechanism can be either passive, using a fixed vertical wing, or active, employing an electric motor [7].

In the "down-wind" configuration, the wind passes behind the rotor and reaches the blades after flowing through the nacelle. This can cause premature equipment wear due to vibration or mechanical fatigue [16].

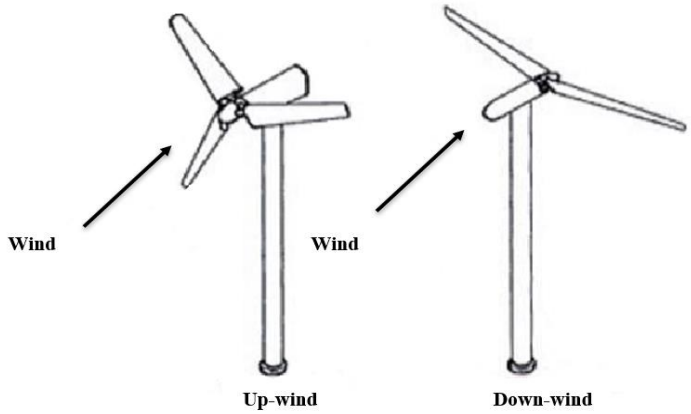

Figure I. 6 Horizontal-Axis Wind Turbines (HAWT).

A. Advantages of HAWT

- Superior efficiency: they can capture wind at higher altitudes, where the wind is less affected by terrain, such as mountains. This enables them to generate more electricity from the same amount of wind [15][17][8].
- Small footprint: HAWTs have a small footprint. Unlike VAWTs, which require a larger surface area, HAWTs only require space for the tower, which usually houses all the connection systems. This makes them suitable for areas where space is limited.
- Simple, robust design: HAWTs have a simple, robust design, reducing the risk of mechanical failure and the need for frequent maintenance.
- Wind orientation system: HAWTs are equipped with a mechanism that allows them to align with the wind direction. This ensures the turbine blades consistently face the wind, maximizing the energy extracted from it.

B. Disadvantages of HAWT

- Horizontal wind turbines emit a lot of noise. This can be problematic in residential areas where wind turbines are installed, as the noise can cause a nuisance for residents.
- Horizontal wind turbines require an orientation system to cope with changes in wind direction. This adds further complexity to the installation and maintenance of the turbine.
- Horizontal wind turbines require non-flexible rotor blades. This means that the blades cannot adapt to variations in wind speed, which can lead to reduced turbine efficiency.

- Faced with strong winds, horizontal wind turbines are less resistant than vertical ones. This means they can be damaged more easily by strong winds, which can lead to high repair costs [15][17][8].

I.4.3 Depending on the size of the wind turbine

In theory, there is no direct correlation between the height of a wind turbine and its power output since the generated power is closely related to the rotor's swept area, which depends on the propeller's diameter rather than the turbine's height. The table I .1 below presents size categories of wind turbines and their associated power ratings, which are approximate and intended to provide a general idea. Additionally, these power ratings are meaningful only when the wind speed at which they are achieved is specified [18].

Table I. 1 Classification of wind turbines by size and associated order of magnitude [18].

Name	Rotor diameter [m]	Swept area [m²]	Power [kW]
Micro	0.5-1.25	0.2-1.2	0.1-0.4
Mini	1.25-3	1.2-7.1	0.4-2
Domestic	3-10	7-79	2-30
Small commercial	10-20	79-314	30-120
Commercial average	20-50	314-1963	120-750
Large commercial	50-100	1963-7854	750-3000
Commercial giant	100-170	7854-22686	3000-8000

I.5 Wind turbine construction

Typically, a wind turbine is composed of three main components [19]:

- The rotor, consisting of blades attached to a hub, can have 1, 2, 3, or more blades, depending on the wind conditions at the installation site. The three-bladed rotor is the most common, offering a balanced compromise between cost, vibration behavior, visual impact, and noise.
- The nacelle houses all the mechanical components needed to connect the turbine rotor to the electric generator, including:
  - ❖ Slow shaft: connects the rotor hub to the gearbox.
  - ❖ Gearbox: links the slow shaft to the fast shaft.
  - ❖ Fast shaft: drives the electric generator.
  - ❖ Generator: typically, a synchronous or asynchronous machine that converts kinetic energy into electrical energy.

- ❖ Cooling system: either air or water-based.
- ❖ Anemometer: measures wind intensity.
- ❖ Electronic management system: controls the wind turbine.
- ❖ Bearings: support rotating parts.
- ❖ Disc brake: different from the aerodynamic brake, it stops the system in case of overload.

- The mast (tower), generally a steel or concrete structure supporting the wind turbine, or possibly a wire mesh, must be as high as possible to avoid disturbance close to the ground. However, the amount of material used is not negligible, and weight must be kept to a minimum. A compromise is generally to choose a mast slightly larger than the diameter of the wind turbine rotor. Figure I.7 shows the main components of a horizontal-axis wind turbine.

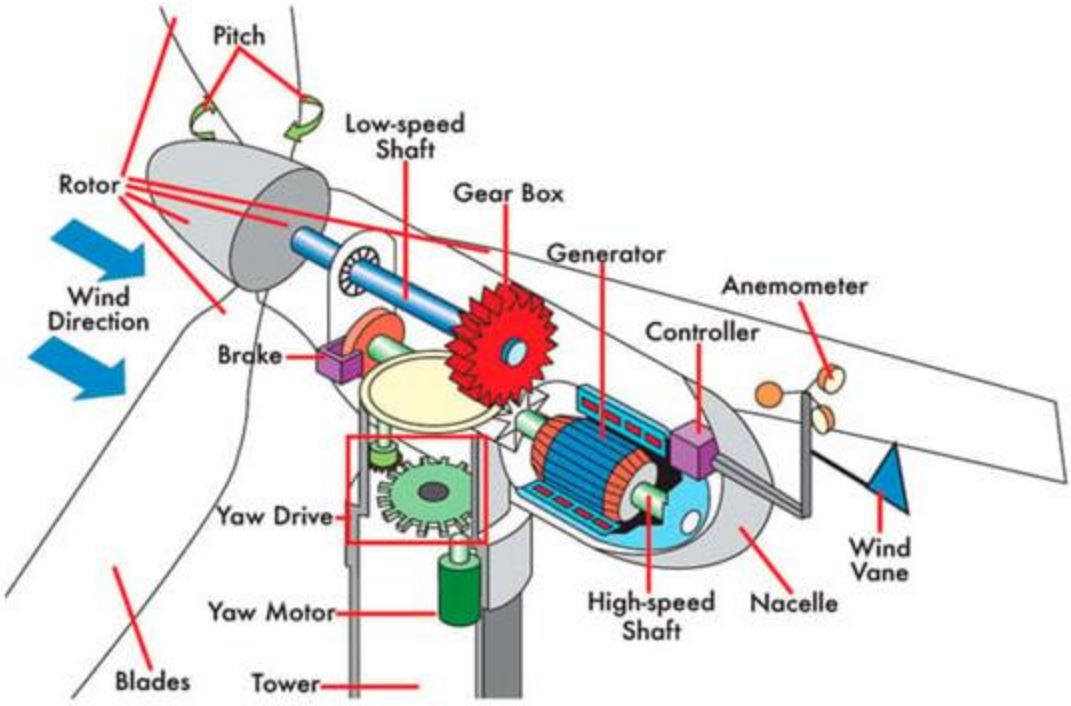

Figure I. 7 Wind Turbine Composition.

I.6 Basic concepts for diagnosis

Methods of fault diagnosis have been of great interest to scientists and researchers, particularly in the field of automated production systems, whose complexity is constantly changing. Troubleshooting is primarily about detecting, locating and identifying anomalies in a system.

It facilitates maintenance by selecting the appropriate method and structure to restore proper system operation. Fault diagnosis is part of a wider monitoring and supervision framework. The complexity of power generation systems, such as wind turbines, requires functions such as monitoring, supervision, technical management and maintenance planning to be taken into account.

This section provides an introduction to the general concepts of monitoring and diagnosis, as well as the different stages and techniques of industrial diagnostics. It addresses different concepts and structures used in diagnosis, highlighting their importance to improve system performance, reliability and safety. It also highlights the importance of fault diagnosis in wind systems and the need to identify and correct apparent faults in these systems.

I.6.1 Normal operation of a system

A system is deemed to be in a normal operating state when its variables (including state variables, output variables, input variables, and system parameters) remain near their nominal values. However, if the variables deviate significantly from their nominal values, the system is considered defective [19][20].

I.6.2 Faults

Faults are manifested by any deviation or deviation of at least one observed feature of the monitored system from its required reference feature, corresponding to the normal and standard operating condition. It usually does not result in a complete shutdown of the system, but it may cause a potential failure. Defects may have a physical origin, resulting from material malfunctions, design errors, errors in the operation of systems, or errors during maintenance actions. As a result of a defect, the system becomes unable to perform the primary function for which it was designed. It is important to note that a defect does not necessarily lead to a failure [7].

I.6.3 Failure

“Failure” means a functional anomaly within a physical system, which means that the system is unable to perform its primary function or one of its functions [8]. “Faults” are included in the category of “failures” but the reverse is not true. This means that a system can have faults without necessarily experiencing a failure, but that a failure always involves the presence of faults. Failure can occur partially when the system maintains the ability to perform some of its required functions, or fully when it is unable to perform all of these functions.

I.6.4 Break-down

A break-down occurs when a component or system is unable to fully perform a required function. This period spans from the moment the failure occurs until the repair work is completed [8][21].

I.6.5 Residual

The residual is a signal that indicates the presence of a defect in a system. It measures the difference between actual or observed system operation and normal or standard operation given by a reference model. When there are no defects, the average residual value is zero, which means that the actual operation of the system corresponds to the expected normal operation. However, in the presence of a defect, the average residual value deviates from zero, indicating that the actual operation differs from the expected normal operation [7].

I.6.6 Diagnostic

Diagnosis is a process aimed at detecting the occurrence of a fault at an early stage before it leads to failure, relying on measurements and observations made on the monitored system.
It also includes the step of fault localization and identification. Its English acronym is FDI (Fault Detection and Isolation), and the diagnostic procedure comprises three essential steps [7][22]:

I.6.6.1 Fault detection

Determination of whether the monitored system is in normal operation or not [7][22].

I.6.6.2 Fault location

This entails determining which functional component or subsystem is affected by the detected fault [7].

I.6.6.3 Fault Identification

This process involves determining the extent, type, and time of occurrence of an observed fault. The goal is to improve the understanding of the system's behavior [7].

I.6.7 Monitoring

Monitoring is a process used to keep a close eye on the operation of a system. It relies on data collected continuously and in real time from the system to analyze and detect any change in its behavior. The collected data is processed and analyzed to identify any deviations from the

normal behavior of the system. If faults or failures are detected, service agents are alerted and can take appropriate action to resolve the problem.

Additionally, the collected data is transferred to a monitoring module for further analysis. There are two types of monitoring: control monitoring and system monitoring. Control monitoring focuses on assessing the performance and behavior of the control system itself, while system monitoring evaluates the overall functioning and behavior of the entire system [7].

I.6.8 Maintenance

is a process of maintaining or restoring the performance of components or the entire system in order to perform the required task. Monitoring and diagnosis improve the reliability, maintainability and availability of a functional entity. These different concepts are defined by [7]:

- **Reliability**

Reliability refers to an entity's ability to perform the required functions under specified conditions for a given duration. This is an important consideration for overall system performance and reliability [7].

- **Availability**

Availability refers to an entity's ability to be in a state where it can perform the required functions under specified conditions. It is a measure of the system's accessibility and readiness to perform its tasks. Availability is crucial to ensure that the system is operational when needed and can meet the demands placed on it [7].

- **Maintainability**

Maintainability is the ability of a system to be restored to a functional state through proper maintenance to perform the functions required under specific conditions [7].

I.6.9 Diagnostic procedures

In the diagnostic process, two main steps are involved: fault detection and localization, followed by, in some methods, an identification step. For industrial equipment, when a fault appears, the diagnostic system first detects the anomaly and then identifies the causes in order to isolate it. The organizational sequence of a system fault diagnostic procedure is defined as [8][23]:

- Extraction of the necessary information,
- Development of signatures associated with defect symptoms,
- Implementation of the diagnostic method,
- Detection of malfunctions,

- Interpretation of data,
- Decision-making guided by the consequences and severity of faults.

I.6.10 Classification of faults (Types of faults)

Faults are classified into three categories based on their location: actuator faults, sensor faults, and system (or component) faults. This classification also takes into account their temporal evolution, distinguishing between abrupt faults, intermittent faults, and gradual faults.

Furthermore, considering their impact on the system, we distinguish between additive and multiplicative faults. Figure 1.8 illustrates the various fault positions within the automated system.

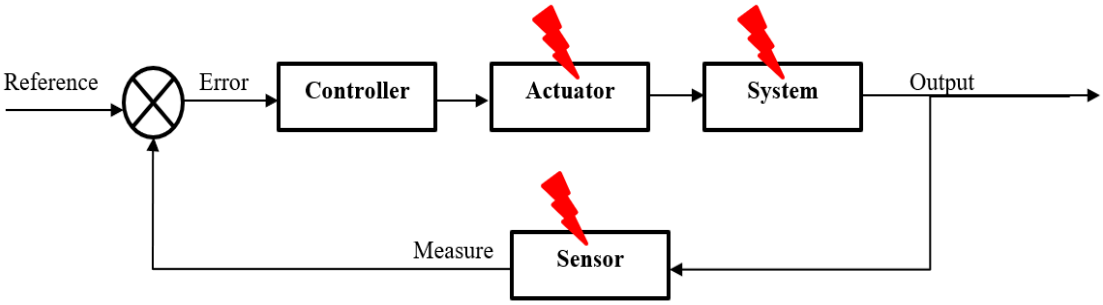

Figure I. 8 Different positions of faults.

I.6.10.1 Depending on the location of the fault

A. Sensor faults

A sensor fault refers to a situation where the sensor inaccurately represents the physical state of the system. There are two types of sensor faults: partial faults and total sensor faults.

A partial fault occurs when the sensor produces a signal that does not fully align with the actual value of the measured variable, potentially causing the displayed value to be lower than the true value. In contrast, a total fault occurs when the sensor outputs a value that is completely unrelated to the measured quantity, meaning the sensor's reading does not correspond at all to the actual physical state of the system.

B. Actuator faults

Actuator faults refer to problems that occur in the operational part of a system and affect the system input signal. These faults may result in a total or partial loss of functionality of an actuator responsible for controlling the system.

Partial actuator faults refer to situations where the actuator still functions to some extent, but its performance is degraded from its normal operation in a healthy system.

C. Component faults

These faults originate from the system itself and are generally not caused by a faulty sensor or actuator. This type of fault can be caused by various factors such as wear, aging of components, environmental conditions or manufacturing errors. This reduces the ability of the system to perform a task. Understanding and analyzing component faults is essential to maintaining system reliability and efficiency.

I.6.11 Diagnostic methods

A fault diagnosis system is specific to its field of application and varies according to various parameters [24]. This variety of parameters and application areas has led to the development of multiple methods for fault diagnosis. Based on the application perspective, we can distinguish two main families of approaches used for diagnosis [25][26][27]:

- Model-Based methods,
- Data-Driven methods.

The following figure shows the hierarchy of diagnostic methods:

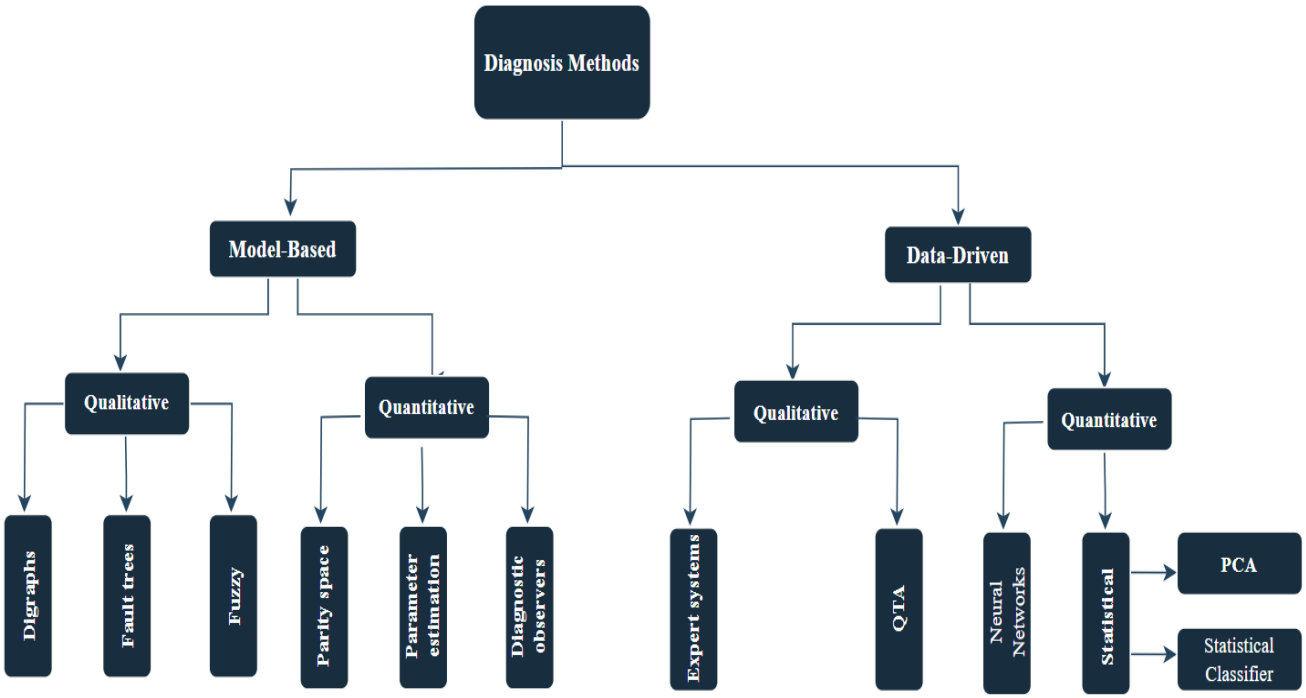

Figure I. 9 Classifications of fault diagnosis methods.

I.6.11.1 Model-Based methods

Within the framework of model-based methods, fault detection and diagnostic systems are generally categorized into qualitative or quantitative approaches.

A. Qualitative methods

Qualitative model-based fault diagnosis methods employ a model that represents the input-output relationship of the plant using qualitative functions focused on different units within the process. This approach is commonly categorized into fault trees, diagraphs, and fuzzy systems [28][29].

- **Diagraph (Causal graphs)**

A graph, or diagraph, is a collection of nodes connected by edges, where each edge has a direction assigned to it. From the "cause" nodes to the "effect" nodes, directed arcs connect them. Every node in the signed digraph represents a variable's departure from its steady state. By identifying faulty components, causal graphs can be used to explain the abnormal operation that was noticed [28][8].

- **Fault trees**

Fault tree analysis originated at Bell Telephone Laboratories in 1961. A fault tree diagram is structured from the top down and visually illustrates possible pathways in a system that could result in an undesired event or failure. These pathways link contributing events and conditions using standard logic symbols, with AND and OR gates being the primary elements utilized in fault trees [28].

- **Fuzzy logic**

Fuzzy logic (FL) is applied in fault diagnosis, especially within qualitative model-based and process-history-based methodologies. Fuzzy logic systems (FLS) utilize qualitative linguistic terms to account for the inherent imprecision observed in real-world processes and systems.

FLS provides the following benefits: they enable the management of processes that are either inadequately modeled or not expressible mathematically; They characterize process behavior using empirical or experiential information from sensor systems and/or human operators; and they can manage complex non-linear, multi-variable, and time-varying processes without necessitating precise mathematical definitions [28].

B. Quantitative methods

Quantitative models are formulated using mathematical functional relationships that connect the input and output of the system [29].

- **Parity space**

The parity space method enables verifying the parity or consistency of the system model with measurements from sensors and known inputs generated by actuators.

Generally, this approach involves identifying a projection matrix that maps the system's inputs and outputs into a subspace that is independent of the system's states. This helps to eliminate the influence of states on residues. Parity relationships are characterized by the fact that they relate only to known variables, such as inputs and outputs. These relationships can be either static, which means that they relate to inputs and outputs of the system at a specific time, be dynamic, meaning that there is a dynamic relationship between the measured outputs and the system inputs at different time points. The parity space method employs linear algebra techniques, particularly matrix projections, to eliminate unknown state variables. Even for nonlinear systems, parity relations remain applicable. However, the resulting residual is expressed as a constraint function independent of the system's state [7].

- **Parameter estimation**

This principle involves estimating the parameters of the studied systems using input and output measurements, as illustrated in Figure I.10. It then calculates the difference between these estimated parameters and the reference values that represent the normal state of the process. This method has been used to detect faults in non-linear systems [30][8].

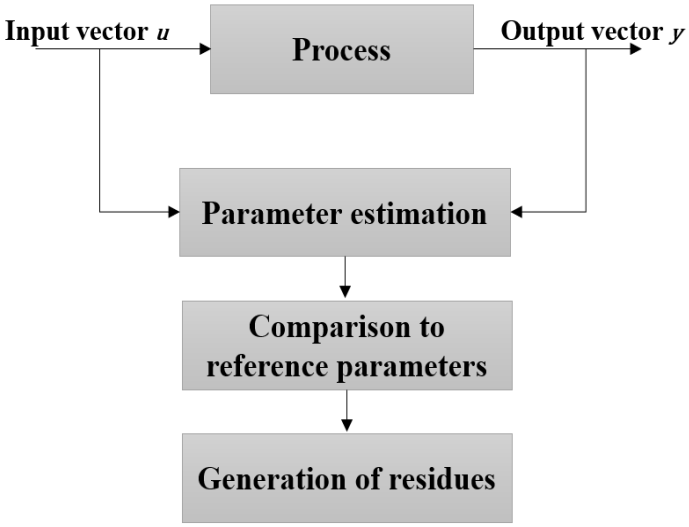

Figure I. 10 Generations of residues by parameter estimation.

- **Diagnostic observers**

Diagnostic observers are intended to estimate system output based on control knowledge (input), as illustrated in Figure I.11. Discrepancies between estimated and measured outputs generate a vector called the residue vector, intended to be a reliable indicator of process behavior [8].

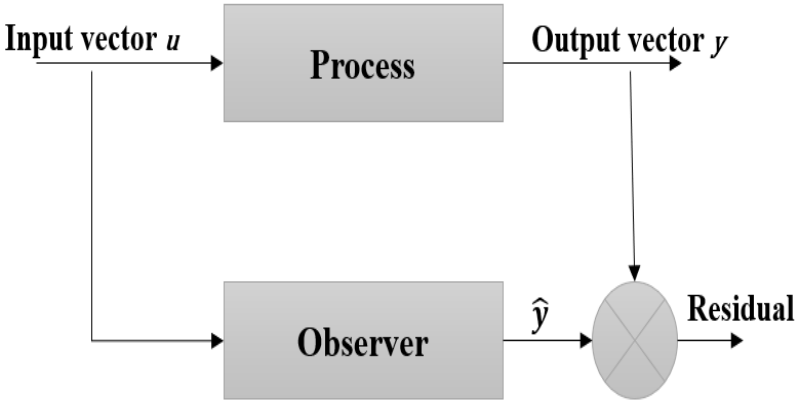

Figure I. 11 Generation of residues by observer.

I.6.11.2 Data-Driven methods

In the data-driven approach, techniques devoid of any specific model assumptions are employed, relying solely on previously processed data. This method operates under the assumption of having access to substantial amounts of pre-processed data. The data, which may vary in form,

can be integrated into a diagnostic system as preliminary information [29]. This approach can be classified into either qualitative or quantitative methods.

A. Qualitative methods

Methods for feature extraction can be divided into qualitative methods, which encompass expert systems and qualitative trend analysis (QTA) [31][32].

- **Expert systems**

Expert systems are computer-based tools utilized to leverage the insights, knowledge, and/or guidance of individuals possessing expertise in a specific domain. Typically, key stages in the development of an expert system involve acquiring knowledge, selecting appropriate knowledge representation methods, encoding knowledge into a knowledge base, designing inference procedures for diagnostic reasoning, and developing input-output interfaces [28].

They use heuristic information to link symptoms to faults. From all the symptoms at his disposal, he deduces possible conclusions and develops new hypotheses to deepen the diagnosis by exploiting the additional information collected on the system to be diagnosed.

The development of expert systems for diagnostic problem-solving offers several advantages, including ease of creation, transparent reasoning, the ability to handle uncertainty, and the provision of explanatory solutions. However, these systems also present significant weaknesses: they are often highly specialized to particular systems, prone to failure outside their knowledge boundaries, and difficult to update or modify [8].

- **Qualitative trend analysis**

QTA is a qualitative signal analysis technique that uses information from the first and second derivatives to segment signals based on their convexity and slope. It is used for process monitoring and fault detection. The QTA consists of two basic steps: identifying trends in measurements and interpreting these trends in terms of scenarios [33][34]. It is a semi-quantitative method that provides fast and useful information for fault diagnosis [35].

B. Quantitative methods

Principal component analysis (PCA) [36], neural network [37], and statistical classifier methods [27] are some of the quantitative techniques utilized for feature extraction.

- **Neural networks**

A neural network (ANN) is a network of interconnected elementary processors that process information from external signals to reproduce the behavior of the system to be modeled.

ANNs are a type of artificial intelligence that imitates the way biological neurons send signals to each other. They are composed of nodal layers, each containing an input layer, one or more hidden layers, and an output layer. Each node, or artificial neuron, performs a mathematical operation on the input it receives and passes the result to the next layer.

ANNs are particularly effective in diagnosing faults within non-linear dynamic systems. They possess noteworthy features such as learning abilities, self-organization, and the capacity to model a large class of non-linear systems, making them both intriguing and appealing [28].

- **Statistical methods**

Several statistical techniques are employed to establish the connection between the inputs and outputs of a system undergoing fault diagnosis. Among these are linear regression, multiple regressions, polynomial regression, principal component analysis, partial least squares, and logistic regression. These methods are commonly known as black-box statistical approaches for fault diagnosis. As fault diagnosis involves classification, it can be framed within the classical statistical pattern recognition framework [28].

- **Principal Component Analysis (PCA)**

PCA is a statistical technique aimed at reducing the dimensionality of multivariate datasets while preserving most of their variance. It is based on the transformation of the initial variables into a new set of orthogonal linear components, called principal components, which are both uncorrelated and ordered according to their decreasing variance [38].

PCA is used to decrease the dimensionality of the data, thus making it possible to visualize the links between the variables and detect the underlying patterns in the data. In addition, BCP can be used to reduce the number of dimensions of data before applying other statistical techniques such as regression or classification.

- **Statistical classifier**

Statistical classification is a supervised learning technique employed to categorize new observations into predetermined classes using a training dataset containing labeled examples. The primary objective is to develop a model capable of accurately predicting the target class for each instance in the dataset. Commonly used algorithms for statistical classification encompass decision trees, Naive Bayes, logistic regression, support vector machines, random forests, and neural networks. Model training entails selecting a suitable algorithm and dataset with known labels, followed by validation using an independent dataset to evaluate its ability to generalize.

Performance assessment relies on metrics such as accuracy, precision, recall, F1 score, ROC curve, and confusion matrix. Challenges in classification include combating overfitting, addressing class imbalance, and optimizing feature selection. Given the absence of a universally superior method, careful consideration must be given to selecting the appropriate algorithm. Understanding these principles and challenges is indispensable for effectively applying classification techniques in real-world scenarios, thereby contributing to ongoing advancements in machine learning and classification methodologies [39].

I.7 Advent of AI in fault diagnosis

Data-driven methods that take advantage of AI remain primarily in the research stage [40]. However, compared to model-based approaches, the data-centric approach offers a new paradigm for solving increasingly complex problems [41]. Interest in data-driven approaches stems from various elements associated with the use of artificial intelligence algorithms. The main advantages and disadvantages of the approaches discussed can be compared according to the criteria presented in Table I.2.

Table I. 2 Comparison between fault diagnostic methods [42].

Features	Model-Based	Data-Driven
Detection method Type of approaches used to perform the diagnosis	Mathematical model	Machine learning
Nature of system Type of systems typically used with the approach	Determinist	Non-deterministic
Transparency of diagnosis Ability to understand the diagnosis	Transparent	Black Box
Expertise required Illustrates the level of expertise needed for development	High	Low to moderate
Flexibility Illustrates the ability to adapt following changes	Weak	High
Development complexity Illustrates the degree of difficulty in development	High	High

- **Nature of system**: the use of AI methods differs from other approaches by facilitating the processing of non-linear data or incomplete models [26]. This approach is suitable for systems with large datasets whose underlying physics remain poorly understood. For other methods, the creation of a complete model or the definition of significant features required

for diagnosis can be difficult, especially when representing a complex system using signal processing methods [43].

- **Flexibility**: Due to the nature of AI tools, this approach provides the ability to periodically adjust the system in response to changes [40]. For example, it is possible to retrain the diagnostic model regularly as new data is generated. In contrast, conventional methods would involve revising the initial model or assessing its impact.
- **Expertise required**: Implementing a data-driven approach requires less expertise on the system under study than other diagnostic methods. Indeed, developing a complete model often requires the collaboration of multiple experts and a significant investment of time. Furthermore, in the case of a signal-based approach, diagnosis relies on the expertise of the individuals who designed the diagnostic system [37].
- **Development complexity**: Accumulating the data needed to train AI tools can be difficult. In addition, AI approaches are prone to overtraining, which can decrease their effectiveness compared to model- or signal-based methods. Developing a model that can effectively simulate various failure conditions for a model-based approach is also a complex challenge. Only the signal-based approach offers a simple and uncomplicated solution to develop [44].
- **Diagnostic transparency**: AI learning methods are generally considered as black boxes, which means that they can sometimes produce undesirable results due to overtraining or use in scenarios not covered by training data, thus causing them to operate outside their area of expertise [40]. In contrast, model-based approaches provide a clearer understanding of diagnosis, as they rely on underlying physical or mathematical models of the system.

I.8 Conclusion

In this chapter, we have presented a general study on wind turbines and their main characteristics in the first part. We have also listed the existing types of wind turbines and their constituent components. The second part focuses on the state of the art in system fault diagnosis: we initially defined terms used in the field of fault diagnosis, then classified system faults based on their location, temporal evolution, and their impact on the performance of monitored systems. Furthermore, we established a classification of fault diagnosis methods and addressed the emergence of AI in fault diagnosis.

To study the wind system and develop fault diagnosis methods, we will establish a mathematical model that satisfactorily and realistically represents the behavior of the wind system,

followed by the implementation of an efficient control. Thus, the next chapter will be devoted to the establishment of the mathematical model and to the control of the variable speed wind system based on DFIG.

CHAPTER II

Modeling and Control of a Variable Speed Wind Turbine, based on a DFIM

II.1 Introduction

The dominance of horizontal-axis wind turbines is primarily due to economic considerations related to their manufacturing and installation. Among horizontal-axis wind turbines, there are two main types: fixed-speed and variable-speed models. Variable-speed wind turbines are more commonly used for electricity production on the grid because they can operate over a wide range of wind speeds, optimizing energy production for low winds and maintaining constant power in high winds.

In our work, we have chosen to study a variable-speed wind turbine using an asynchronous generator with a wound rotor, also known as a Doubly-Fed Induction Generator (DFIG). This second chapter focuses on the modeling and control of a variable-speed wind turbine system based on a DFIG. We will begin by explaining why this type of wind turbine is the most widely used for electrical energy production. Next, we will present the models of the various components in the wind turbine's electromechanical conversion chain. In the second part, we will detail the various control laws that enable optimal operation of the wind turbine and independent control of active and reactive power using PI, FLC, and NN controllers. The chapter will conclude with a presentation and explanation of the simulation results.

II.2 Description of the WECS based in DFIG

In our research focus, we've opted to examine a variable-speed wind turbine utilizing a wound rotor asynchronous generator, commonly termed a doubly-fed induction machine (DFIM), illustrated in Figure II.1.

Here's how the system operates: the turbine propels the DFIM via a multiplier. The stator of the DFIM is directly linked to the grid, while the rotor connects to the grid through three-phase static converters IGBT (Insulated Gate Bipolar Transistor). These power converters, referred to as RSC and GSC within our study, will be controlled using Pulse Width Modulation (PWM).

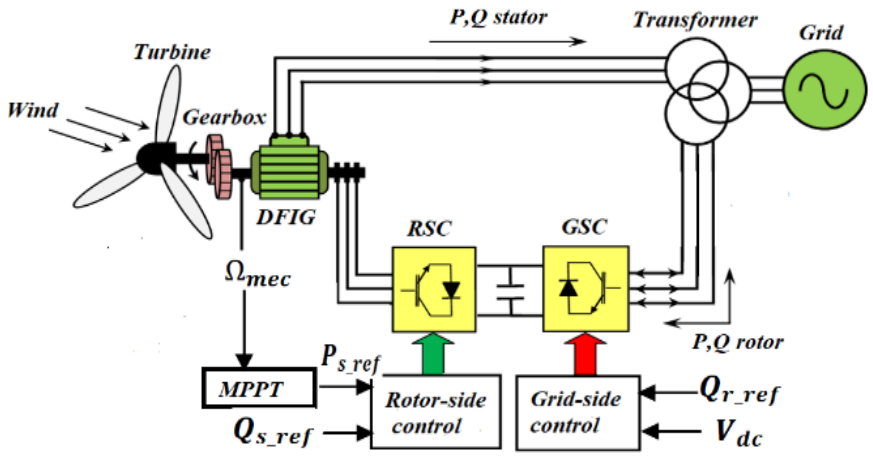

Figure II. 1 WECS based on DFIG.

The operation of this arrangement can be explained as follows: When wind passes through, the rotor, also known as the propeller, begins to rotate, thereby setting the blades in motion. This rotational action of the propeller induces movement in a shaft located within the nacelle, known as the slow shaft, which is connected to the gearbox. The gearbox then increases the slow rotational speed of the turbine to match the rotation speed of the rotor. The generator, linked to the gearbox via a shaft known as the fast shaft, is responsible for converting this mechanical energy into electrical energy.

The bidirectional capability of the converters enables operation in hypo or hypersynchronous modes. In hypersynchronous mode, electrical energy can be transferred not only from the stator to the grid but also from the rotor to the grid, enhancing the efficiency of the wind system. Furthermore, the power factor at the connection point of the wind turbine to the power grid can be managed by adjusting reactive powers in various inverter controls [45].

The primary advantage of this wind system is that the RSC and the GSC, which transfer the slip power to the power grid, are designed to handle only a portion of the nominal power of the DFIM. Specifically, if the DFIM operates at nominal power in hypersynchronous mode with a maximum slip of -30%, then a maximum of 25% of the machine's nominal power passes through the converters. This allows the converters to be sized for a power range between 25% and 30% of the machine's nominal power [45].

The additional costs linked to maintenance resulting from the use of a speed multiplier and the ring/brush system of the DFIM are thus counterbalanced by the savings made on the converters,

compared to a wind system where the converters would be sized for the rated power of the generator [45].

We will now study the transformation of the kinetic energy of wind into electrical energy by modeling the different elements of the electromechanical conversion chain of the wind turbine.

II.3 Wind energy conversion system modeling

In this section, we introduce the aerodynamic model of the turbine and the multiplier, followed by the mechanical model of the wind turbine. We then discuss the conversion of mechanical energy into electrical energy. A brief overview of the operation of the DFIG will be provided, after which the DFIG will be modeled in the Park reference frame to present the control of the RSC. Finally, we will model the connection of the GSC to the electrical grid via the RL filter in the Park reference frame to explain the GSC control.

II.3.1 Wind turbine modeling

II.3.1.1 Aerodynamic model

The turbine or propeller, positioned at the front of the turbine, typically features three blades of length R and is mounted on a rotor. Its primary function is to capture the kinetic energy of the wind and convert it into mechanical energy, which is then transferred to the slow rotating shaft.

Wind power is expressed by the following mathematical equation [46].

$$P_W = \frac{1}{2}.\rho.S.v^3 \tag{II. 1}$$

The aerodynamic power, converted by a wind turbine, P_{tur}, depends on the power coefficient C_p, and is expressed by equation (2) [47]:

$$P_{tur} = \frac{1}{2}C_p(\lambda,\beta) * \rho * S * v^3 \tag{II. 2}$$

λ represents the tip speed ratio:

$$\lambda = \frac{\Omega_{tur} * R}{v} \tag{II. 3}$$

Where:

ρ: Air density (Kg/m3);

v: Wind speed (m/s);

$S = \pi R^2$: Surface area swept by the wind turbine blades (m2);

R: Rotor radius of the turbine (m);

$C_p(\lambda, \beta)$: The power coefficient is dependent on both the tip speed ratioλ and the pitch angle β.

$\Omega_{tur}$is the angular speed of the wind turbine rotor.

The C_p represents the aerodynamic efficiency of the wind turbine and is influenced by its specific characteristics. This value is theoretically limited by the Betz limit, set at 0.593, though this limit is never actually achieved in practice [45].

In this thesis, we use an approximation based on analytical functions to estimate the $C_p$as a function of λ and the β, as expressed in equation (II.4) [48]:

$$\begin{cases} C_p(\lambda,\beta) = 0.73\left(\frac{151}{\lambda_i} - 0.58\beta - 0.002\beta^{2.4} - 13.2\right).e^{\frac{-18.4}{\lambda_i}} \\ \lambda_i = \frac{1}{\lambda + 0.02\beta} - \frac{0.003}{\beta^3 + 1} \end{cases} \quad \text{(II. 4)}$$

Figure II.2 shows the power coefficient curves plotted for various values of β against λ.

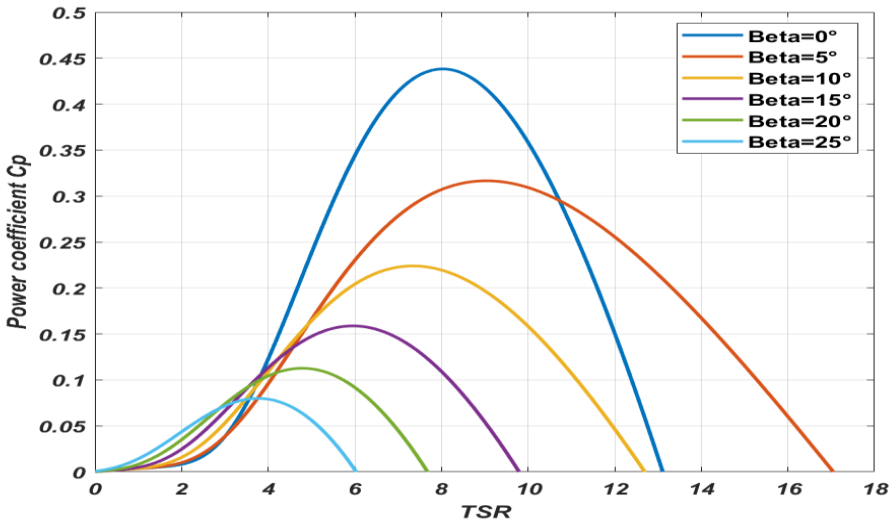

Figure II. 2 The power coefficient Cp (λ,β).

Given the turbine's rotational speed, the mechanical torque T_{tur} available on the slow-rotating shaft can be expressed as follows:

$$T_{tur} = \frac{P_{tur}}{\Omega_{tur}} = \frac{\pi}{2.\lambda} * \rho * R^3 * v^2 * C_p(\lambda, \beta) \quad \text{(II. 5)}$$

II.3.1.2 Multiplier model

The multiplier plays an essential role between the turbine and the generator in a wind power system. Its purpose is to adjust the turbine speed (Ω_{tur}), which is relatively slow, to the generator

speed (Ω_{mec}), which is higher. The multiplier is ideally rigid and lends itself to simplified modeling in the form of a simple gain [49].

In this approach, we neglect the elasticity and friction of the multiplier and the associated energy losses. In sum, although the multiplier is a complex device, we represent it concisely by the following two equations:

$$T_{mec} = \frac{T_{tur}}{G} \quad \text{(II. 6)}$$

$$\Omega_{mec} = G * \Omega_{tur} \quad \text{(II. 7)}$$

Where: T_{mec} is mechanical torque,

Ω_{mec} the generator speed, and G is the multiplier ratio.

II.3.1.3 Modeling of the mechanical shaft

The shaft incorporates a mass that simulates the inertia of the turbine rotor, supporting both the blades and the hub, alongside a smaller mass representing the inertia of the generator rotor.

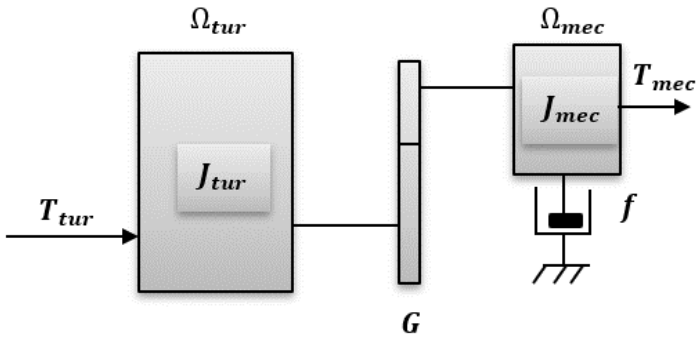

Figure II. 3 Model of the mechanical part of the wind turbine.

According to Figure II.3, we can determine the rotation speed of the turbine. The mechanical equation of the turbine shaft, linked to that of the generator used, is given as follows:

$$\left(\frac{J_{tur}}{G^2} + J_{mec}\right)\frac{d\Omega_{mec}}{dt} + f\Omega_{mec} = T_{mec} - T_{em} \quad \text{(II. 8)}$$

f is the viscous friction coefficient,

T_{em} is the electromagnetic torque of the generator,

J_{tur} is the moment of inertia of the turbine,

J_{mec} is the moment of inertia of the generator.

II.3.2 Modeling of the doubly-fed induction generator

In the domain of converting mechanical energy into electrical energy for electricity production, a variety of generators tailored for wind systems can be found. These diverse machines are classified based on factors such as power output, operational speed, torque capabilities, weight, volume, and other pertinent criteria. Among the primary types of electrical machines commonly used in the wind industry are synchronous machines and asynchronous machines [50]. For the purposes of this study, we have chosen to utilize the DFIG, renowned for its high efficiency and widespread adoption in wind energy production.

The DFIM is a variant of the three-phase asynchronous machine. Its particularity lies in the fact that it is simultaneously powered by two sources: its stator and its rotor. The major advantage of the DFIM lies in its ability to control power flow in hyposynchronous and hypersynchronous regimes, whether in motor or generator mode. Additionally, it enables variable-speed operation in integrated systems [51].

In the context of variable-speed wind energy systems, two primary configurations are used for double feeding of asynchronous machines:

Stator-Only Double Feeding: In this configuration, the stator provides one source of power, and the machine's rotor is also fed directly from the grid. This setup allows for better control of power flow and is commonly used.

Stator-Rotor Double Feeding with Converters: Another configuration employs converters positioned between the rotor of the machine and the electrical grid. These converters are smaller and more economical since they manage lower rotor power. Additionally, this setup enables simultaneous adjustment of both rotor voltage amplitude and frequency. Consequently, it is preferred in variable-speed wind turbine systems over turbines powered solely by the stator and equipped with power converters [52].

In a three-phase reference frame, the electrical equations of the DFIG are expressed as follows:

$$\begin{cases} [U_s] = [R_s] * [I_s] + \dfrac{d}{dt}[\varphi_s] \\ [U_r] = [R_r] * [I_r] + \dfrac{d}{dt}[\varphi_r] \end{cases} \quad \text{(II. 9)}$$

With;

$$[U_s] = \begin{bmatrix} U_{as} \\ U_{bs} \\ U_{cs} \end{bmatrix} ; [I_s] = \begin{bmatrix} I_{as} \\ I_{bs} \\ I_{cs} \end{bmatrix} \text{ et } [R_s] = \begin{bmatrix} R_s & 0 & 0 \\ 0 & R_s & 0 \\ 0 & 0 & R_s \end{bmatrix}$$

$$[U_r] = \begin{bmatrix} U_{ar} \\ U_{br} \\ U_{cr} \end{bmatrix} ; [I_r] = \begin{bmatrix} I_{ar} \\ I_{br} \\ I_{cr} \end{bmatrix} \text{ et } [R_r] = \begin{bmatrix} R_r & 0 & 0 \\ 0 & R_r & 0 \\ 0 & 0 & R_r \end{bmatrix}$$

Where: $[U_s]$, $[U_r]$: stator and rotor voltage vector,

$[I_s]$, $[I_r]$: stator and rotor current vector,

$[R_s]$,$[R_r]$: are respectively the stator and rotor resistors.

The equations related to fluxes are expressed in terms of currents and various self and mutual inductances, as follows:

$$\begin{cases} [\varphi_s] = [L_{ss}] * [I_s] + [M_{sr}] * [I_r] \\ [\varphi_r] = [L_{rr}] * [I_r] + [M_{rs}] * [I_s] \end{cases} \quad (\text{II. } 10)$$

With;

$$[L_{ss}] = \begin{bmatrix} l_s & M_s & M_s \\ M_s & l_s & M_s \\ M_s & M_s & l_s \end{bmatrix} \quad ; \quad [L_{rr}] = \begin{bmatrix} l_r & M_r & M_r \\ M_r & l_r & M_r \\ M_r & M_r & l_r \end{bmatrix}$$

Where:

$[L_{ss}]$, $[L_{rr}]$: are respectively the self-inductances of the stator and rotor phases,

M_s, M_r: are the mutual inductances between stator and rotor phases,

$[M_{sr}]$: is the matrix of mutual inductances or the stator-rotor coupling matrix given by:

$$[M_{sr}] = [M_{rs}]^T = \begin{bmatrix} \cos(\theta) & \cos\left(\theta + \frac{2\pi}{3}\right) & \cos\left(\theta - \frac{2\pi}{3}\right) \\ \cos\left(\theta - \frac{2\pi}{3}\right) & \cos(\theta) & \cos\left(\theta + \frac{2\pi}{3}\right) \\ \cos\left(\theta + \frac{2\pi}{3}\right) & \cos\left(\theta - \frac{2\pi}{3}\right) & \cos(\theta) \end{bmatrix}$$

$[M_{sr}]\ and\ [M_{rs}]^T$: is the stator-rotor mutual inductance.

The Park transformation is used to simplify and reduce the equations related to the machine by performing a change of reference frame in the electrical plane, designated as the (d-q) frame.

This transformation is described by:

$$P(\theta)=\sqrt{\frac{2}{3}}\begin{bmatrix}\cos(\theta) & \cos\left(\theta-\frac{2\pi}{3}\right) & \cos\left(\theta-\frac{4\pi}{3}\right)\\ -\sin(\theta) & -\sin\left(\theta-\frac{2\pi}{3}\right) & -\sin\left(\theta+\frac{2\pi}{3}\right)\\ \frac{1}{\sqrt{2}} & \frac{1}{\sqrt{2}} & \frac{1}{\sqrt{2}}\end{bmatrix} \quad \text{(II. 11)}$$

The Park transformations applied to currents and voltages in the equations of DFIG result in obtaining a biphasic model. This model is formulated as follows:

$$\begin{cases} U_{ds}=R_s*I_{ds}+\frac{d\varphi_{ds}}{dt}-\dot{\theta}_s*\varphi_{qs}\\ U_{qs}=R_s*I_{qs}+\frac{d\varphi_{qs}}{dt}+\dot{\theta}_s*\varphi_{ds}\\ U_{dr}=R_r*I_{dr}+\frac{d\varphi_{dr}}{dt}-\dot{\theta}_r*\varphi_{qr}\\ U_{qr}=R_r*I_{qr}+\frac{d\varphi_{qr}}{dt}+\dot{\theta}_r*\varphi_{dr}\end{cases} \quad \text{(II. 12)}$$

$$\begin{cases}\varphi_{ds}=L_s*I_{ds}+M*I_{dr}\\ \varphi_{qs}=L_s*I_{qs}+M*I_{qr}\\ \varphi_{dr}=L_r*I_{dr}+M*I_{ds}\\ \varphi_{qr}=L_r*I_{qr}+M*I_{qs}\end{cases} \quad \text{(II. 13)}$$

With respectively:

U_{ds}, U_{qs}, U_{dr} and U_{qr} : direct and quadrature stator and rotor voltages of the two-phase system,

$\dot{\theta}_s$ and $\dot{\theta}_r$: the angular speed of the d and q axes in the stator reference frame (S, abc) and in the rotor reference frame (R, abc), respectively,

ω_s et ω_r : sont les pulsations des grandeurs électriques statoriques et rotoriques ;

$\varphi_{ds}, \varphi_{qs}, \varphi_{dr}$and φ_{qr} : direct and quadrature stator and rotor flux of the system,

L_s and L_r : the stator and rotor cyclic inductors of the machine,

M : mutual inductance.

The electromagnetic torque is expressed as:

$$T_{em}=p\frac{M}{L_s}\left(I_{dr}\varphi_{qs}-I_{qr}\varphi_{ds}\right) \quad \text{(II. 14)}$$

Where p represents the number of pole pairs of the DFIG.

The active and reactive power components generated by the stator and rotor of the DFIG are respectively expressed as:

$$\begin{cases} P_s = U_{ds}I_{ds} + U_{qs}I_{qs} \\ Q_s = U_{qs}I_{ds} + U_{ds}I_{qs} \\ P_r = U_{dr}I_{dr} + U_{qr}I_{qr} \\ Q_r = U_{qr}I_{dr} + U_{dr}I_{qr} \end{cases} \quad (\text{II. } 15)$$

II.3.3 Modeling the GSC connection

In this section, we examine the modeling of the GSC connection to the electrical grid via an RL filter. Figure II.4 illustrates the entire link to the electrical grid, consisting of the DC bus, the GSC, and the input filter.

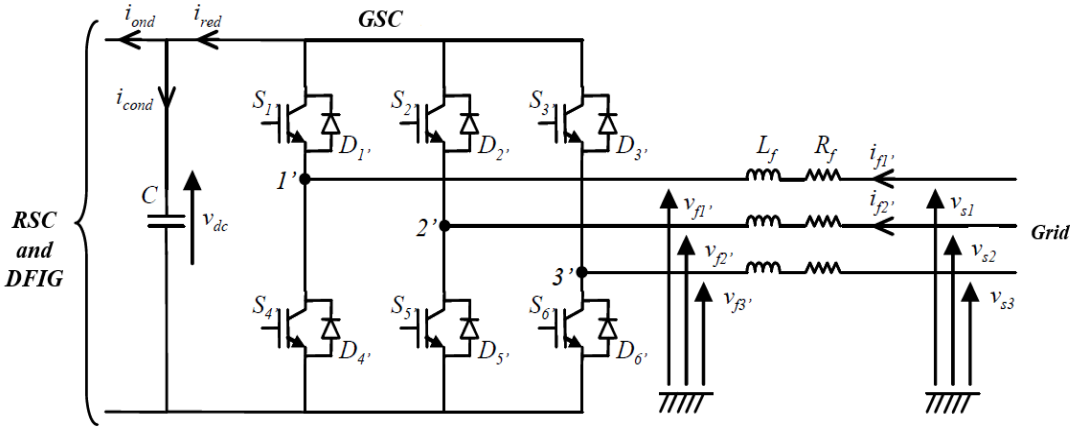

Figure II. 4 Connection of the GSC to the grid.

With:

$\boldsymbol{i_{ond}, i_{red,}}$ **:** the currents modulated by the RSC and the GSC, respectively,

$\boldsymbol{i_{cond}}$ **:** the current through the capacitor,

$\boldsymbol{v_{dc}}$ **:** DC bus voltage,

$\boldsymbol{S_{i'}, D_{i'}}$ **:** respectively, the IGBT transistors and the diodes connected in antiparallel ($i \epsilon \{1, 2, 3,4, 5, 6\}$),

$\boldsymbol{R_f, L_f}$ **:** the resistance and inductance of the filter RL,

$\boldsymbol{v_{f1'}, v_{f2'}, v_{f3'}}$: simple voltages modulated by the GSC,

$\boldsymbol{v_{s1}, v_{s2}, v_{s3}}$ **:** the simple voltages of the grid,

$\boldsymbol{i_{f1'}, i_{f2'}}$ **:** the currents flowing through the RL filter.

II.3.3.1 Modeling the DC bus

The voltage across the DC bus capacitor is determined by integrating the current that flows through the capacitor [53]:

$$\frac{dv_{dc}}{dt} = \frac{1}{C} \cdot i_{cond} \tag{II.16}$$

The current in the capacitor originates from a node through which two currents flow, modulated respectively by the RSC and the GSC (see Figure II.4).

$$i_{cond} = i_{red} - i_{ond} \tag{II.17}$$

II.3.3.2 Model of the connection to the grid in the Park frame

According to Figure II.4, in the three-phase frame system and using Kirchhoff's laws, we can formulate the following expressions [54]:

$$v_{f1'} = -R_f * i_{f1'} - L_f \frac{di_{f1'}}{dt} + v_{s1} \tag{II.18}$$

$$v_{f2'} = -R_f * i_{f2'} - L_f \frac{di_{f2'}}{dt} + v_{s2} \tag{II.19}$$

$$v_{f3'} = -R_f * i_{f3'} - L_f \frac{di_{f3'}}{dt} + v_{s3} \tag{II.20}$$

Using the Park transformation on the three previous equations, we arrive at the following expression [55][56]:

$$v_{fd} = -R_f * i_{fd} - L_f \frac{di_{fd}}{dt} + \dot{\theta}_s * L_f * i_{fq} + U_{ds} \tag{II.21}$$

$$v_{fq} = -R_f * i_{fq} - L_f \frac{di_{fq}}{dt} - \dot{\theta}_s * L_f * i_{fd} + U_{qs} \tag{II.22}$$

The powers active and reactive produced by the GSC are defined by [57]:

$$P_f = U_{ds} * i_{fd} + U_{qs} * i_{fq} \tag{II.23}$$

$$Q_f = U_{qs} * i_{fd} - U_{ds} * i_{fq} \tag{II.24}$$

II.4 Wind energy conversion system control

According to Figure II.1, it is therefore imperative to execute three specific controls to ensure the proper functioning of the wind turbine:

- The MPPT,
- The RSC, using IFOC with a power loop,
- The GSC; consists of controlling the DC bus voltage as well as the active and reactive power exchanged with the grid.

II.4.1 MPPT control strategy

The MPPT method is employed to enhance the efficiency of wind energy conversion systems by maximizing the power extracted from the wind. This is achieved through precise control of the rotor speed using a variable speed drive, which adjusts the electromagnetic torque to maintain the rotor speed at its designated reference value [58].

In this control strategy, the output of the speed controller uses the reference electromagnetic torque T_{em}^{*} to achieve a rotor speed Ω_{mec} equal to its desired value Ω_{mec}^{*}. To regulate the rotor speed and mitigate the impact of mechanical torque T_{mec}, considered a disturbance, an integral proportional (PI) controller is implemented. This method ensures effective tracking and maintenance of the maximum power point, thereby optimizing power generation in wind energy conversion systems.

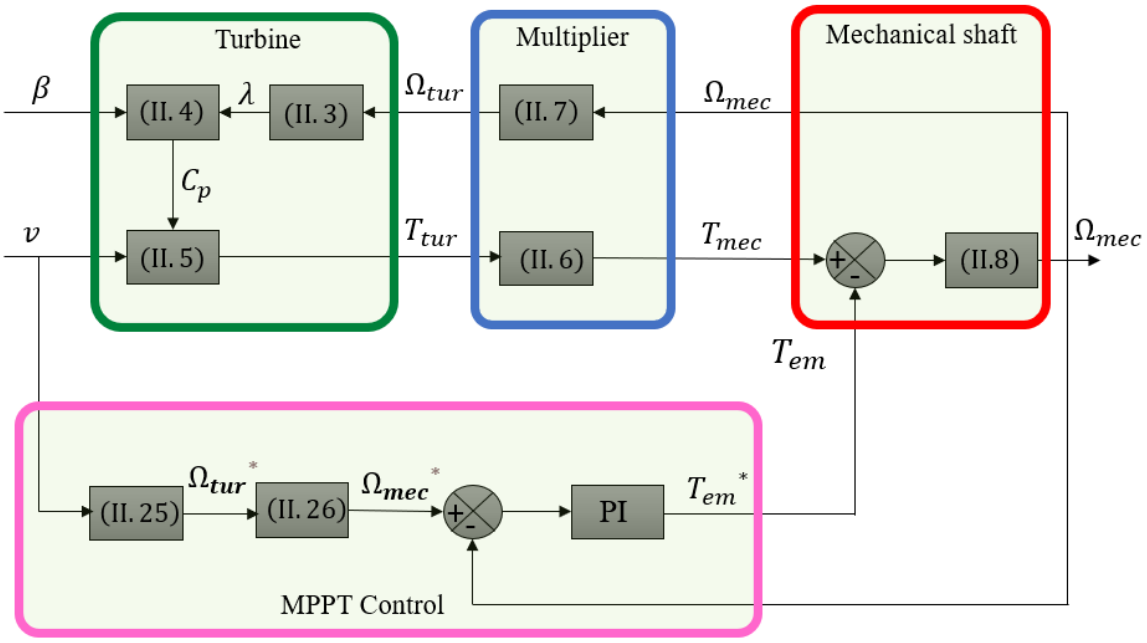

Figure II. 5 Block diagram of MPPT strategy.

For a given operating point (at a fixed wind speed), the objective is to maximize mechanical power, which corresponds to the maximum value of the coefficient C_p. This value is achieved when the relative speed λ equals its optimal value λ_{opt} (for a constant value of β equal to 0°), as illustrated in Figure II.6.

The reference rotation speed of turbine Ω_{tur}^{*} is obtained using equation (II.3) and is defined as follows:

$$\Omega_{tur}{}^{*} = \frac{\lambda_{opt}.v}{R} \quad (II.25)$$

We deduce the rotation speed reference of the DFIG by taking into account the gain of the multiplier by:

$$\Omega_{mec}{}^{*} = G.\Omega_{tur}{}^{*} \quad (II.26)$$

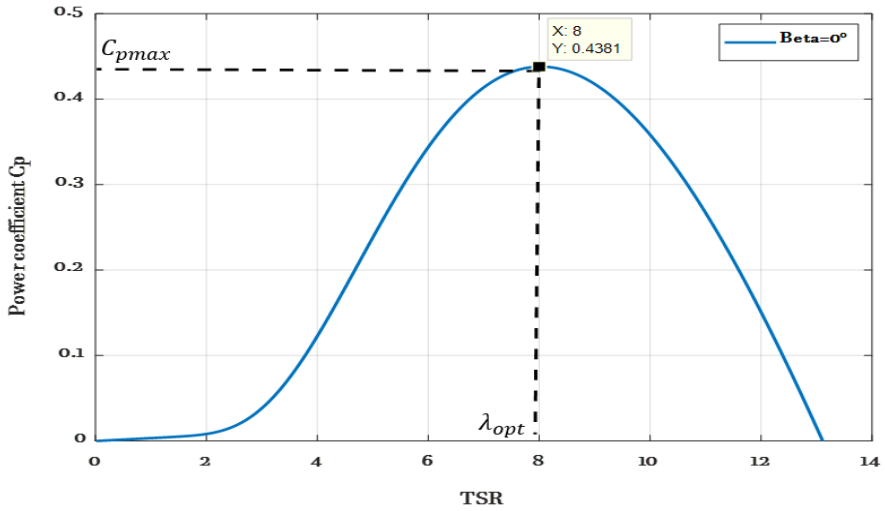

Figure II. 6 Cp as a function of λ for β =0°.

II.4.2 Grid side converter control (GSC)

The GSC is connected between the direct current DC bus and the electrical grid via an RL filter. This converter serves two essential functions [45][59]:

- ✓ Maintaining a constant DC bus voltage, regardless of the magnitude and direction of the rotor power flow in the DFIG.
- ✓ Ensuring a unity power factor at the point of connection with the electrical grid.

Figure II.7 illustrates the control of the GSC, which achieves these two functions by simultaneously regulating the currents flowing through the RL filter and the DC bus voltage.

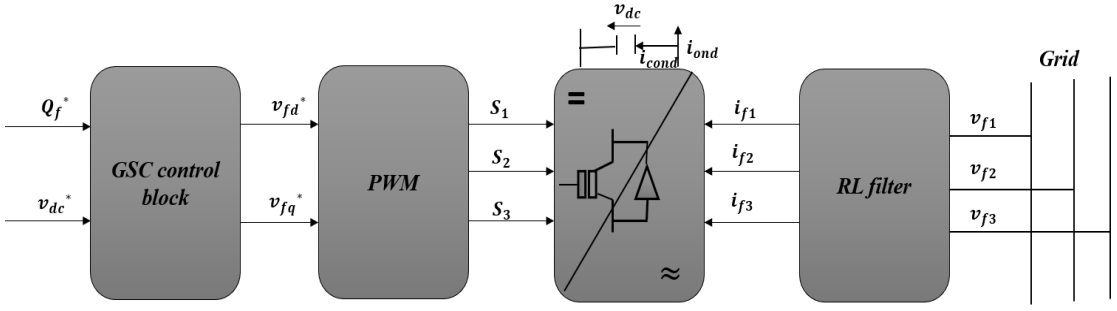

Figure II. 7 Principle of GSC control.

A. Control of currents passing through the RL filter

In the frame system (d, q) associated with the stator rotating field, we have the following equations [60]:

$$v_{fd} = -R_f . i_{fd} - L_f \frac{di_{fd}}{dt} + e_{fd} \quad \text{(II. 27)}$$

$$v_{fq} = -R_f . i_{fq} - L_f \frac{di_{fq}}{dt} + e_{fq} \quad \text{(II. 28)}$$

Where:

$$e_{fd} = \omega_s . L_f . i_{fq} \quad \text{(II. 29)}$$

$$e_{fq} = -\omega_s . L_f . i_{fd} + U_{qs} \quad \text{(II. 30)}$$

The connection model between the GSC and the grid, in the dq reference frame based on the stator rotating field, allows us to establish precise control over the currents flowing through the RL filter. Taking couplings into account, each axis (d and q) can be independently controlled, each with its own controller [45]. The references for these controllers are the currents in the RL filter of the dq axes.The block diagram of the current control loops for the dq axes is illustrated in Figure II.8. The controllers used are of the PI type. These regulation schemes include compensation and decoupling terms for the dq axes, as well as models of the GSC and its connection to the grid via the RL filter in the dq reference frame [60].

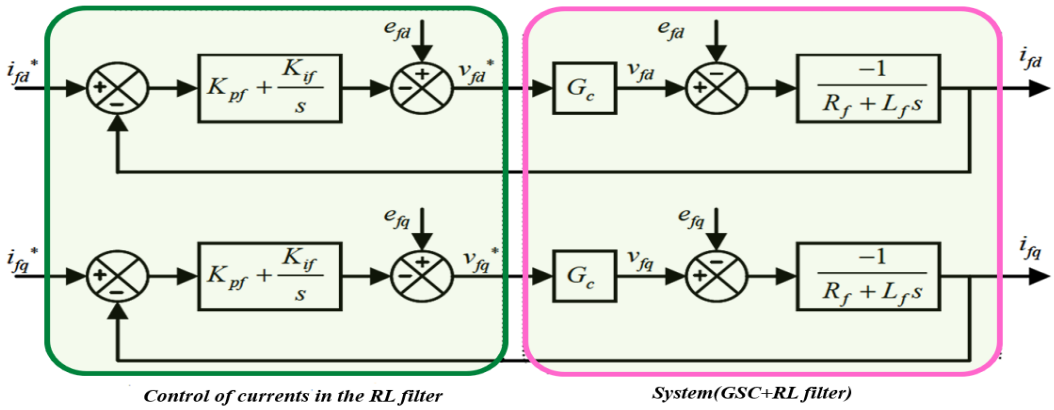

Figure II. 8 Control of currents in the RL filter.

For the control of rotor currents, we represent the RSC by a gain G_c. We assume that the converter is ideal, which means we neglect the dead times imposed by the power switch drivers of the RSC. In this case, the value of G_c is equal to 1.

The reference currents i_{fd}^{*} and i_{fq}^{*}come from the DC bus voltage control block and the reactive power control respectively at the connection point of the GSC with the power grid.

By neglecting losses in the resistance R_f of the RL filter and taking into account the orientation of the dq reference associated with the rotating stator field (U_{ds} = 0), equations (II.23) and (II.24) are rewritten as follows [61]:

$$P_f = U_{qs}.i_{fq} \quad (II.31)$$

$$Q_f = U_{qs}.i_{fd} \quad (II.32)$$

Using these equations, we can impose the reference active and reactive powers, denoted as P_f^{*} and Q_f^{*}, by imposing the corresponding reference currents [45]:

$$i_{fd}^{*} = \frac{Q_f^{*}}{U_{qs}} \quad (II.33)$$

$$i_{fq}^{*} = \frac{P_f^{*}}{U_{qs}} \quad (II.34)$$

The i_{fd}^{*} component is used to control the reactive power at the point of connection between the GSC and the grid. On the other hand, the quadrature component $i_{fq}^{*}$is employed to control the DC bus voltage. Thanks to this principle, it is possible to impose a zero reference reactive power (Q_f^{*}= 0 VAr) [45].

B. Control of DC bus voltage

The powers involved in the DC bus can be expressed as follows [45]:

$$P_{red} = v_{dc}.i_{red} \quad (II.35)$$

$$P_c = v_{dc}.i_{cond} \quad (II.36)$$

$$P_{ond} = v_{dc}.i_{ond} \quad (II.37)$$

The connection between these powers is expressed by the relation [45]:

$$P_{red} = P_c + P_{ond} \quad (II.38)$$

Assuming that all Joule losses are negligible compared to the power exchanged between the rotor of the DFIG and the grid (including losses in the capacitor, converter, and RL filter), we can express this as follows [45]:

$$P_f = P_{red} = P_c + P_{ond} \quad (II.39)$$

The reference power for the capacitor is associated with the reference current flowing through it [45]:

$$P_c^* = v_{dc}.\, i_{cond}^* \qquad (II.40)$$

The Figure II.9 illustrates the block diagram of the DC bus voltage control loop. To simplify the control chain, we assume that the reference current i_{fq}^* is always equal to the current i_{fq}, as the response time of the internal loop is shorter than that of the external loop [45].

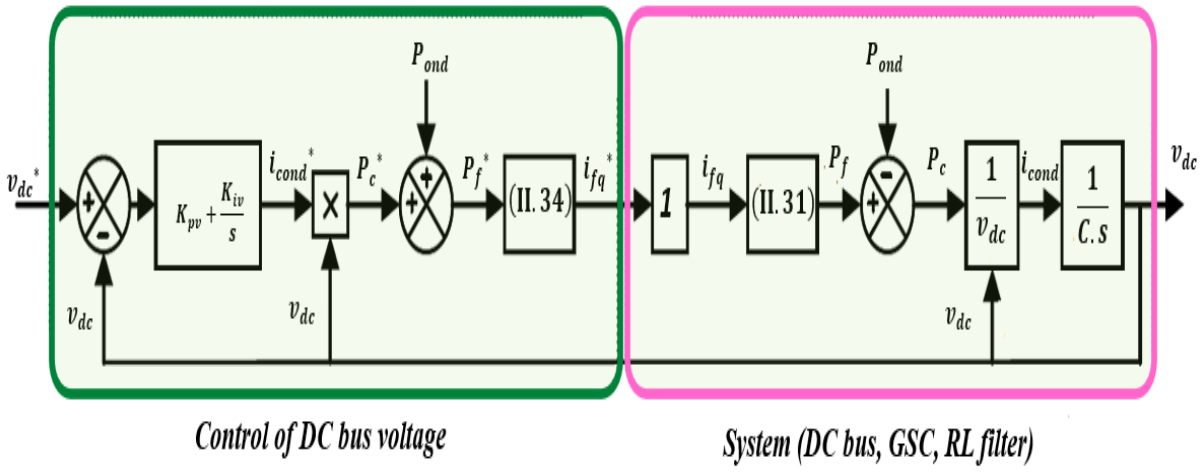

Figure II. 9 DC bus voltage control loop.

II.4.3 Rotor side converter control (RSC)

II.4.3.1 Indirect field-oriented control (IFOC)

Vector control remains the predominant technique for controlling DFIG-based wind turbines. In this approach, the rotor current vector is split into two components using a synchronously rotating (dq) reference frame [62]. The direct rotor current governs reactive power control, while the quadrature current is associated with real power. This configuration allows the DFIG to closely resemble the structure of a DC machine, where torque and flux control magnitudes are naturally decoupled [63].

For an AC machine, achieving this straightforward vector control performance directly is not feasible. Two options exist to address this challenge. The first option involves aligning the d-axis with the stator flux. Alternatively, the second option is to orient the q-axis along the stator voltage and introduce a 90° delay to the d-axis, considering that the two vectors are phase-shifted

by 90°. The first one is widely adopted in wind power generation using DFIG and is a classical method documented in the literature [64][65].

The system employs an indirect vector approach to independently regulate the generator's powers and address coupling issues. Specifically, a closed-loop control scheme governs the rotor currents, while an open-loop control scheme manages the powers. Assuming constant stator flux aligned with the d-axis, the elimination of stator winding resistance results in a quadratic nullification of the quadrature stator flux (φ_{qs}=0), yielding a direct stator flux of (φ_{ds}= φ_s) [66]. This simplifies the equations (II.12), (II.13) and (II.14) to their concise form:

$$\begin{cases} U_{ds} = R_s I_{ds} \\ U_{qs} = R_s I_{qs} + \dot{\theta}_s \varphi_{ds} \\ U_{dr} = R_r I_{dr} + \dfrac{d\varphi_{dr}}{dt} - \dot{\theta}_r \varphi_{qr} \\ U_{qr} = R_r I_{qr} + \dfrac{d\varphi_{qr}}{dt} + \dot{\theta}_r \varphi_{dr} \end{cases} \quad (II.41)$$

The resistance of the stator windings is negligible in high-power machines.

$$\begin{cases} U_{ds} = 0 \\ U_{qs} = \dot{\theta}_s \varphi_{ds} = V_s \end{cases} \quad (II.42)$$

$$\begin{cases} \varphi_{ds} = \varphi_s = L_s I_{ds} + M I_{dr} \\ 0 = L_s I_{qs} + M I_{qr} \\ \varphi_{dr} = L_r I_{dr} + M I_{ds} \\ \varphi_{qr} = L_r I_{qr} + M I_{qs} \end{cases} \quad (II.43)$$

$$T_{em} = -p \frac{M}{L_s} I_{qr} \varphi_s \quad (II.44)$$

The power stator equations (II.15) can be simplified as shown below:

$$\begin{cases} P_s = V_s I_{qs} \\ Q_s = V_s I_{ds} \end{cases} \quad (II.45)$$

From Equation (II.43), one can deduce the connection between the stator and rotor currents:

$$\begin{cases} I_{ds} = \dfrac{\varphi_s}{L_s} - \dfrac{M}{L_s} . I_{dr} \\ I_{qs} = -\dfrac{M}{L_s} . I_{qr} \end{cases} \quad (II.46)$$

By substituting equation (II.46) into the rotor flux expressions (II.43), they can be expressed in terms of rotor currents as shown below:

$$\begin{cases} \varphi_{dr} = \left(L_r - \frac{M^2}{L_s}\right) I_{dr} + M\frac{\varphi_s}{L_s} \\ \varphi_{qr} = \left(L_r - \frac{M^2}{L_s}\right) I_{qr} \end{cases} \quad (II.47)$$

The connection between the rotor voltages and the rotor currents can be determined by substituting equation (II.47) into the expressions for U_{dr} and U_{qr} [67]:

$$\begin{cases} U_{dr} = R_r . I_{dr} + \left(L_r - \frac{M^2}{L_s}\right)\frac{dI_{dr}}{dt} - g\omega_s\left(L_r - \frac{M^2}{L_s}\right) I_{qr} \\ U_{qr} = R_r . I_{qr} + \left(L_r - \frac{M^2}{L_s}\right)\frac{dI_{qr}}{dt} + g\omega_s\left(L_r - \frac{M^2}{L_s}\right) I_{dr} + g.\frac{\varphi_s M}{L_s} \end{cases} \quad (II.48)$$

Where :

$\omega_s$and ω_r: stator and rotor angular velocity, respectively;

g: represents the slip of the asynchronous machine.

$$g = \frac{\omega_s - \omega_r}{\omega_r} \quad (II.49)$$

By replacing Equation (II.46) into Equation (II.45), the expressions for active and reactive power can be reformulated in terms of rotor currents, as shown below:

$$\begin{cases} P_s = -V_s . \frac{M}{L_s} I_{qr} \\ Q_s = V_s \frac{\varphi_s}{L_s} - V_s \frac{M}{L_s} . I_{dr} \end{cases} \quad (II.50)$$

From equation (II.42) the expression for the stator flux can be written as follows:

$$\varphi_{ds} = \varphi_s = \frac{V_s}{\omega_s} \quad (II.51)$$

So, equation (II.50) becomes like this:

$$\begin{cases} P_s = -V_s . \frac{M}{L_s} I_{qr} \\ Q_s = \frac{{V_s}^2}{M . \omega_s} - V_s \frac{M}{L_s} . I_{dr} \end{cases} \quad (II.52)$$

Utilizing the equations recently derived, we can construct a streamlined representation for the rotor windings of the DFIG. This enables us to define the relationships between the applied

voltages on the rotor and the consequent stator powers. Specifically, equations (II.48) and (II.52) allow us to illustrate in Figure II.10 a model with rotor voltages as inputs and stator active and reactive powers as outputs. This model serves as the foundation for subsequent regulation efforts.

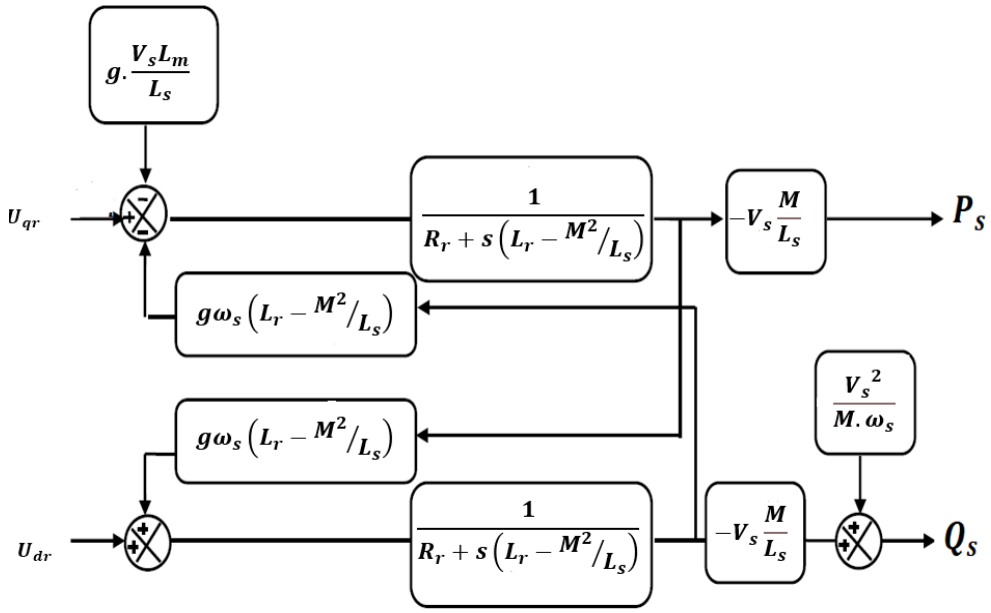

Figure II. 10 Block diagram of the DFIG.

From Figure II.10, we can observe that power and voltage are connected through a first-order transfer function. Additionally, because the slip value g is low, it will be feasible to establish vector control effectively. The impact of couplings will remain minimal, allowing independent control of the d and q axes using their respective controllers.

Unlike direct control, the IFOC method aims to regulate both the rotor powers and currents. It accounts for the coupling terms and employs two proportional-integral (PI) controllers on each axis [68]. The figure below illustrates the model of IFOC that we selected for our study.

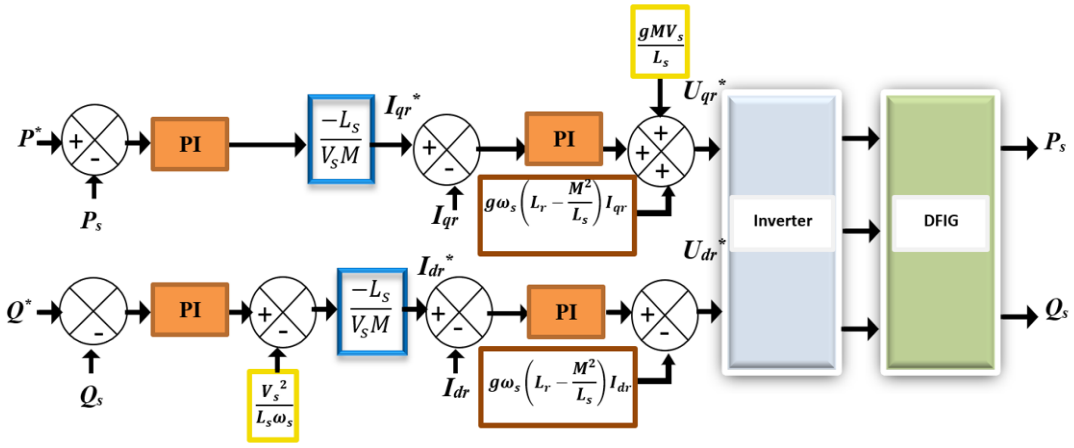

Figure II. 11 Block diagram of IFOC with PI controllers.

II.4.3.1.1 PI synthesis

A. Power controller

The block diagram illustrating the power control loop with a PI controller is depicted in the figure below:

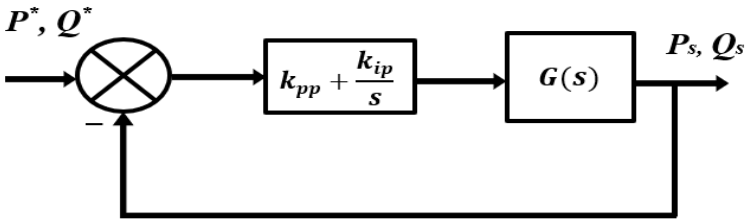

Figure II. 12 Block diagram of the power PI controller.

In the context of control systems, the terms K_{pp} and K_{ip} represent the proportional and integral gains, respectively. This particular type of controller emerges from the balanced interplay of two fundamental actions:

- Proportional Action: Its purpose is to fine-tune the system's dynamic response speed.
- Integral Action: This action aids in minimizing the discrepancy (static error) between the desired reference value and the actual controlled output.

The transfer function to be regulated, denoted as $G(s)$, is defined as follows:

$$G(s) = \frac{MV_s}{L_s.R_r + s.L_s.\left(L_r - \frac{M^2}{L_s}\right)} \qquad \text{(II. 53)}$$

The transfer function of the open loop becomes:

$$H_{p-ol}(s) = \left(K_{pp} + \frac{K_{ip}}{s}\right).G(s) = \frac{MV_s.\left(K_{pp}.s + K_{ip}\right)}{s\left[L_sR_r + s.L_s.\left(L_r - \frac{M^2}{L_s}\right)\right]} \quad (II.54)$$

The transfer function of the closed loop is expressed by:

$$H_{p-cl}(s) = \frac{\frac{MV_s.\left(K_{pp}.s+K_{ip}\right)}{L_s.\left(L_r-\frac{M^2}{L_s}\right)}}{s^2 + \frac{s.\left(L_sR_r+MV_sK_{pp}\right)}{L_s.\left(L_r-\frac{M^2}{L_s}\right)} + \frac{MV_sK_{ip}}{L_s.\left(L_r-\frac{M^2}{L_s}\right)}} \quad (II.55)$$

The transfer function of a second-order system is expressed by the following equation:

$$TF = \frac{K.{w_n}^2}{s^2 + 2.\xi w_n.s + {w_n}^2} \quad (II.56)$$

Where:

K :is the system's gain,

w_n:is the natural frequency of the system,

ξ :is the damping ratio.

By identifying equation (II.56) with equation (II.55), we obtain:

$$\begin{cases} K_{pp} = \dfrac{2.\xi.w_n.L_s.\left(L_r - \frac{M^2}{L_s}\right) - L_sR_r}{L_s.\left(L_r - \frac{M^2}{L_s}\right)} \\ {w_n}^2 = \dfrac{MV_sK_{ip}}{L_s.\left(L_r - \frac{M^2}{L_s}\right)} \\ K_{ip} = \dfrac{{w_n}^2L_s.\left(L_r - \frac{M^2}{L_s}\right)}{MV_s} \end{cases} \quad (II.57)$$

B. Current controller

The figure below depicts the simplified block diagram for the synthesis of PI controllers for the rotor currents of the DFIG.

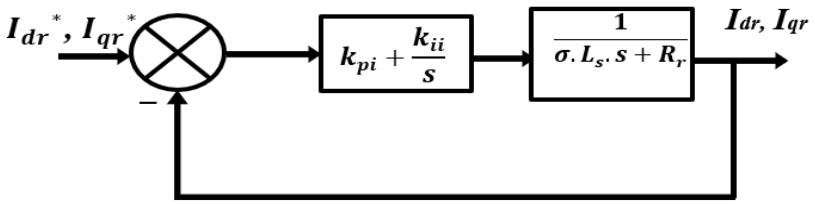

Figure II. 13 Block diagram of the current PI controller.

With:

$$\sigma = \left(1 - \frac{M^2}{L_s L_r}\right) \tag{II.58}$$

The open loop transfer function is given by:

$$H_{i-ol}(s) = \left(K_{pi} + \frac{K_{ii}}{s}\right).\left(\frac{1}{\sigma . L_s . s + R_r}\right) = K_{ii}.\left(\frac{1 + \frac{K_{pi}}{K_{ii}}.s}{s}\right) \tag{II.59}$$

To eliminate the zero in the transfer function, we employ the pole compensation method for controller synthesis. In other words, this translates to:

$$\frac{K_{pi}}{K_{ii}} = \frac{\sigma . L_r}{R_r} \tag{II.60}$$

The H_{i-ol} then becomes.

$$H_{i-ol}(s) = \frac{K_{ii}}{R_r . s} \tag{II.61}$$

The Closed Loop Transfer Function has the following form:

$$H_{i-cl}(s) = \frac{1}{1 + \frac{R_r}{K_{ii}}.s} \tag{II.62}$$

The formula for adjusting the controller gains based on machine parameters and response time is presented as follows:

$$\begin{cases} K_{pi} = \dfrac{\sigma . L_r}{t_r} \\ K_{ii} = \dfrac{R_r}{t_r} \end{cases} \tag{II.63}$$

Where: $\boldsymbol{t_r}$is the response time.

II.4.3.2 Fuzzy Logic Control

This section focuses on applying fuzzy logic to improve the performance of the IFOC technique by replacing PI controllers with FLCs. One major advantage of fuzzy control over traditional methods is its independence from precise mathematical models of the system [69].

Typically, designing an FLC for electric drives involves decisions concerning the following parameters:

- Selection of linguistic variables,
- Choice of membership functions,
- Selection of inference method,
- Choice of defuzzification strategy.

In single-variable systems, the inputs to the FLC typically consist of the error (the deviation between the setpoint and the process output) and its rate of change (which indicates the system's dynamics) [23]. Many advanced controllers adopt the simple scheme proposed by Mamdani, as depicted in the following diagram:

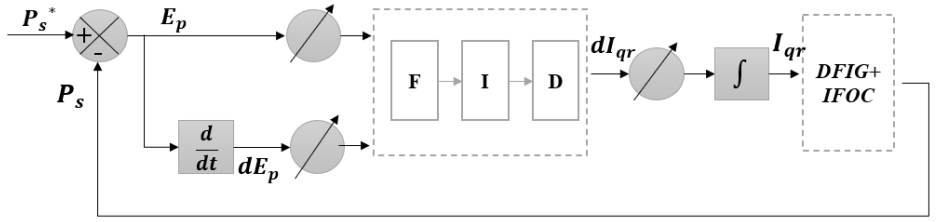

Figure II. 14 Block diagram of a FLC.

The inputs for the FLC are computed as depicted at time k [69].

$$E_p(k) = P_s^*(k) - P_s(k) \quad \text{(II. 64)}$$

$$dE_p(k) = E_p(k) - E_p(k-1) \quad \text{(II. 65)}$$

By integrating the FLC output dI_{qr} ,we obtain the control signal for the ${I_{qr}}^*$system, as was presented in the Figure II.14.

$${I_{qr}}^*(k) = I_{qr}(k-1) - {dI_{qr}}^*(k) \quad \text{(II. 66)}$$

Figure II.15 illustrates the comprehensive diagram of IFOC utilizing FLC.

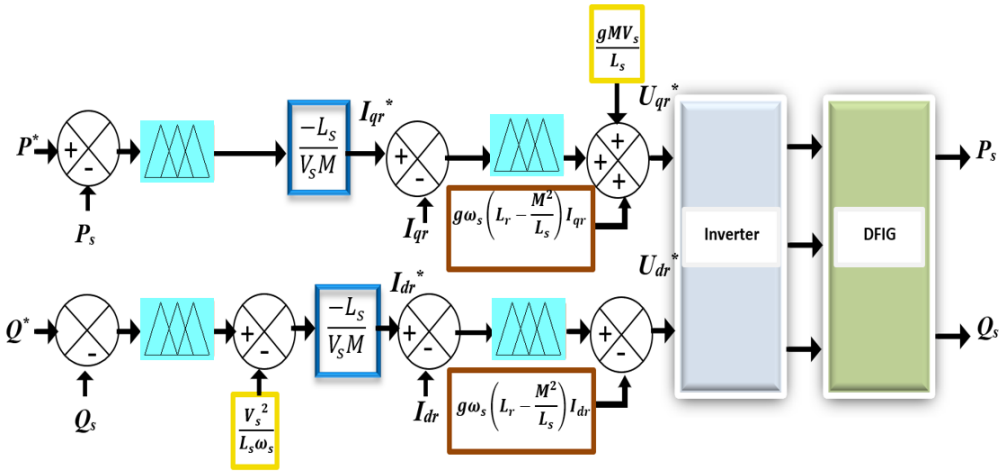

Figure II. 15 Block diagram of IFOC with FLC.

This method relies on four fundamental steps:

a. Fuzzification

The evaluation of a membership function that converts a numerical value into a fuzzy degree is shown in Figure II.16.

The membership functions for the input variables E_p, dE_p, and dI_{qr} were chosen to be triangular and trapezoidal shapes[58]. This choice is based on their simple implementation and their effectiveness in representing linguistic variables and their corresponding fuzzy sets[58].

These shapes enable smooth transitions between different linguistic terms and provide flexibility in representing fuzzy sets.

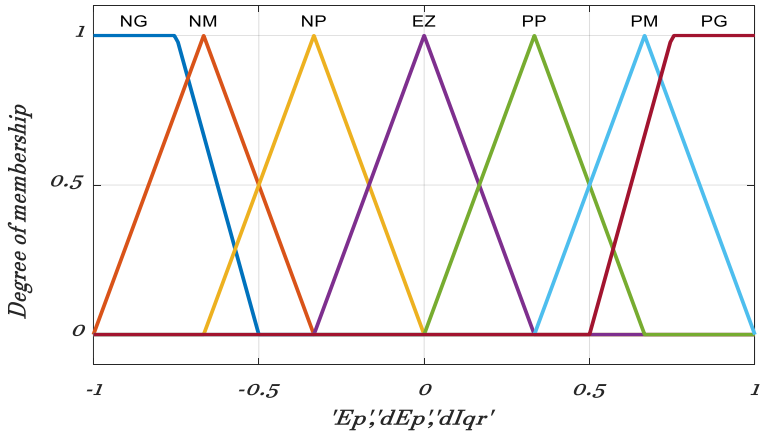

Figure II. 16 Membership functions for input variables Ep,dEp and output dIqr of the FLC.

b. Evaluation of the rules

The process involves converting fuzzy input into fuzzy output using fuzzy If-Then rules. In this study, we employed Mamdani's fuzzy inference method, along with a fuzzy Max-Min operation, as detailed in Table II.1. The FLC's inference process is based on a set of 7x7 rules that define the relationship between the input variables and the resulting control signal.

Table II. 1 Table of fuzzy rules.

dE_p \ E_p	NG	NM	NP	E Z	PP	PM	PG
NG	NG	NM	NG	NG	NM	NP	EZ
NM	NG	NM	NG	NM	NP	EZ	PP
NP	NG	NP	NM	NP	EZ	PP	PM
EZ	NG	NP	NP	EZ	PP	PM	PG
PP	NM	NM	EZ	PP	PM	PG	PG
PM	NP	EZ	PP	PM	PG	PB	PG
PG	EZ	PP	PM	PG	PG	PB	PG

c. Rule output aggregation

The aggregation process entails combining the outputs from all the rules into a single unified result.

d. Defuzzification

To obtain a numerical value from the aggregated fuzzy output set, a technique called defuzzification is used. In the context of the FLC for controlling active and reactive power in a DFIG, the defuzzification process uses the center of gravity method.

This method calculates the crisp output value by determining the weighted average of the fuzzy output sets, with each set's weight based on its degree of membership within the output fuzzy set.

The defuzzification equation for the FLC in this context can be represented as follows:

$$dI_{qr} = \frac{\sum \mu_{Ri}(I_{qri}) dI_{qri}}{\sum \mu_{Ri}(I_{qri})} \quad \text{(II. 67)}$$

Where, μ_{Ri}denotes the membership degree of I_{qri}.

II.4.3.3 Improvement of IFOC performance by ANN

This section delves into the practical application of ANN. Our goal is to enhance the performance of the IFOC technique by replacing the PI controllers with NNC.

ANNs are inspired by the complex structure of the human brain. In our study, we implemented an NN controller using Matlab's nftool. Concurrently, we simulated a DFIG-based wind turbine using a PI controller and collected data to represent the desired control behavior of the DFIG-based WECS both before and after the controller's operation.

We then trained a feed-forward neural network using supervised learning. The neural network architecture was configured as (1-10-1), meaning one input neuron, ten neurons in the hidden layer, and one output neuron. The training process focused on optimizing the network's performance by minimizing a cost function, and we refined the network iteratively using the Levenberg-Marquardt optimization algorithm until achieving satisfactory results.

Once fully trained, the NNC can be seamlessly integrated into the control system of the DFIG-based WECS, effectively regulating power generation. Figure II.17 illustrates the structure of a NNC used, and Figure II.18 illustrates the comprehensive diagram of IFOC with NNC.

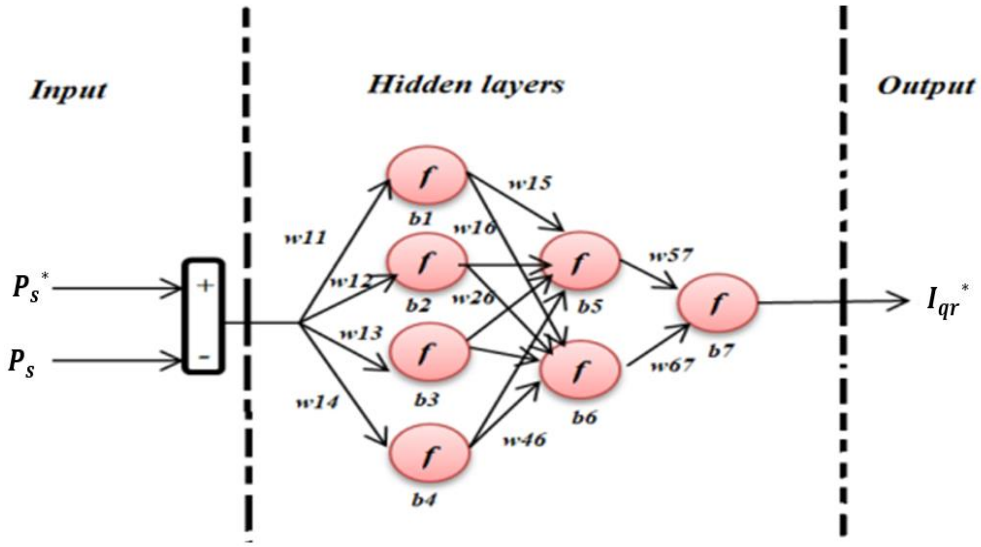

Figure II. 17 General structure of Artificial Neural Network

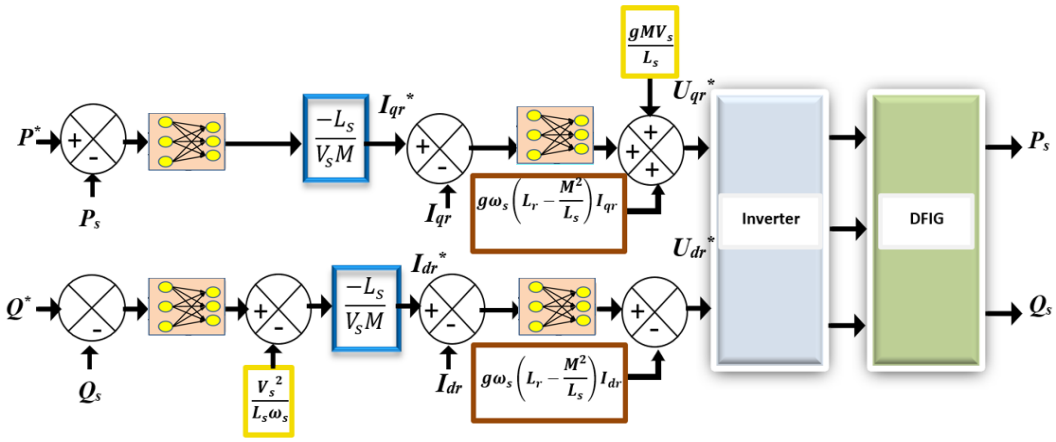

Figure II. 18 Block diagram of IFOC with NNC.

II.5 Results and discussion

This section evaluates and compares the performance of the proposed methods in terms of reference tracking, dynamic response, static error, system stability, and robustness. The complete system was modeled by simulating a 10 Kw wind turbine with the parameters specified in Table II.2 using Matlab/Simulink.

Table II. 2 Parameters of turbine and DFIG.

Turbine parameters	
Parameters	**Value**
Nominal power	10Kw
Number of blades	3
Diameter of a blade	3m
Multiplier gain	5.4
Moment of inertia	0.042Kg.m^2
Coefficient of friction	0.017N.m.s^{-1}
DFIG parameters	
Nominal power	7.5Kw
Rated frequency	50Hz
Stator resistance	0.455Ω
Rotor resistance	0.62Ω
Stator inductance	0.084H
Rotor inductance	0.081H
Mutual inductance	0.078H
Moment of inertia	0.3125 Kg.m2
Coefficient of friction	6.73*10^{-3} N.m.s^{-1}
Number of pole pairs	2
Air density	1.225 Kg/m^3

Figures (II.19), (II.20), (II.21), and (II.22) illustrate the reference tracking responses for active and reactive power control employing PI, FLC, and NN controllers. To assess the performance of

the proposed controllers, the simulation entails incrementally adjusting both active and reactive reference powers. Specifically, the active reference power is modified at 2s and 3s, while the reactive reference power is adjusted at 3s.

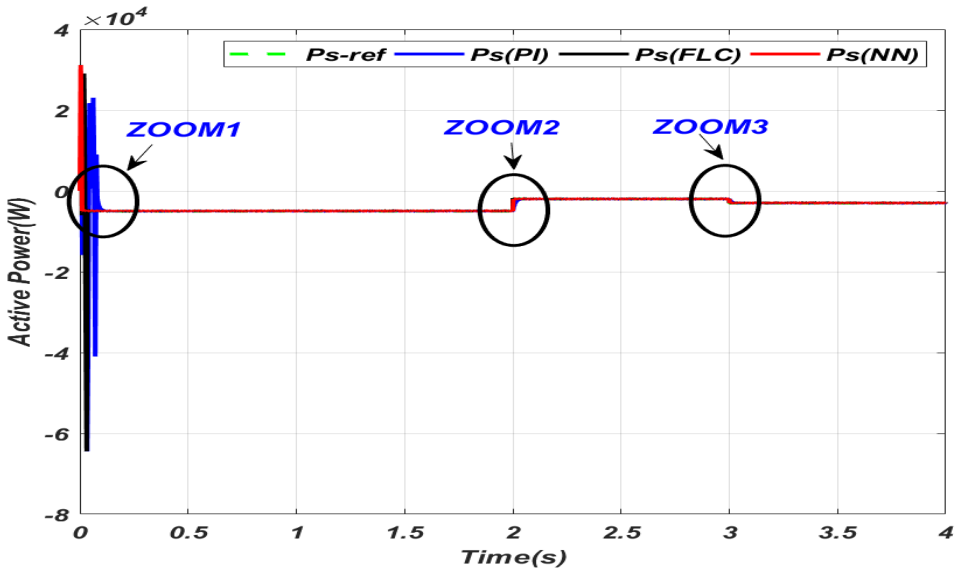

Figure II. 19 Active power.

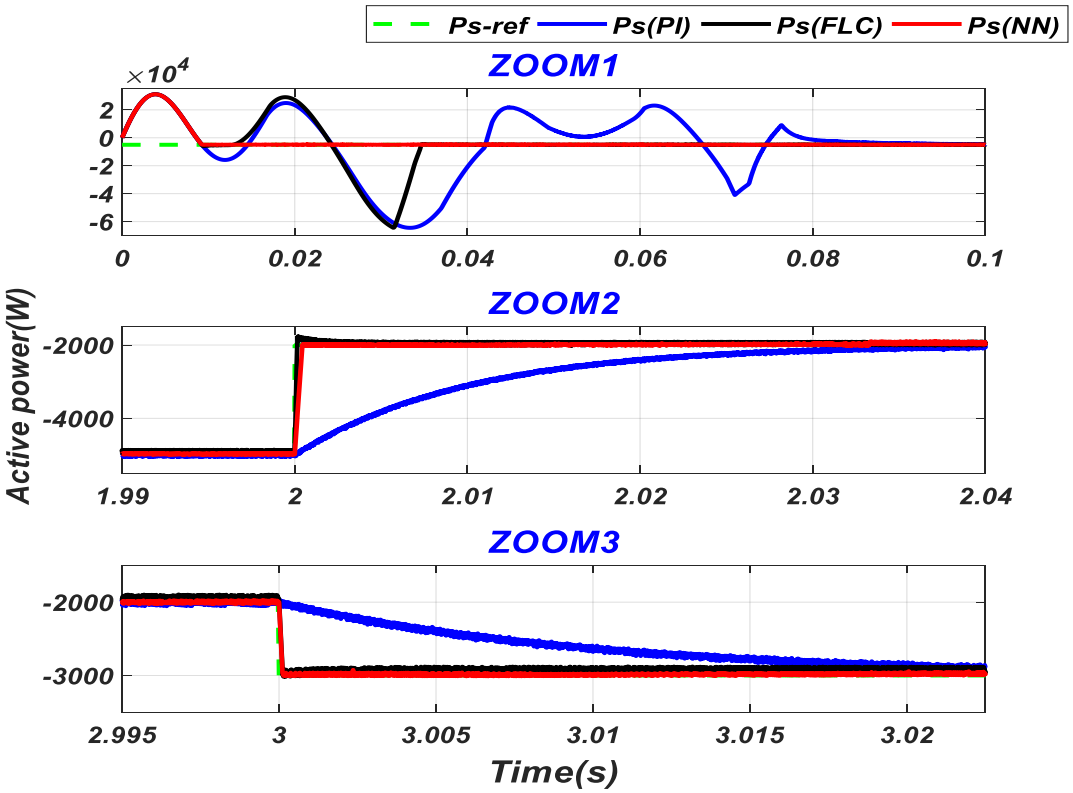

Figure II. 20 Zoom in active power behavior.

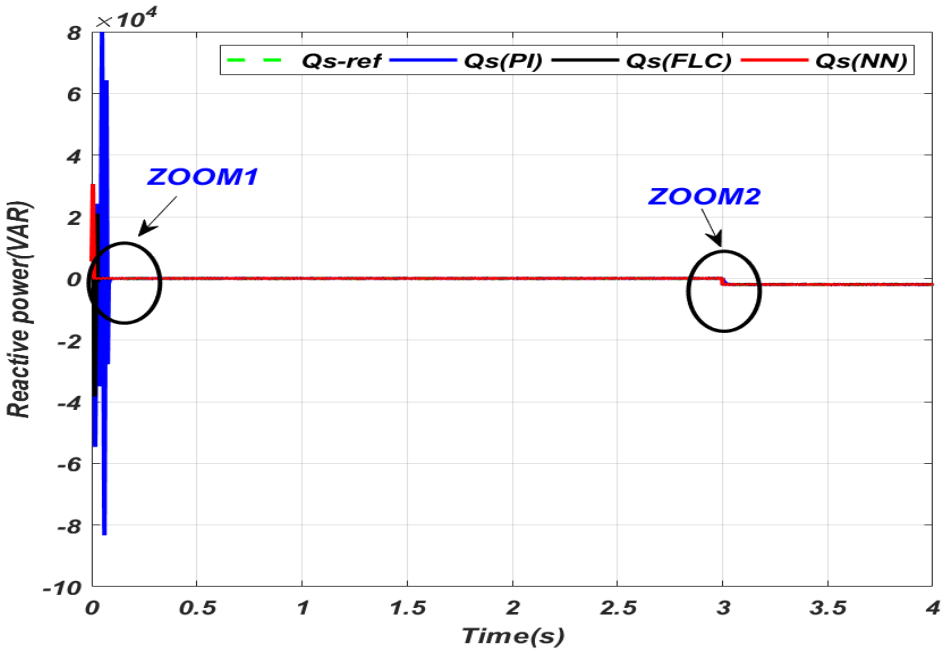

Figure II. 21 Reactive power.

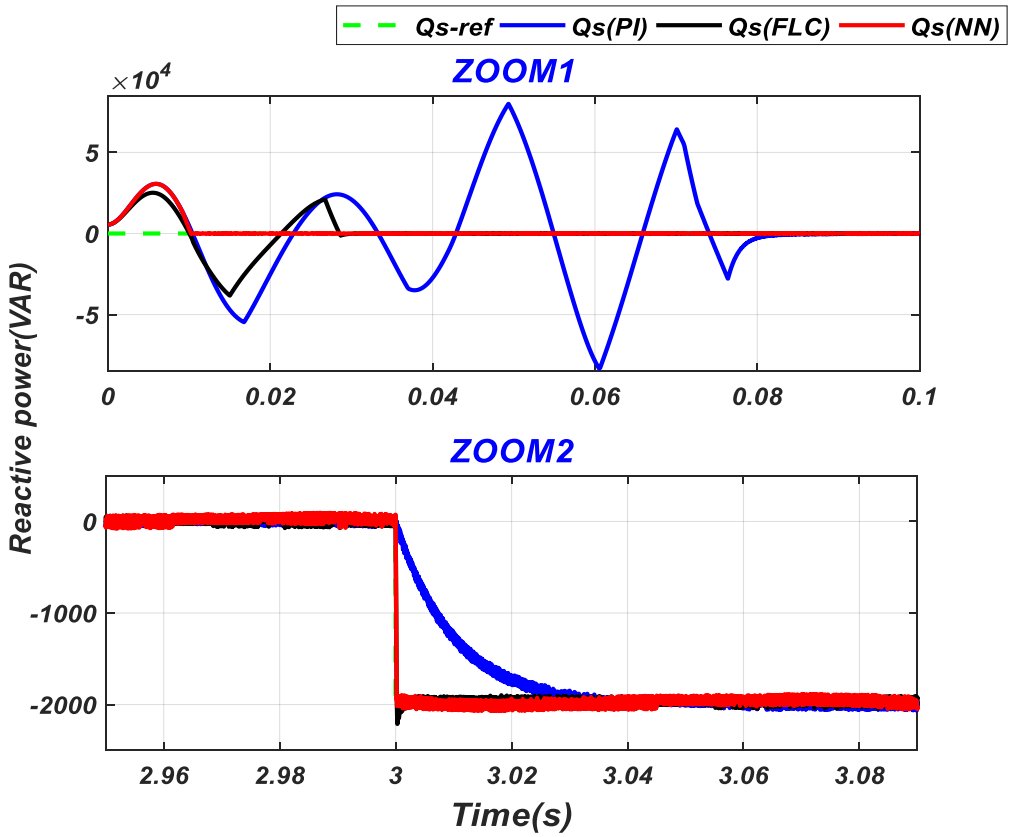

Figure II. 22 Zoom in reactive power behavior.

The dynamic and static performance of the three controllers during normal operation can be succinctly summarized in Tables II.3 and II.4, respectively.

Table II. 3 Performance comparison of the three active power controllers.

Active power			
Controller / Performances	PI	FLC	NN
Rise time(s)	2.9486e-04	2.9206e-04	2.9745e-04
Maximum overshoot (%)	2061.4898	2080.7327	67.3400
Settling time(s)	0.078728	0.034608	0.00923
Conception	Simple	Simple	Medium

Table II. 4 Performance comparison of the three reactive power controllers.

Reactive power			
Controller / Performances	PI	FLC	NN
Rise time(s)	5.2314e-04	6.2824e-04	2.9903
Maximum overshoot (%)	4093.5473	1888.5716	5.8815
Settling time(s)	0.08462	0.03056	0.01022
Conception	Simple	Simple	Medium

- The classical PI controller performs well in tracking active and reactive power, considering rise time, settling time, and peak values.
- However, it exhibits a significant overshoot, indicating an oscillatory response. To mitigate this, controller tuning is necessary.
- Sensitivity to variations in system parameters requires careful attention during implementation and tuning.
- The FLC shows similar performance in terms of rise time, settling time, and peak compared to the PI controller.
- It appears slightly more robust to parameter variations.
- Like the PI controller, it also exhibits a significant overshoot, which may require tuning.
- The NNC demonstrates remarkable performance across rise time, settling time, overshoot, and robustness to parameter variations.
- Notably, it has a low overshoot compared to other controllers.
- However, it does exhibit a noticeable undershoot.

- Overall, the NNC design complexity is moderate.

II.5.1 Robustness test

In this simulation section, our main goal is to evaluate the robustness of the three controllers when faced with varying parameters, specifically the inductances L_s, L_s, and the mutual inductance M. We will compare the performance of these controllers based on criteria such as rise time, maximum peak overshoot, and settling time.

To conduct the robustness assessment, we employed the following approaches:

1. Stator and Rotor Inductance Variation: We intentionally increased the stator and rotor inductances of the DFIG by 25% above their nominal values. Subsequently, we analyzed the system's behavior using the PI, FLC, and NN controllers while these parameters were modified.
2. Mutual Inductance Variation: Conversely, we reduced the mutual inductance of the DFIG by 25% below its nominal value. We then observed how the system responded to this parameter change when controlled by the three different controllers.

Figure II.23 and Table II.5 display the simulation outcomes with a +25% variation in L_s.

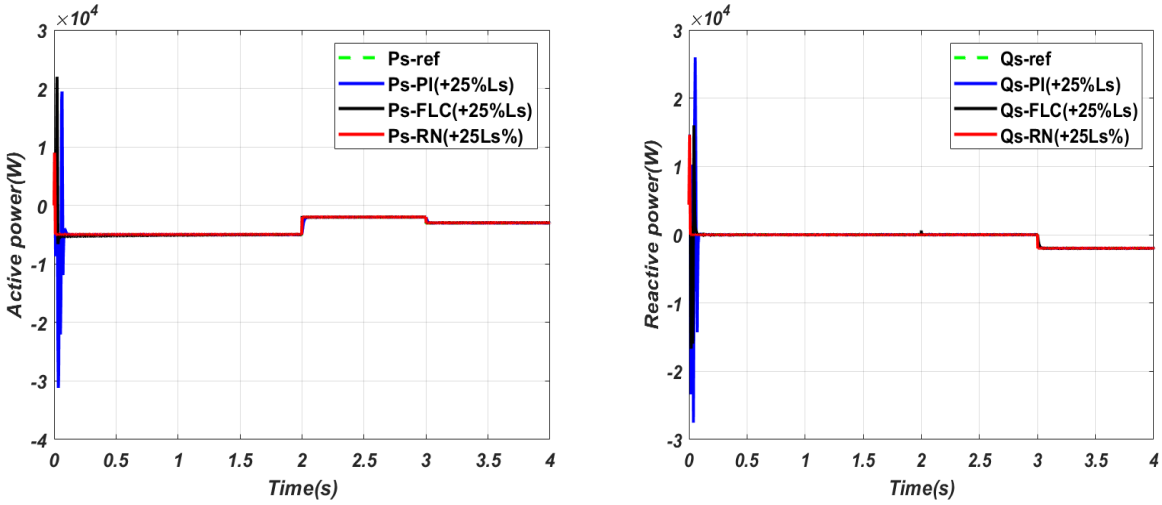

Figure II. 23 Active and reactive power behavior using the three controllers with +25% variation of *Ls.*

Table II. 5 Performance comparison of the three active power controllers with +25% variation of *Ls*.

Active power			
Controller / Performances	PI	FLC	NN
Rise time(s)	7.7744e-4	4.9143e-4	7.7203e-4
Maximum overshoot (%)	941.1434	125.1498	67.6828
Settling time(s)	0.1024	0.04711	0.01036
Reactive power			
Rise time(s)	1.0614e-2	1.5885e-3	2.9891
Maximum overshoot (%)	1279.1335	746.1308	1.1689
Settling time(s)	0.08478	0.06909	0.01213

Figure II.24 and Table II.6 present the simulation results with +25% variation of L_r.

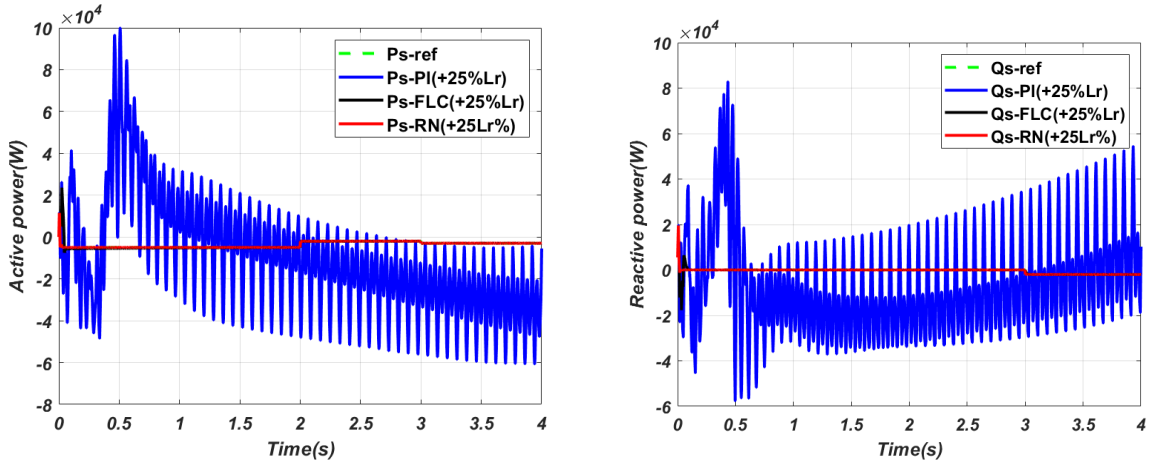

Figure II. 24 Active and reactive power behavior using the three controllers with +25% variation of *Lr*.

Table II. 6 Performance comparison of the three active power controllers with +25% variation of *Lr*.

Active power			
Controller / Performances	**PI**	**FLC**	**NN**
Rise time(s)	1.2407e-3	8.6182e-4	6.4654e-4
Maximum overshoot (%)	1006.3462	153.7652	67.4897
Settling time(s)	unstable	0.05089	0.01193
Reactive power			
Rise time(s)	1.8857e-3	1.8196e-3	2.9884
Maximum overshoot (%)	709.1956	803.1542	0.91166
Settling time(s)	unstable	0.09309	0.01294

Figure II.25 and Table II.7 present the simulation results with -25% variation of M.

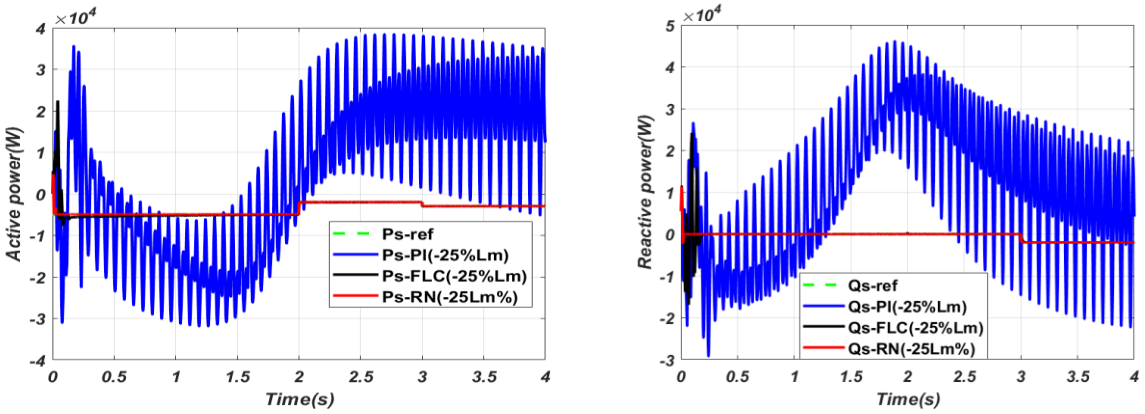

Figure II. 25 Active and reactive power behavior using the three controllers with -25% variation of *M*.

Table II. 7 Performance comparison of the three active power controllers with -25% variation of *M*.

Active power			
Controller / Performances	**PI**	**FLC**	**NN**
Rise time(s)	2.1116e-2	9.1929e-4	1.4402e-3
Maximum overshoot (%)	196.486	159.4129	67.3609
Settling time(s)	unstable	0.809	0.01245
Reactive power			
Rise time(s)	4.1798e-4	6.2902e-3	3.6251e-3
Maximum overshoot (%)	1001.8854	752.9087	16.7727
Settling time(s)	unstable	0.1838	0.02345

Through an examination of the impact of stator/rotor inductance variation and mutual inductance on the dynamics of controllers (PI, FLC, and NN), it becomes evident that both FLC and NN controllers exhibit robustness across different parametric variations (L_s, L_r, and M). However, the PI controller loses its robustness entirely when subjected to a -25% variation in M. Furthermore, the neural controllers outperform the fuzzy controller, particularly in terms of settling time and overshoot.

II.6 Conclusion

This chapter addressed the modeling and control of a variable-speed wind system based on a DFIG directly connected to the electrical grid via the stator and through static three-phase converters using IGBTs on the rotor. The modeling of various components of the wind system was

presented, including the aerodynamic and mechanical models of the turbine. To establish control strategies for both converters, models for the DFIG and the connection of the GSC to the grid via an RL filter were developed. The MPPT control method was examined in detail to extract the maximum available power from the wind. Control schemes for the RSC and GSC were elaborated to ensure independent control of active and reactive powers while optimizing wind turbine operation. These controls were implemented using PI, FLC, and NN controllers.

Finally, simulations were conducted to validate the overall modeling and control of the wind system. The results demonstrated that active and reactive powers of the wind system could be independently controlled while ensuring optimal active power supply to the electrical grid. Furthermore, the NN controller outperformed the PI and FLC controllers in terms of power, efficiency, and robustness, enhancing both the dynamic and static performance of the DFIG.

The robustness of the controllers was also assessed by varying the machine's mutual inductance. Notably, the PI controller was significantly affected by this variation, while the NN controller remained nearly unchanged.

CHAPTER III

Electrical fault diagnosis of the DFIG

III.1 Introduction

DFIGs are essential components of modern wind farms, efficiently converting wind energy into electricity. However, due to their continuous operation in harsh environmental conditions, these machines are prone to various electrical and mechanical faults that can compromise their performance and durability. This chapter examines diagnostic methods for electrical faults in DFIGs primarily used in wind systems. We begin with a thorough analysis of the various types of faults encountered by wind systems, ranging from mechanical issues such as bearing and gear failures to electrical faults including short circuits and phase openings. Next, we explore advanced diagnostic methods used to detect these faults, including model-based techniques and data-driven approaches. Special attention is given to artificial intelligence techniques such as the use of neural networks and fuzzy logic for precise fault detection and localization. We present in this chapter the proposed approach for detecting and locating short circuit and phase opening faults in the stator of a DFIG using fuzzy logic. Finally, we analyze the simulation results to demonstrate their effectiveness in a real operational environment.

III.2 Different Faults of Wind Systems

A wind turbine system is a complex device that converts wind energy into electrical energy. Composed of several components, wind turbines can be subject to malfunctions or faults caused by temporary events or natural aging. These problems can lead to interruptions and economic consequences. Temporary events may include extreme weather conditions, while faults due to aging occur over time. When these problems arise, wind turbines may fail to function properly, resulting in disruptions in electricity production and high repair costs.

To better understand these faults, it is crucial to analyze statistics based on the frequency of faults and their downtime. This approach allows for the identification of the most critical faults for effective predictive maintenance [70]. However, access to this data may be limited by manufacturers, hindering the optimization of wind turbine maintenance [70].

The main components susceptible to faults in wind turbine systems are the electrical system, sensors, blade orientation, and control system. The longest downtimes are generally associated with the control system and the gearbox [19]. Faults are more frequent in the electrical system than in mechanical components such as the gearbox. The number of faults per year of operation increases after the first years, with a relatively constant rate thereafter [71][19].

Generators and power converters are more prone to faults in direct drives than in indirect drives, but less critical than gearbox faults. The electrical system has a significant fault rate in direct drives, exceeding that of the gearbox in indirect drives. Direct-drive generators have a fault rate twice as high as those in indirect drive applications [19].

Below, we outline some common faults that may arise in wind turbine systems due to factors such as environmental conditions, operational stresses, component wear, and manufacturing faults.

Table III. 1 Common faults in wind turbines [72][73][74].

Type of Fault	Origins of Fault
Blade and Rotor Faults	Corrosion, cracks, reduced stiffness, increased surface roughness, deformation of blades, errors in pitch angle, imbalance of rotors
Gearbox Faults	Imbalance and misalignment of shaft, damage to shaft, bearings, and gears, broken shaft, high oil temperature, oil leakage, poor lubrication
Generator Faults	Excessive vibrations, overheating, abnormal noises, insulation damage
Bearing Faults	Overheating, premature wear due to unpredictable stress
Main Shaft Faults	Misalignment, cracks, corrosion, coupling failure
Hydraulic System Faults	Sliding valve blockage, oil leakage
Mechanical Braking System Faults	Hydraulic failures, wind speed exceeding the limit
Tower Faults	Poor quality control during manufacturing, improper installation and loading, harsh environmental conditions
Electrical System/Device Faults	Broken buried metal lines, corrosion or cracks in traces, board delamination, component misalignment, electrical leaks, cold-solder joints
Sensor Faults	Malfunction or physical failure of sensors, malfunction of hardware or communication links, errors in data processing or communication software

These faults can lead to disruptions in system operation, decreased efficiency, and potential safety risks. It is critical to implement robust monitoring, diagnostic, and maintenance strategies to promptly detect and rectify these faults, ensuring the reliable and safe functioning of wind turbine systems.

III.3 Diagnostic Methods on Wind Turbines

The detection and location of faults in wind turbines are achieved through various approaches, including:

- The use of observers to detect faults in rotor and generator angular velocity sensors, as well as to estimate output and adjust detection thresholds [75].

- Model-based methods, such as the use of Coleman transformation and invariant linear time model identification, enabling fault detection using a Kalman filter[77][76].
- Data-based approaches, such as neural networks, for monitoring and fault detection, demonstrating superiority in fault detection compared to other methods [77][78][79].

Regarding fault detection on specific wind turbine components, several studies have focused on:

- Detecting pitch angle sensor faults using piecewise-refined models to generate residual signals [80].
- Detecting speed multiplier faults by extracting fault-related features using wavelets [81].
- Detecting converter faults using an unknown input observer [82].
- Other specific methods are also used to detect defects such as cracks in gears, mechanical brake defects, bearing defects, ...
- Time-frequency analysis-based approaches, such as wavelet transform use, are also used for mechanical and electrical fault monitoring and diagnosis in wind turbines [83]. This method effectively eliminates noise and analyzes non-stationary signals, making it easier to detect various defects in wind turbines.

III.4 Faults in Electric Generators

The asynchronous generator, despite advancements in engineering and materials science, can still have various types of faults. The most common faults in low and medium power generators are stator faults, while mechanical stress-induced faults are more prevalent in high-power generators. Although the DFIG is robust, it can still experience electrical or mechanical faults, which can be caused by various stresses and can lead to structural and functional faults, potentially damaging the machine and causing production losses [84].

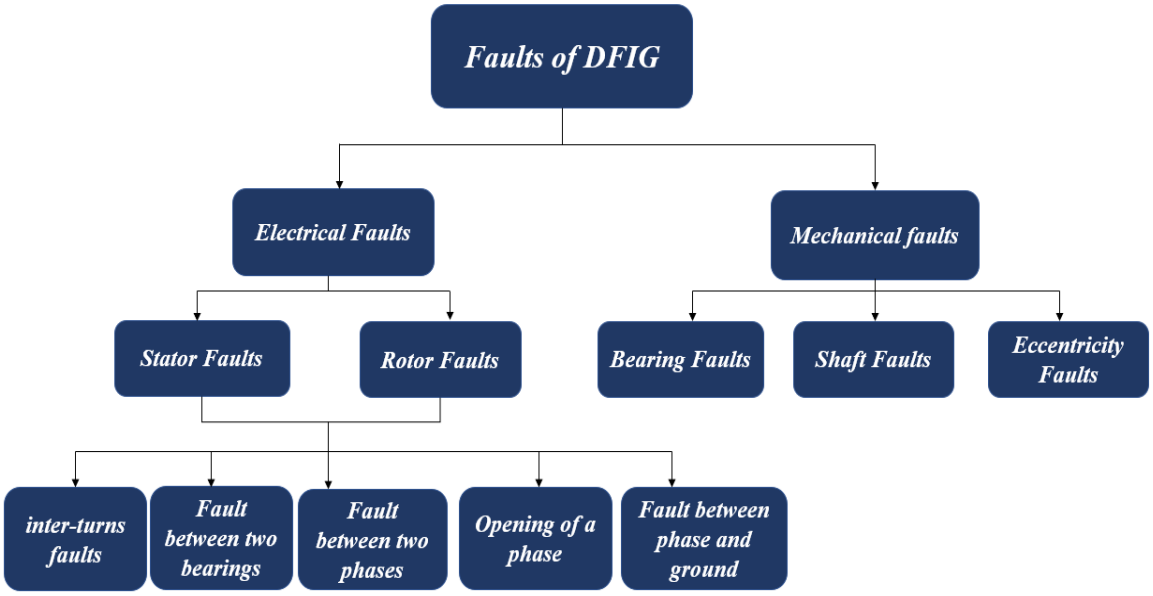

Figure III. 1 The different faults in DFIG.

III.4.1 Electrical faults

The electrical faults of a DFIM can lead to its shutdown and are classified into two categories: those affecting the stator electrical circuits and those affecting the rotor. These faults, such as short circuits between turns of the same phase, can result in an increase in currents in the stator of the affected phase, a slight variation in amplitude on the other phases, a modification of the power factor, and an intensification of currents in the rotor circuit. They can also lead to an increase in temperature at the winding, accelerating the deterioration of the insulators and potentially causing a cascade effect, such as the occurrence of a second short circuit.

Among the short-circuit faults, we find short circuits between the phases of the stator or the rotor, between bearings of the same phase, and between a phase and ground. A short circuit near the power supply between phases can generate very high currents, leading to conductor fusion or triggering of protective devices. Similarly, a short circuit near the neutral between two phases can cause an imbalance without conductor fusion, which may also have a mechanical origin, such as excessive vibrations leading to loosening of bolts or insufficient tightening of a lug at the cable junction, potentially resulting in phase opening.

III.4.2 Mechanical Faults

Mechanical faults in a DFIM are common and can manifest at the level of the ball bearings and the machine shaft. Bearing faults can result from poor material selection during manufacturing, leading to rotation problems and disruptions in the machine's operation. Electrical currents flowing through the bearings can contribute to their deterioration, especially at high speeds.

Shaft faults may be caused by the use of unsuitable materials during construction, potentially leading to cracks and eventually shaft fracture, resulting in irreparable machine shutdown. Corrosive environments can weaken the robustness of the shaft, for example, moisture can cause microcracks and ultimately lead to complete machine failure.

Eccentricity, resulting from rotor displacement relative to the shaft's center of rotation, can cause torque oscillations. Different types of eccentricities, such as static, dynamic, or mixed eccentricity, alter the magnetic and mechanical behavior of the machine, increasing electromagnetic forces in the air gap and causing friction between the stator and rotor, resulting in significant vibrations in the windings.

III.5 Study of Electrical Faults of the DFIG

In this section, we will develop the stator fault model that concerns the malfunctions of induction machines due to short-circuits between the stator windings. Furthermore, the model of the stator phase open-circuit fault.

The short-circuit (SC) inter-turns of the same phase can occur either at the level of the coil heads or inside the winding slots. However, the coil heads are more likely to be affected due to the crossings of the wire bundles. This type of fault leads to a decrease in the effective number of turns in the coil, which can have a significant impact on the operation of the machine.

The short-circuit fault between the turns of the same phase is expressed as a percentage of the total number of short-circuited turns. This means that the severity of the fault is assessed based on the proportion of turns affected by the short-circuit compared to the total number of turns in the winding. This information is essential to diagnose and assess the extent of the damage caused by the SC between the turns, which can help take appropriate corrective measures to ensure the proper operation of the induction machine.

III.5.1 Model of DFIG with SC Fault

In the event of a SC fault in an induction machine, the corresponding voltage and flux equations can be expressed as follows:

$$\begin{cases} [U_s] = [R_s][I_s] + \dfrac{d}{dt}[\varphi_s] \\ [U_r] = [R_r][I_r] + \dfrac{d}{dt}[\varphi_r] \\ 0 = [R_{sci}][I_{sci}] + \dfrac{d}{dt}[\varphi_{sci}] \end{cases} \quad \text{(III. 1)}$$

With;

$$\begin{bmatrix} \varphi_s \\ \varphi_r \\ \varphi_{sci} \end{bmatrix} = \begin{bmatrix} L_{ss} & M_{sr} & L_{ssc} \\ M_{sr} & L_{rr} & L_{rsc} \\ L_{ssc} & L_{rsc} & L_{sci} \end{bmatrix} \begin{bmatrix} I_s \\ I_r \\ I_{sci} \end{bmatrix} \quad \text{(III. 2)}$$

Where;

φ_{sci}: flux of the phase shorted-circuit;

I_{sci}: current of the short-circuit phase;

L_{ssc}: mutual inductance between a stator phase and SC winding;

L_{rsc}: mutual inductance between a rotor phase and SC winding;

R_{sci}: resistance related to the short circuit coil.

In the case of a stator circuit current fault, the inductance of the SC winding can be modeled by considering both the stator and rotor phases [85]:

$$L_{sci} = \eta_{sci}{}^2(M + l_i) \quad \text{(III. 3)}$$

Using the equation below, we can establish the relationship between the number of turns affected by short-circuits N_{sci} and the number of turns in the healthy phase N_i:

$$\eta_{sci} = \frac{N_{sci}}{N_i} \quad \text{(III. 4)}$$

Upon transforming the three-phase system into a two-phase system (α_s, β_s), the voltage and flux equations undergo corresponding modifications and can be expressed in relation to the new two-phase variables as follows:

$$\begin{cases} \underline{U}_{\alpha\beta s} = R_s \underline{I}_{\alpha\beta s} + \dfrac{d}{dt}\underline{\varphi}_{\alpha\beta s} \\ \underline{U}_{\alpha\beta r} = R_r \underline{I}_{\alpha\beta r} + \dfrac{d}{dt}\underline{\varphi}_{\alpha\beta r} - \omega P\left(\dfrac{\pi}{2}\right)\underline{\varphi}_{\alpha\beta r} \\ \underline{0} = \eta_{sci} R_i \underline{I}_{\alpha\beta i} + \dfrac{d}{dt}\underline{\varphi}_{\alpha\beta sc-i} \end{cases} \quad \text{(III. 5)}$$

$$\begin{cases} \underline{\varphi}_{\alpha\beta s} = \underline{\varphi}_{\alpha\beta f_s} + \underline{\varphi}_{\alpha\beta m} = l_s.\underline{I}_{\alpha\beta s} + M\left(\underline{I}_{\alpha\beta s} + \underline{I}_{\alpha\beta r} - \underline{I}_{\alpha\beta sc}\right) \\ \underline{\varphi}_{\alpha\beta r} = \underline{\varphi}_{\alpha\beta f_r} + \underline{\varphi}_{\alpha\beta m} = l_r.\underline{I}_{\alpha\beta r} + M\left(\underline{I}_{\alpha\beta s} + \underline{I}_{\alpha\beta r} - \underline{I}_{\alpha\beta sc}\right) \\ \underline{\varphi}_{\alpha\beta sc_i} = \eta_{sci}.\delta.(\theta_{sc}).\underline{\varphi}_{\alpha\beta m} \end{cases} \quad \text{(III. 6)}$$

With; $\delta.(\theta_{sc}) = \begin{bmatrix} cos^2(\theta_{sc}) & \cos(\theta_{sc})\sin(\theta_{sc}) \\ \cos(\theta_{sc})\sin(\theta_{sc}) & cos^2(\theta_{sc}) \end{bmatrix}$

$$\begin{cases} \underline{\tilde{I}}_{\alpha\beta sc_i} = \sqrt{\frac{3}{2}}\eta_{isc}\underline{I}_{\alpha\beta sc_i} \\ \underline{\tilde{\varphi}}_{\alpha\beta sc_i} = \sqrt{\frac{3}{2}}\eta_{isc}\underline{\varphi}_{\alpha\beta sc_i} \end{cases} \quad \text{(III. 7)}$$

$\underline{\varphi}_{\alpha\beta m}$: the common magnetizing flux;

$\underline{\varphi}_{\alpha\beta f\_s}$, $\underline{\varphi}_{\alpha\beta f\_r}$: stator and rotor leakage flux, respectively.

The line currents are determined by combining the SC currents with the currents accounted for by the conventional Concordia model. This combined total represents the overall line currents. Through this approach, it becomes feasible to derive the winding equation for the faulty component with respect to the stator reference [85]:

$$\underline{\tilde{I}}_{\alpha\beta sc_i} = \frac{2}{3}\frac{\eta_{scs}}{R_s}\delta.(\theta_{sc}).\underline{U}_{\alpha\beta s} \quad \text{(III. 8)}$$

III.5.2 Stator Phase Open Fault of The DFIG Model

The faults of open circuits (OC) in the stator or rotor phases can have various origins [86]. These faults result in the cancellation of current in the damaged phase, lead to an imbalance of currents in the other phases, and cause significant fluctuations in torque. Their consequences are less severe than those of a SC because they do not pose the risk of overheating that could lead to a sudden machine failure. However, these faults disrupt the operation of the generator in the mode of supplying electrical energy [84]. In the event of a phase "a" open fault, the DFIG stator and rotor voltages become unbalanced. The voltages and fluxes are then represented by the following equations:

$$\begin{cases} [U_s] = [R_s^{def\_o}][I_s] + \frac{d}{dt}[\varphi_s] \\ [U_r] = [R_r][I_r] + \frac{d}{dt}[\varphi_r] \end{cases} \quad \text{(III. 9)}$$

$$\begin{cases} [\varphi_s] = [L_{ss}^{def\_o}][I_s] + [M_{sr}^{def\_o}][I_r] \\ [\varphi_r] = [L_{rr}][I_r] + [M_{rs}^{def\_o}][I_s] \end{cases} \quad \text{(III. 10)}$$

Where; $R_s^{def\_o} = \begin{bmatrix} 0 & 0 & 0 \\ 0 & R_s & 0 \\ 0 & 0 & R_s \end{bmatrix}$; $L_{ss}^{def\_o} = \begin{bmatrix} 0 & -\frac{1}{2}M_s & -\frac{1}{2}M_s \\ 0 & l_s + M_s & -\frac{1}{2}M_s \\ 0 & -\frac{1}{2}M_s & l_s + M_s \end{bmatrix}$

$$L_{sr}^{def\_o} = M_s = \begin{bmatrix} 0 & 0 & 0 \\ \sin(\theta_r + \frac{2\pi}{3}) & sin\theta_r & \sin(\theta_r - \frac{2\pi}{3}) \\ \sin(\theta_r - \frac{2\pi}{3}) & \sin(\theta_r + \frac{2\pi}{3}) & sin\theta_r \end{bmatrix}$$

$$L_{rs}^{def\_o} = M_s = \begin{bmatrix} 0 & \sin(\theta_r + \frac{2\pi}{3}) & \sin(\theta_r - \frac{2\pi}{3}) \\ 0 & sin\theta_r & \sin(\theta_r + \frac{2\pi}{3}) \\ 0 & \sin(\theta_r - \frac{2\pi}{3}) & sin\theta_r \end{bmatrix}$$

With;

$R_s^{def\_o}$: fault stator resistance;

$L_{ss}^{def\_o}$: fault stator inductance;

$L_{sr}^{def\_o}$: stator-rotor mutual fault inductance;

$L_{rs}^{def\_o}$: rotor-stator mutual fault inductance.

III.6 Diagnosis By Fuzzy Logic

Monitoring and diagnostic techniques for energy conversion systems are widely used to prevent unexpected shutdowns of these systems. These techniques were initially developed from traditional methods and have since evolved to incorporate AI techniques, including fuzzy logic, artificial neural networks, and combined structure techniques. Compared to conventional fault diagnostic approaches, these artificial intelligence-based techniques offer numerous advantages [87][88].

In this section, we will introduce a methodology based on fuzzy logic for monitoring the DFIG condition. This methodology enables the detection of short-circuit or open-phase faults in the stator windings, as well as the detection and localization of these types of faults.

III.6.1 Stator Fault Detection Using Fuzzy Logic

In order to evaluate the condition of the DFIG stator, a compositional rule based on fuzzy logic is employed and managed by a fuzzy interference block. A monitoring system is proposed to implement this diagnostic approach, with its architecture illustrated in Figure III.2.

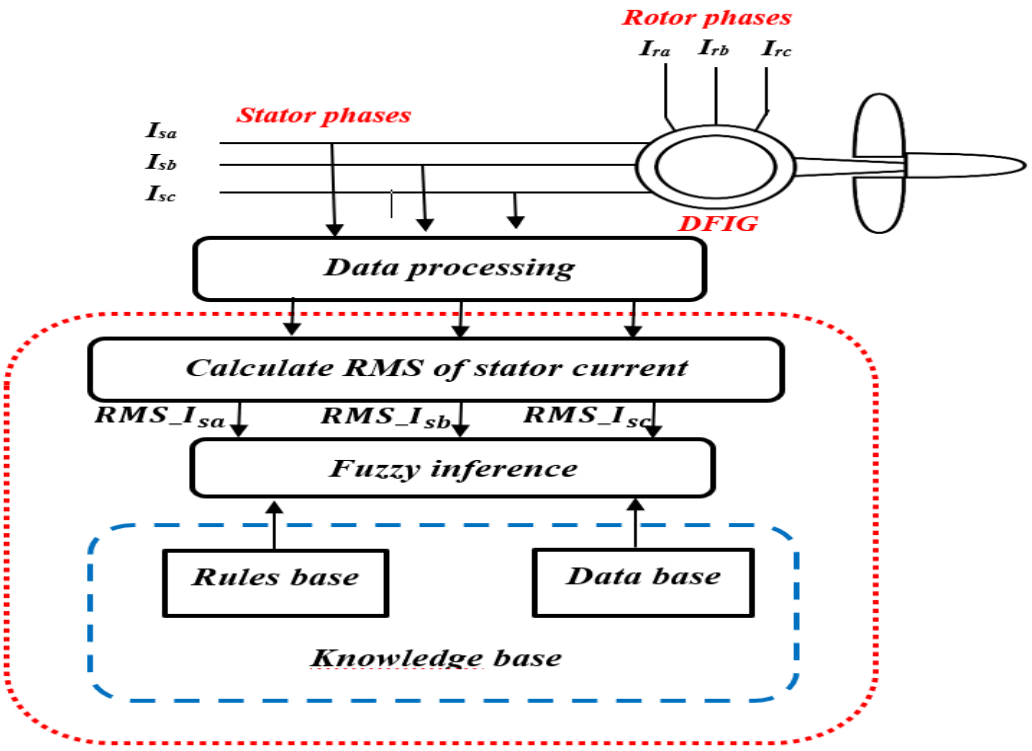

Figure III. 2 Fault monitoring and detection system.

In the proposed diagnostic methodology, the amplitudes of the stator currents (Ias, Ibs, and Ics) and the stator's condition (CM) are chosen as input membership functions and outputs of the fuzzy system. These variables are defined using fuzzy set theory and play a crucial role in the analysis process. The stator's condition is expressed as a linguistic variable in the CM, with values like "Healthy, Short-circuit, Critical short circuit and Open-phase" as shown in Figure III.3. Furthermore, the input variables Ias, Ibs, and Ics are also treated as linguistic variables, with values such as "Very-small, Small, Medium, and Big" as depicted in Figure III.4.

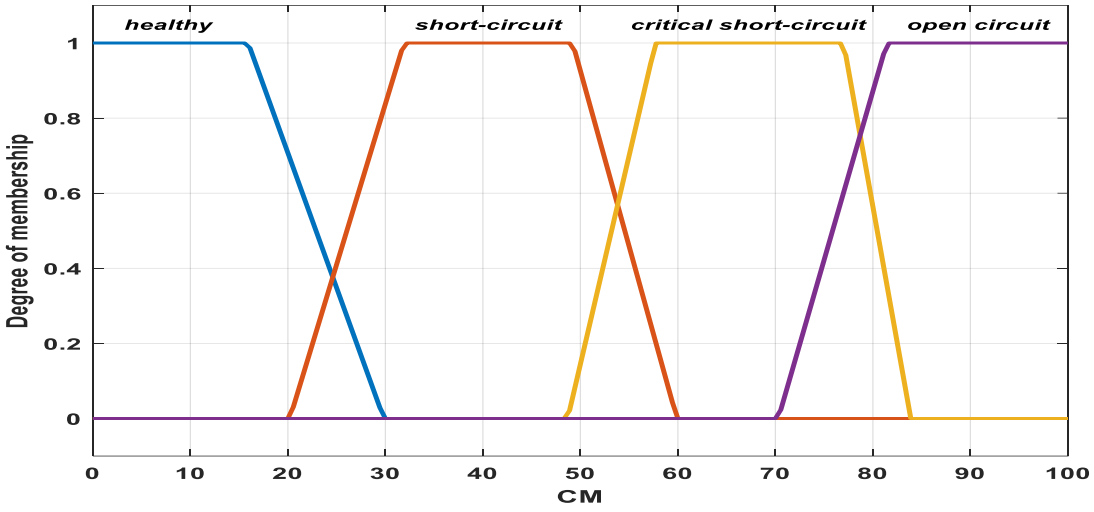

Figure III. 3 Membership functions for output variables.

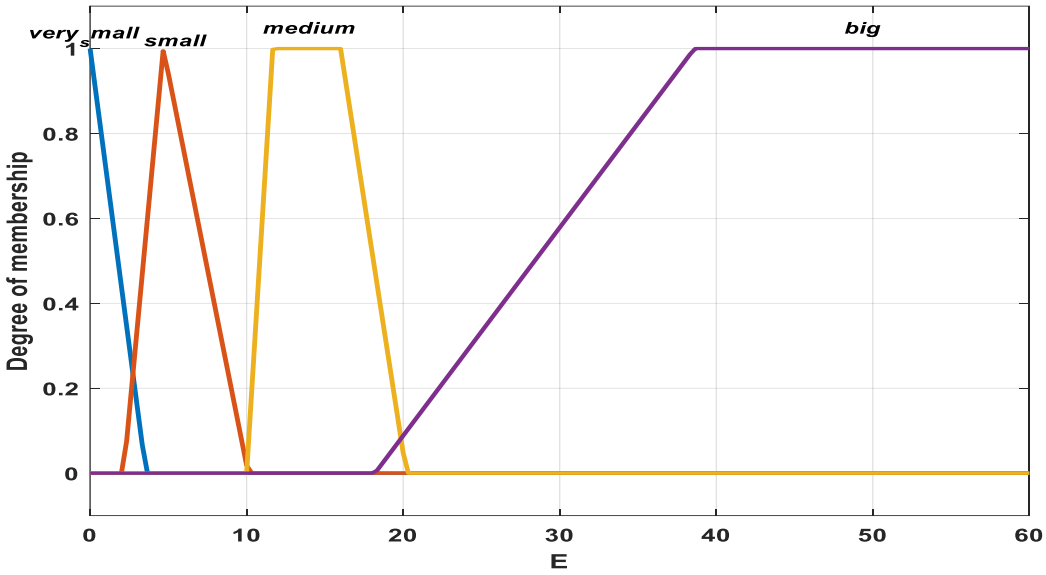

Figure III. 4 Membership functions for input variables.

The fuzzy rules for membership functions are developed using the entire dataset presented in Table III.2 A total of fourteen rules are applied, incorporating both input and output membership functions. These rules are defined as follows:

Table III. 2 Fuzzy rules of the membership functions (Detection Cas).

Rules		I_{as}		I_{bs}		I_{cs}		CM
1		very-small						OC
2				very-small				OC
3						very-small		OC
4		big						Critical SC
5				big				Critical SC
6	If		***And***		***And***	big	***Then***	Critical SC
7		small		small		small		Healthy
8		medium		medium		medium		Healthy
9		small		small		medium		SC
10		Small		medium		medium		SC
11		medium		small		medium		SC
12		small		medium		small		SC
13		medium		small		small		SC
14		medium		medium		small		SC

III.6.1.1 Simulation Results (Detection Cas)

A. Characteristics Under Normal Operating Conditions (Healthy Case)

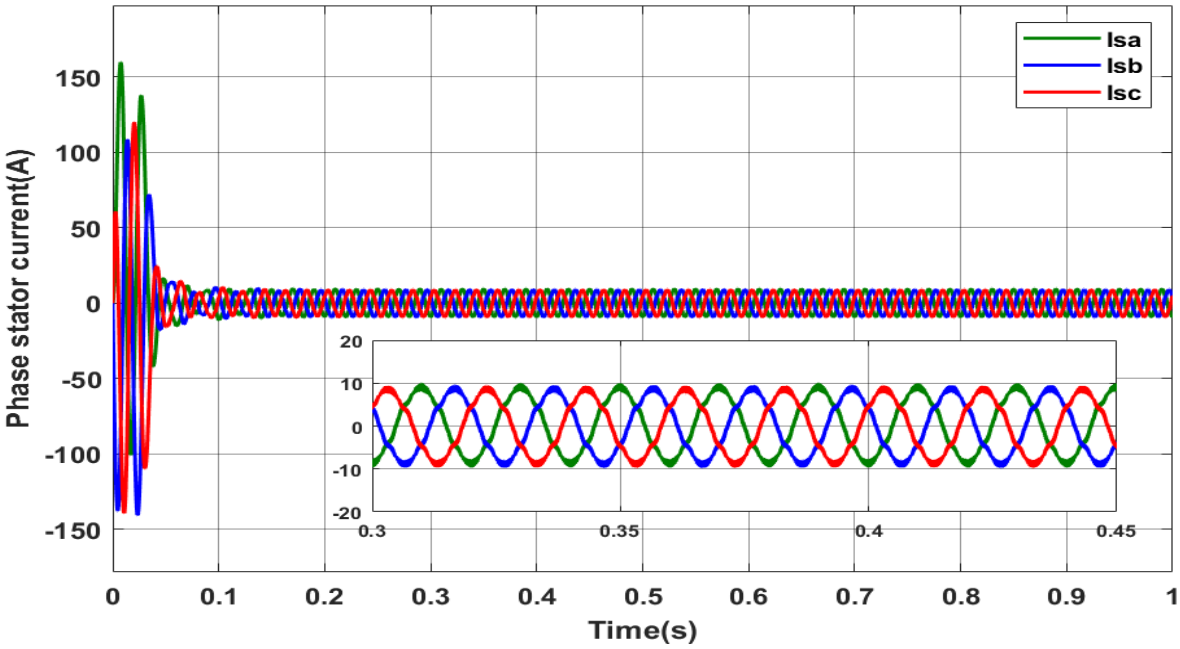

Figure III. 5 The curve of the stator current (Detection Cas).

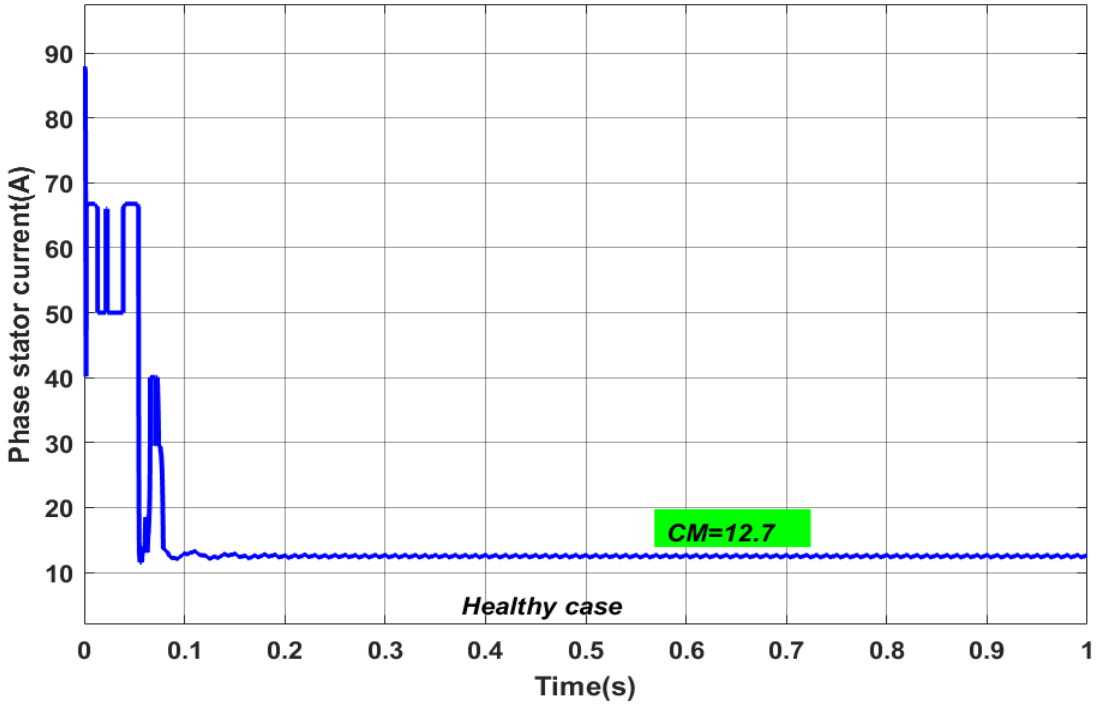

Figure III. 6 Fuzzy output values (Detection Cas).

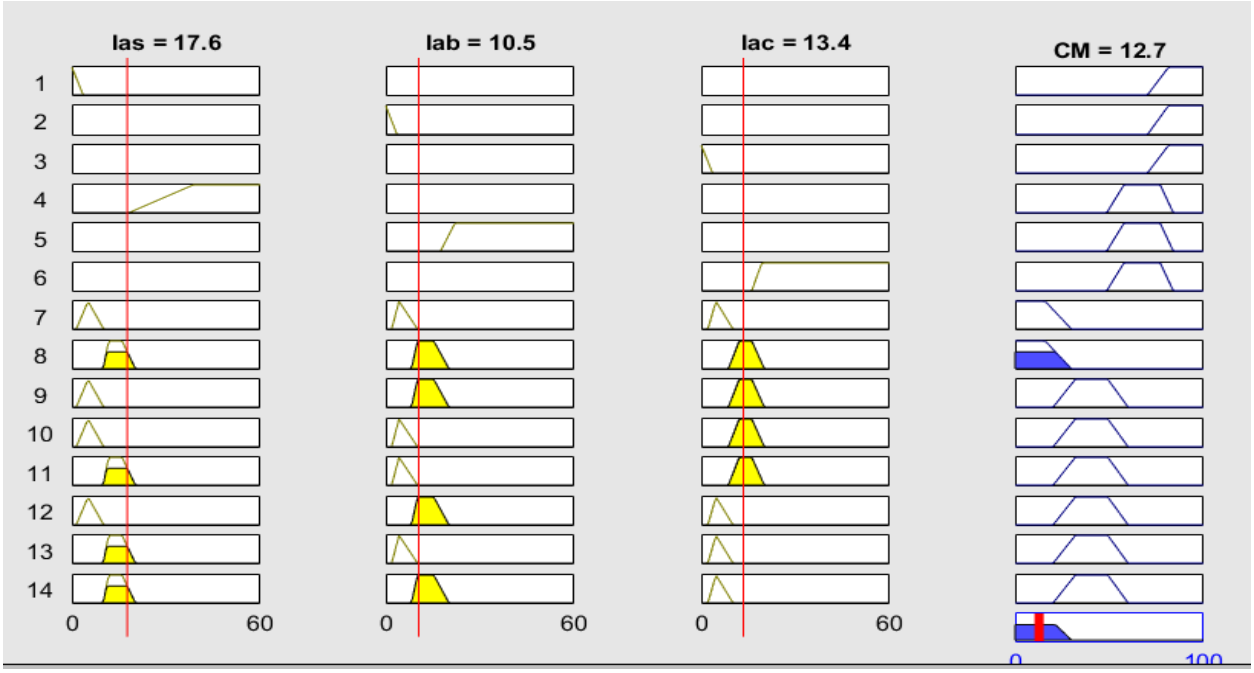

Figure III. 7 Fuzzy inference diagram (Detection Cas).

B. DFIG Characteristics Under Open Phase Conditions

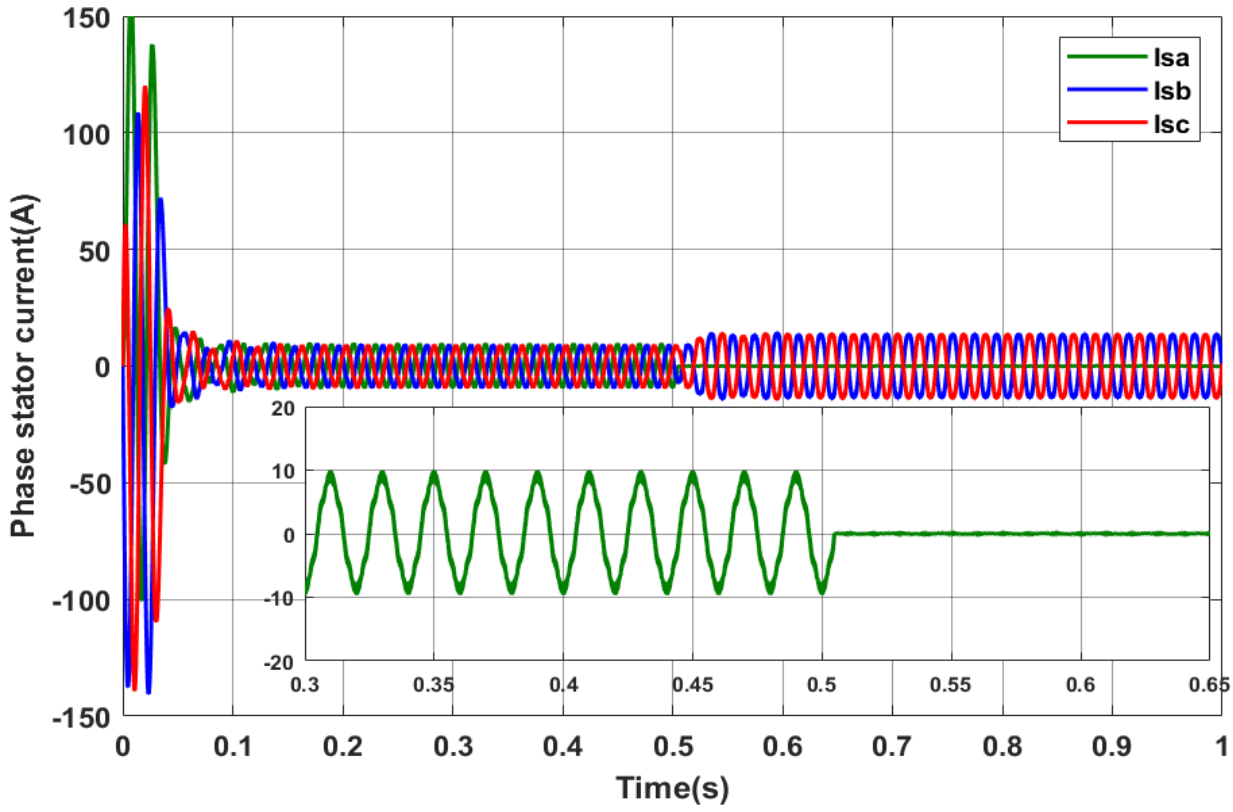

Figure III. 8 The curve of the stator current (Detection Cas).

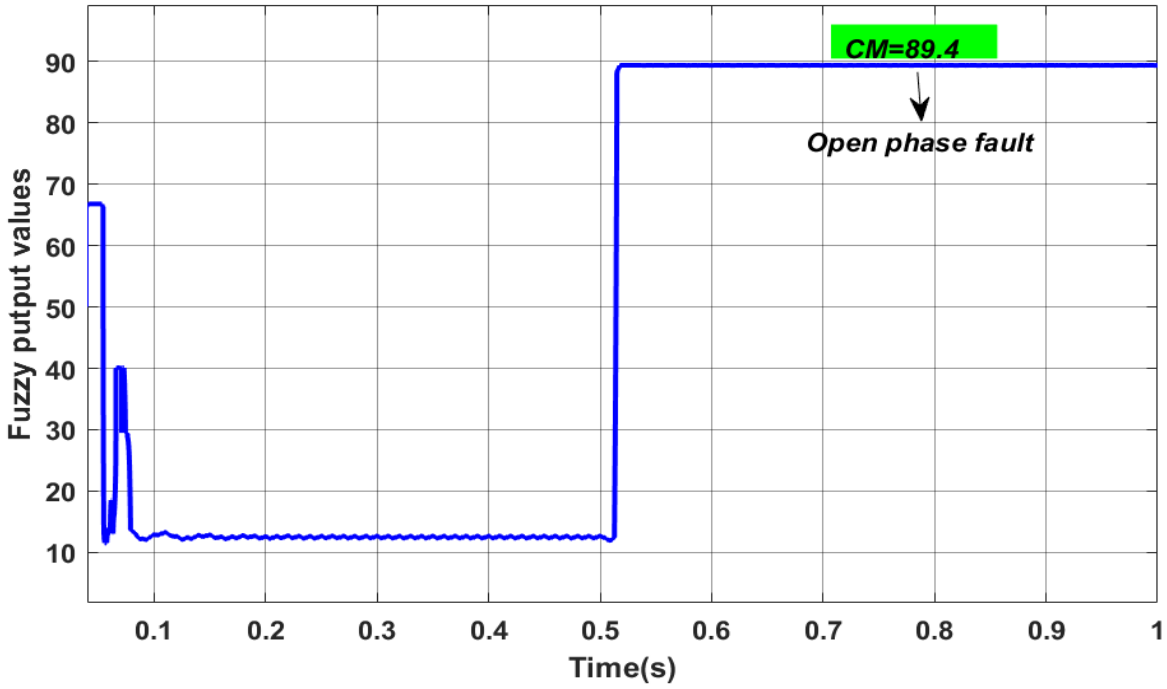

Figure III. 9 Fuzzy output values (Detection Cas).

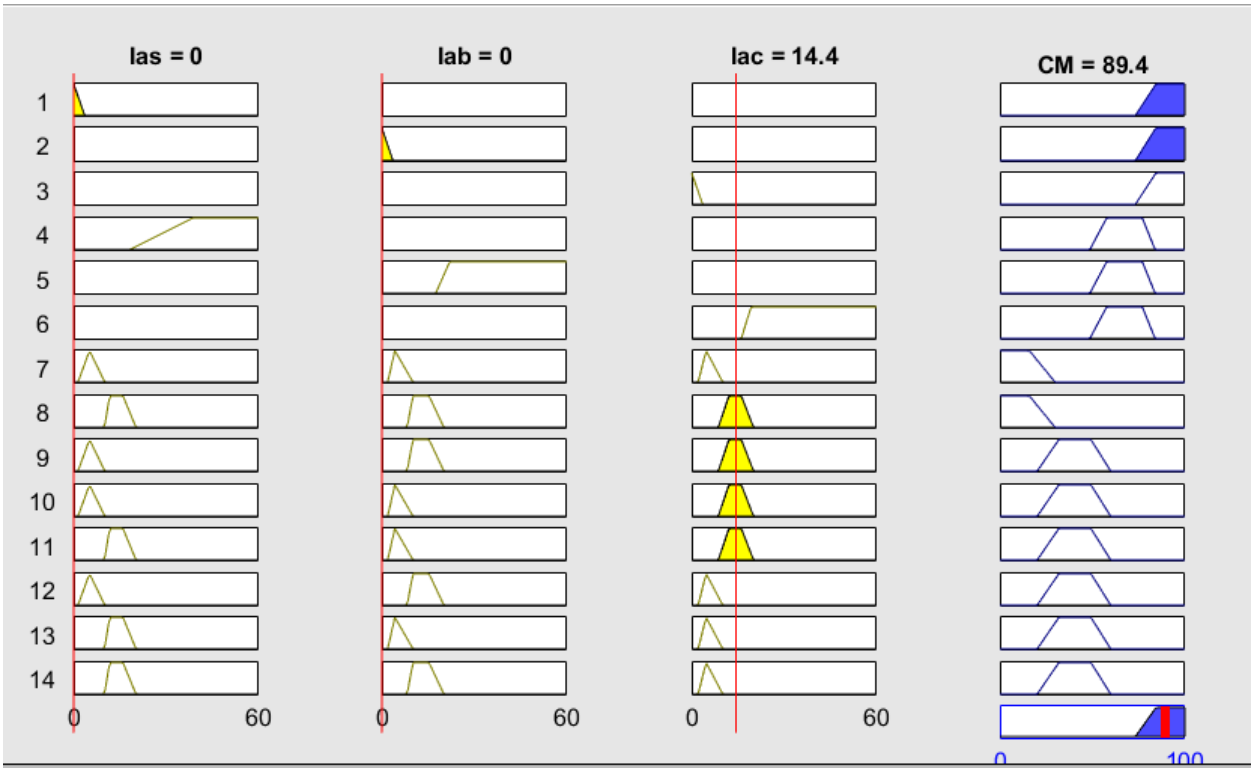

Figure III. 10 Fuzzy inference diagram (Detection Cas).

C. DFIG Characteristics Under Short-Circuit Conditions

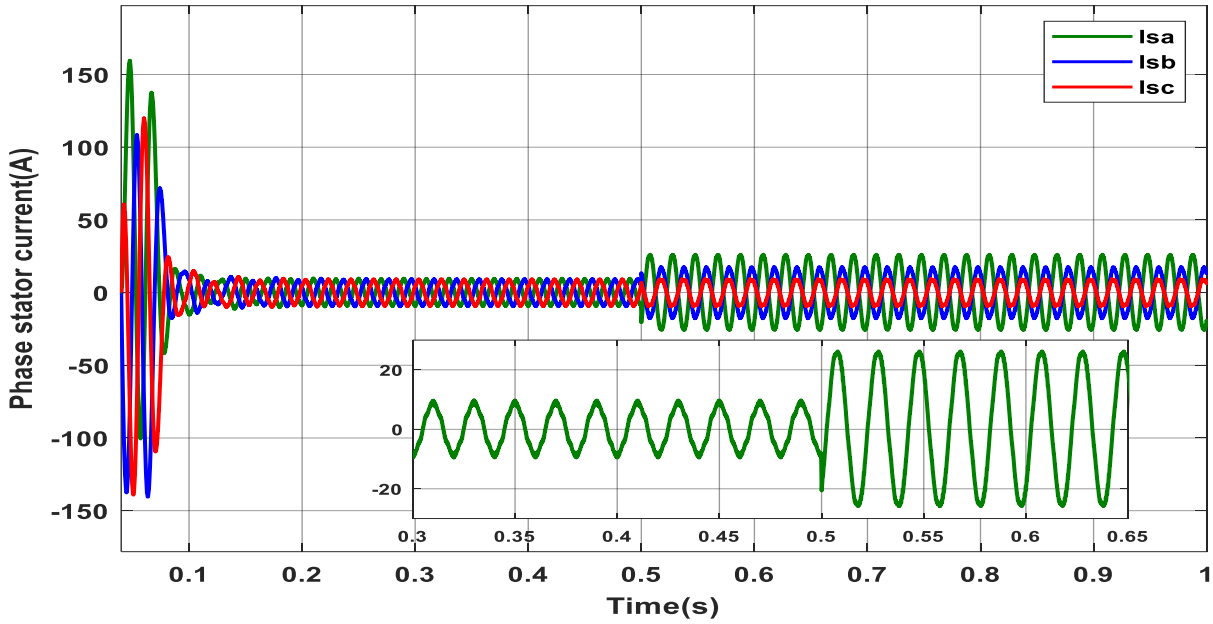

Figure III. 11 The curve of the stator current (Detection Cas).

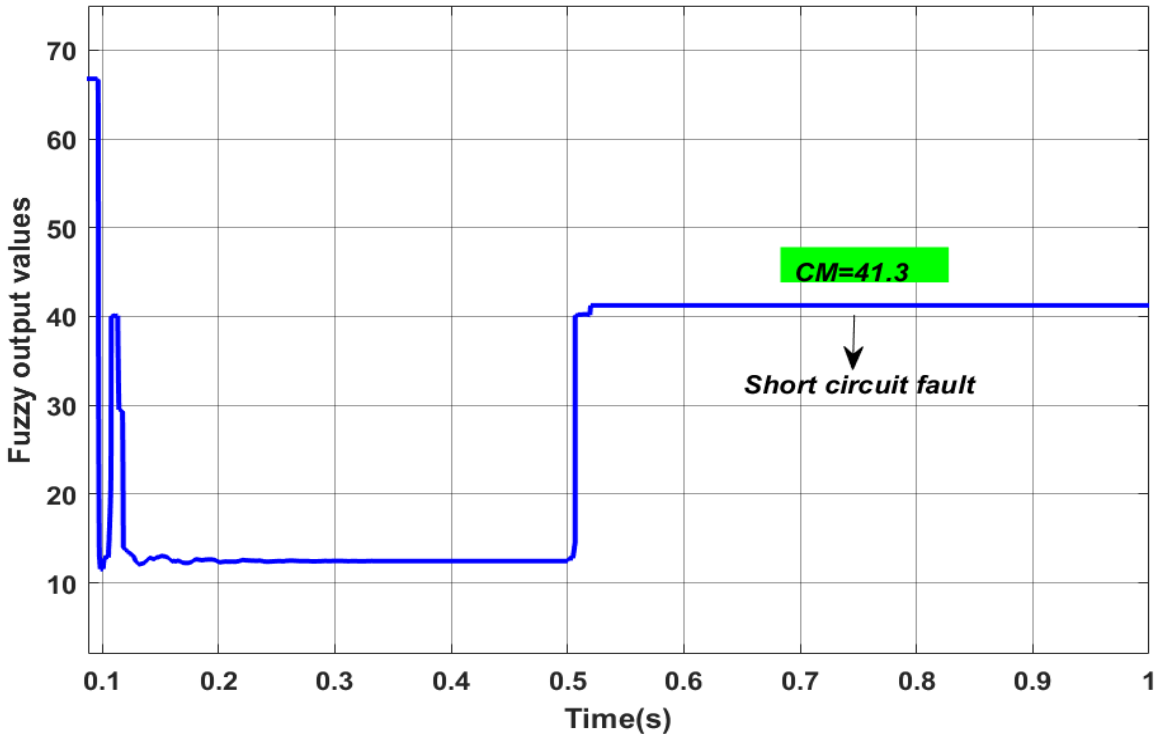

Figure III. 12 Fuzzy output values (Detection Cas).

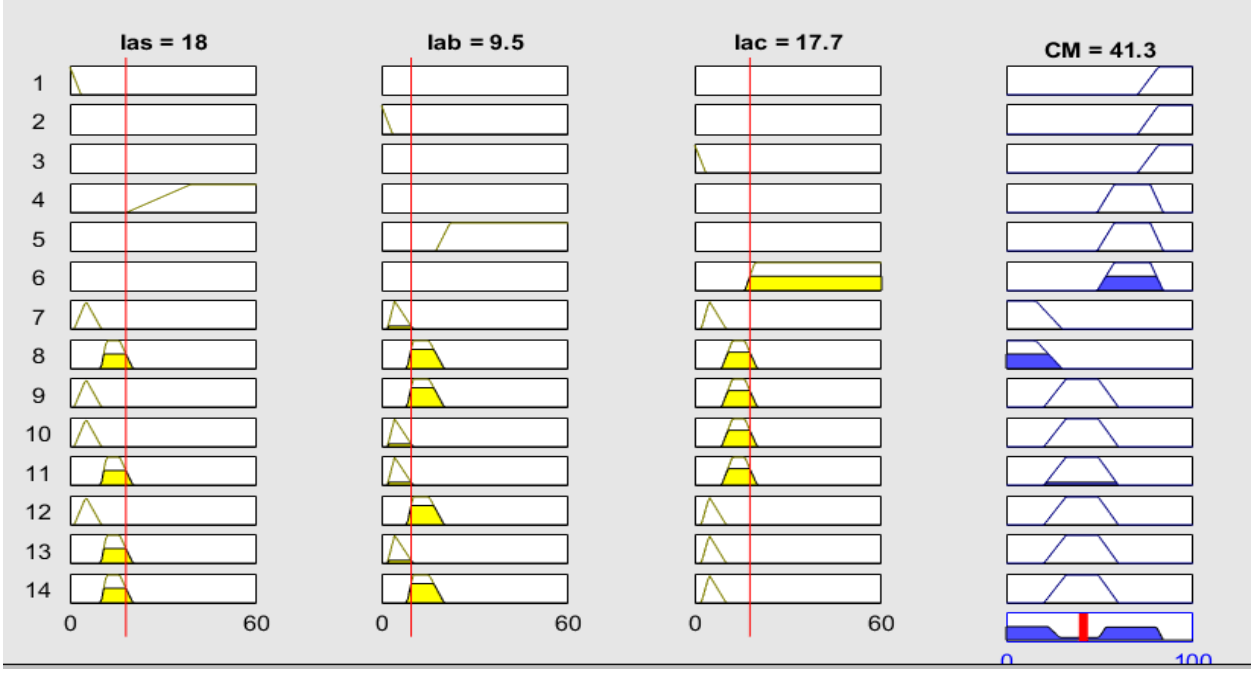

Figure III. 13 Fuzzy inference diagram (Detection Cas).

D. DFIG Characteristics Under Critical Short-Circuit Conditions

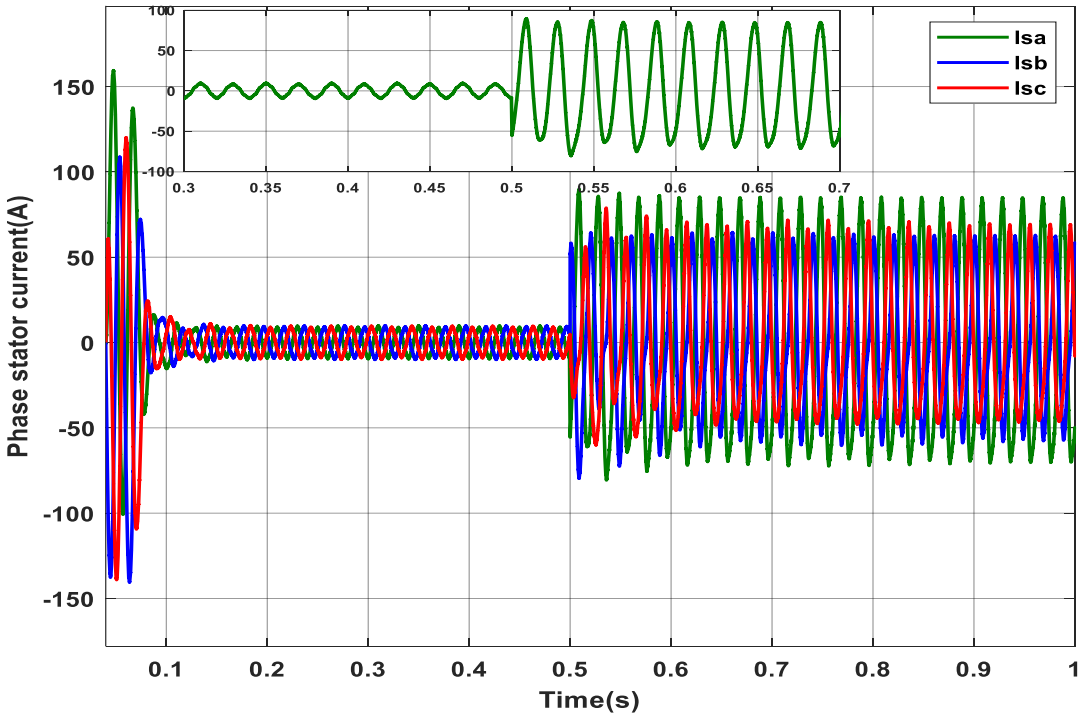

Figure III. 14 The curve of the stator current (Detection Cas).

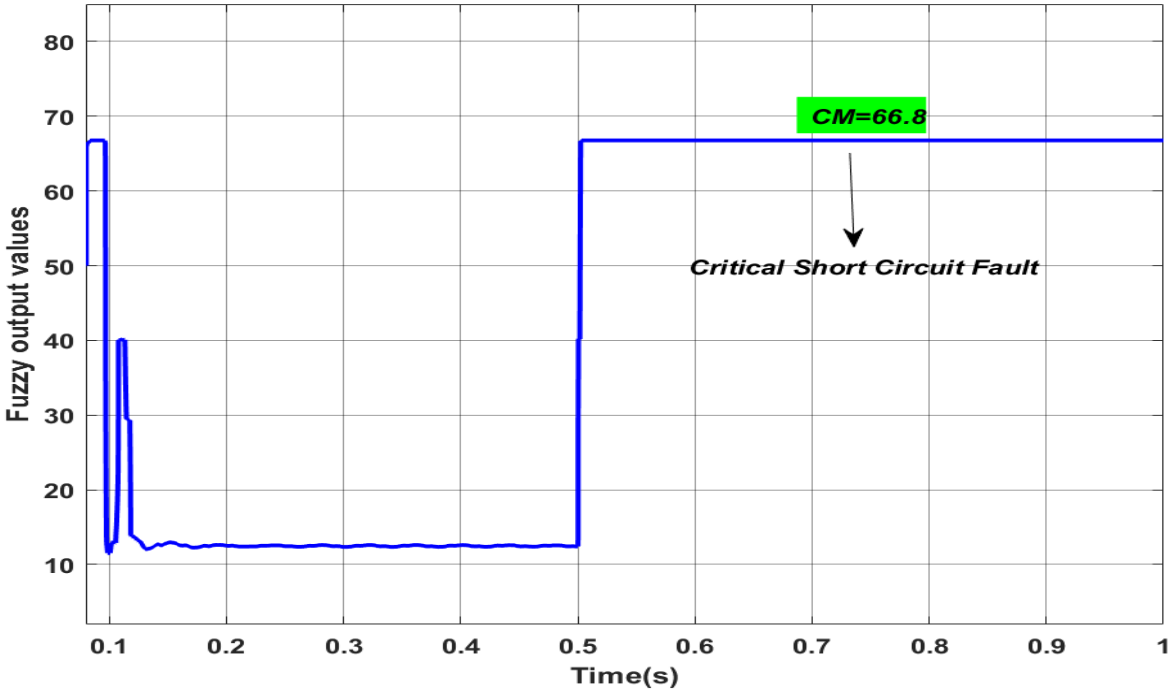

Figure III. 15 Fuzzy output values (Detection Cas).

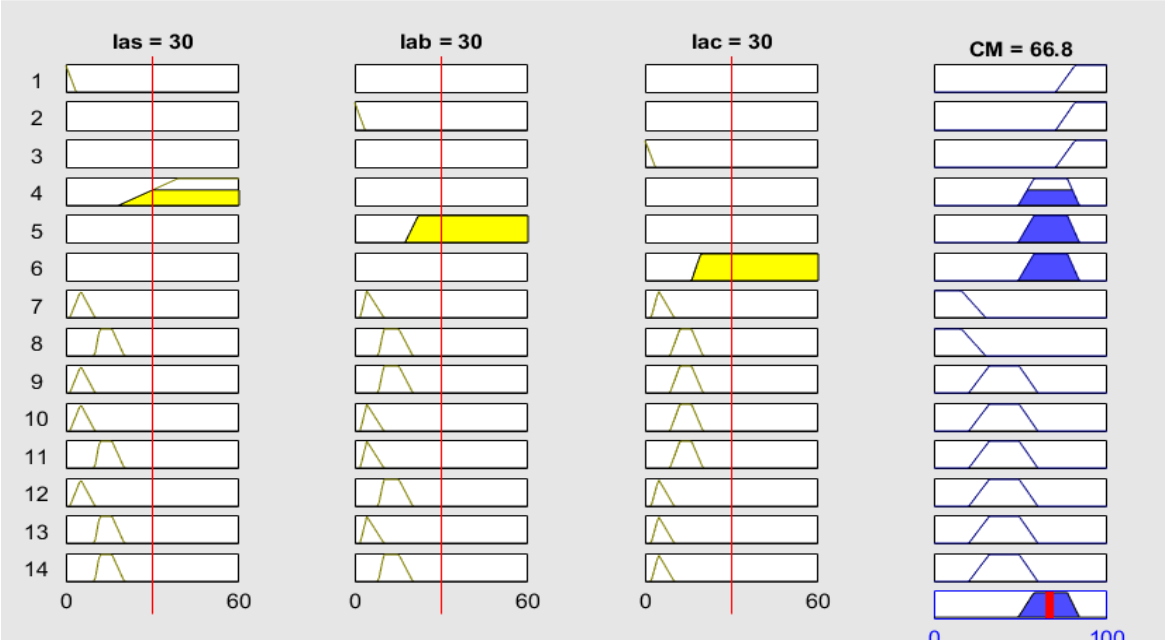

Figure III. 16 Fuzzy inference diagram (Detection Cas).

- Figure III.5 illustrates the stator phase currents with a zoom on the section where the operation is in a steady state. This clearly indicates that the current is balanced.

- Figure III.6 depicts the output fuzzy value, reflecting the decision taken, falling within the CM range of healthy [0 30], denoting the boundaries of a healthy state. Furthermore, Figure III.7 showcases the fuzzy inference system for the current phases.
- Figures III.8 until III.16 illustrate the same parameters under different scenarios.
- Figure III.8,III.9 and III.10 displays the parameters when the generator has an open circuit in phase (a) a stator, while Figure III.11, III.12 and III.13 presents the parameters in the event of a SC with 10% of turns occurring in the same phase. Additionally, Figure III.14, III.15 and III.16 showcases the parameters when critical SC faults with 35% of turns occur in the same phase.
- Observing figures III.8, III.11, and III.14, it is notable that a stator short circuit or a phase opening fault leads to an imbalance in the generator's stator currents and a significant increase in the amplitudes of the three stator phase currents, even if the fault is only present in phase "a".
- Expanding on this, an open stator phase results in suppressed current, significantly affecting the generator's performance. Conversely, in the case of a short circuit, the current amplitude rises in correlation with the number of stator turns affected by the short circuit. Hence, precise detection and diagnosis of these faults are crucial for maintaining the DFIG's optimal operation.
- Figures (III.9) ,(III.12) and (III.15) outline the criteria used to detect these faults. In the scenario of an open stator phase, the criterion is defined as CM = {open circuit [60 100]}. This signifies that if the current amplitude in the affected phase falls between 60% and 100% of the nominal current amplitude, an open phase fault is identified. Similarly, in the case of a short circuit involving 10% of the windings, the criterion is CM = {short circuit [20 60]}. This indicates that if the current amplitude in the affected phase ranges from 20% to 60% of the nominal current amplitude, a short circuit fault is detected. For critical short circuit faults involving 35% of the turns, the decision criterion is CM = {critical short circuit [50 85]}.
- The reliability of the current phase-related approach is confirmed through the fuzzy inference diagrams illustrated in Figures III.10, III.13, and III.16. These tests validate the methodology, demonstrating its reliability and applicability. Moreover, to showcase the effectiveness of our approach in detecting and monitoring the state of the DFIG stator, even

in the presence of open or short-circuit phase faults in other phases (b and c), we investigated a 10% and 35% fault in the short circuit of the turn and the opening fault of phases "b" and "c."

III.6.2 Stator Fault Detection and Localization Using Fuzzy Logic

The system for detecting and locating short-circuit or phase opening faults at the stator level maintains the same basic principle as the previous methodology but incorporates a second membership function for the input variables. This precision function aims to pinpoint the faulty stator phase. Thus, the input precision variables (Delta_E1, Delta_E2, and Delta_E3) are interpreted as linguistic variables, with categories such as Negative(N), Zero (Z), and Positive(P), as illustrated in Figure III.17.

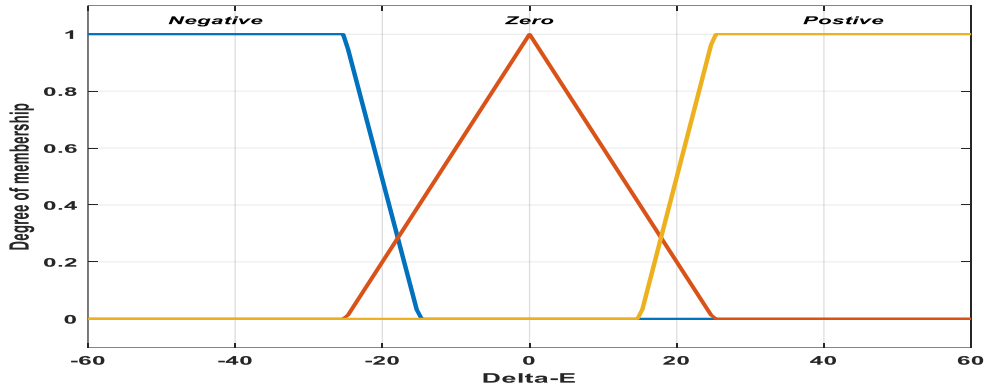

Figure III. 17 Membership functions of input precision variables.

The membership functions of the output variables in this case are shown in Figure III.18, with values such as: "Healthy, OC-A, OC-B, OC-A, CSC-A, CSC-B, CSC-C, SC-A, SC-B, SC-C."

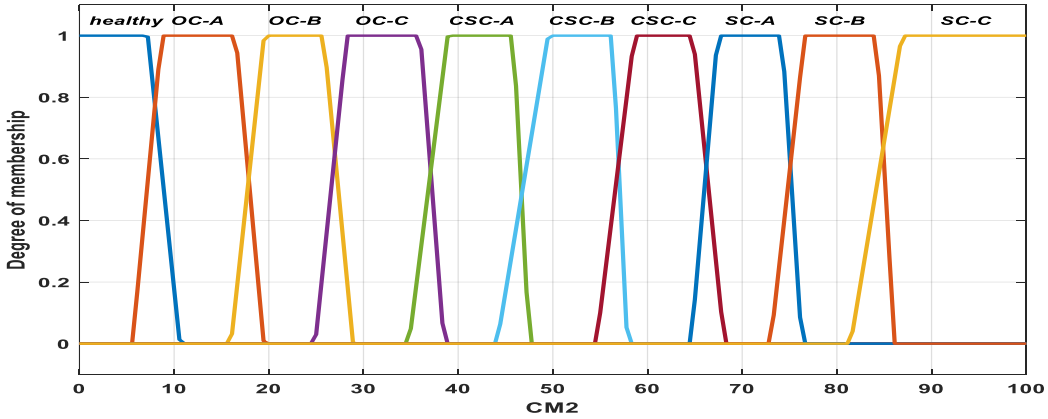

Figure III. 18 Membership functions of output variables.

The fuzzy rules for the membership functions used in localizing stator phase faults are determined from the data provided in Table III.3. A set of 17 rules is applied, integrating the membership functions of two inputs and one output, and they are defined as follows:

Table III. 3 Fuzzy rules of the membership functions (Detection and Localization Cas).

Rules		I_{as}		I_{bs}		I_{cs}		Delta E1		Delta E2		DeltaE3		CM
1		very-small												OC-A
2				very-small										OC-B
3	If		***And***		***And***	very-small	If		***And***		***And***		***Then***	OC-C
4		big												CSC-A
5				big										CSC-B
6						big								CSC-C
7		small		small		small		Z		Z		Z		Healthy
8		medium		medium		medium		Z		Z		Z		Healthy
9		small		small		medium								SC-C
10		Small		medium		medium						P		SC-B
11		Small		medium		medium						N		SC-C
12		medium		Small		medium				P				SC-A
13		medium		small		medium				N				SC-C
14		Small		medium		small								SC-B
15		medium		Small		Small								SC-A
16		medium		medium		Small		P						SC-A
17		medium		medium		Small		N						SC-B

III.6.2.1 Simulation Results (Detection and Localization Cas)

Figures III.19, III.20, III.21, III.22,III.23 and III.24 illustrate the results of the test for detecting and locating faults in the stator phases, specifically the open phase fault of phase C, the short-circuit fault of phase A, and the critical short-circuit fault of phase B. This methodology enables the detection and localization of faults in any stator phase.

A. Case of Open-Circuit Fault in Stator Phase C

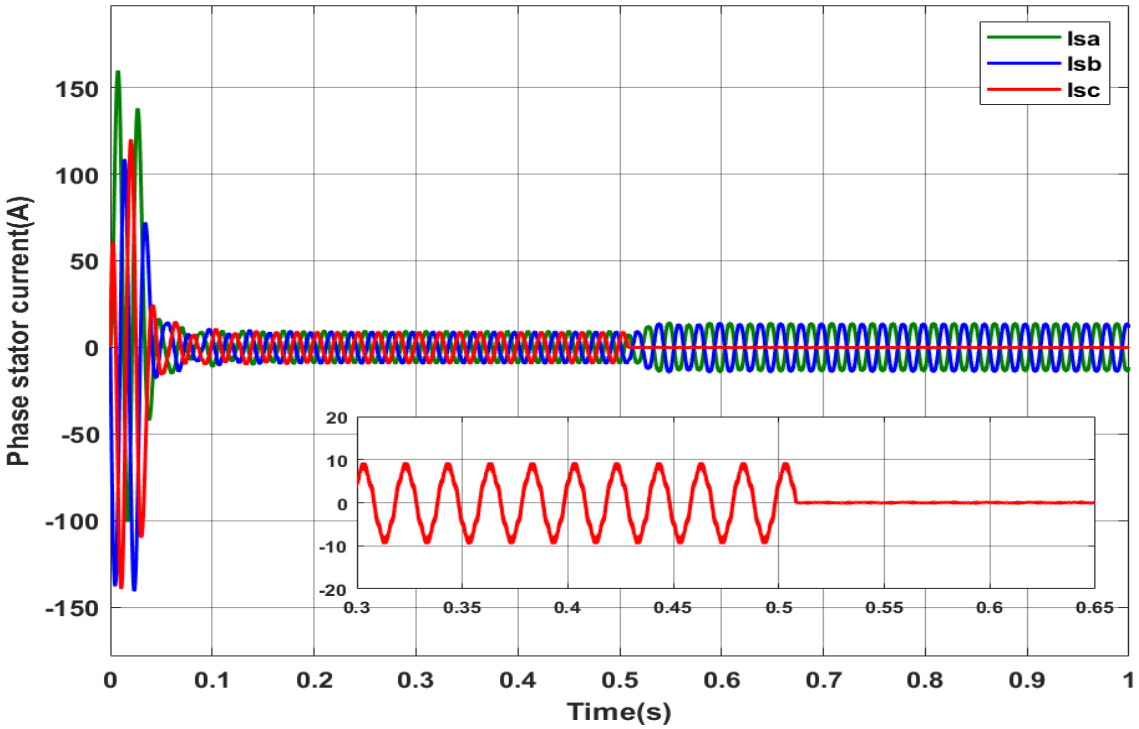

Figure III. 19 The curve of the stator current (Detection and Localization Cas).

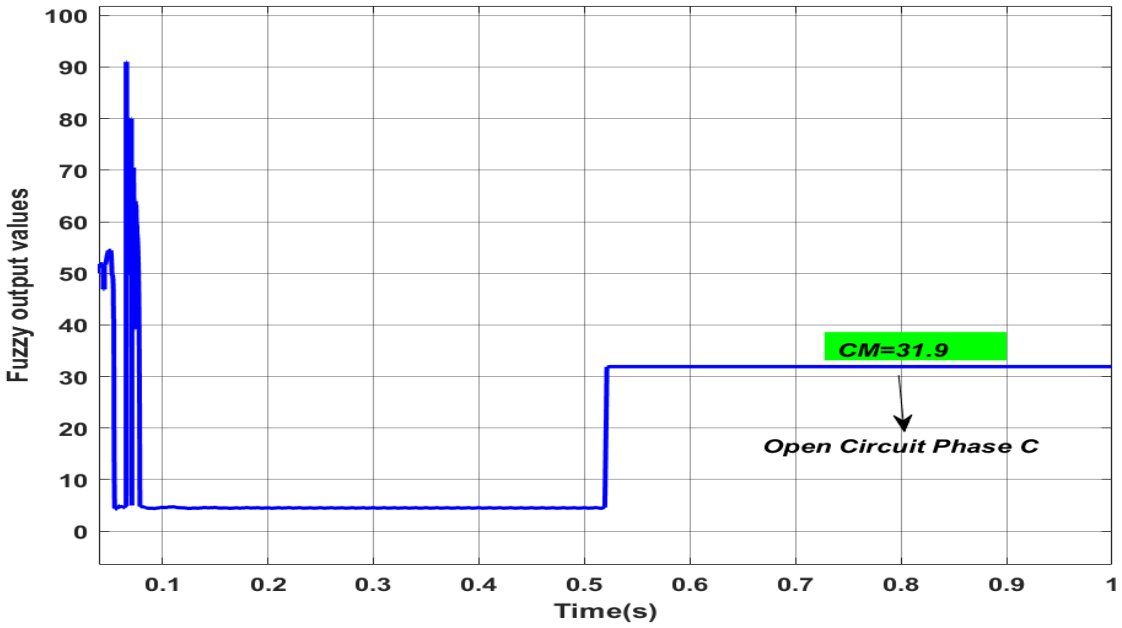

Figure III. 20 Fuzzy output values (Detection and Localization Cas).

B. Case of Short-Circuit Fault in Stator Phase A

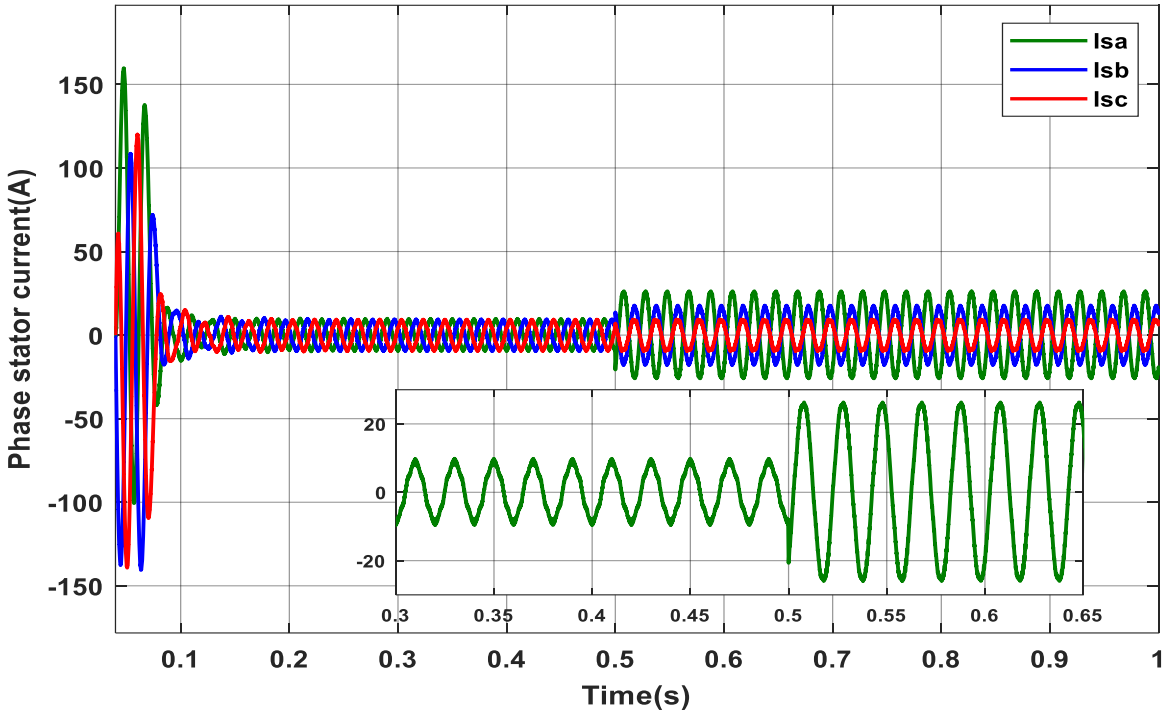

Figure III. 21 The curve of the stator current (Detection and Localization Cas).

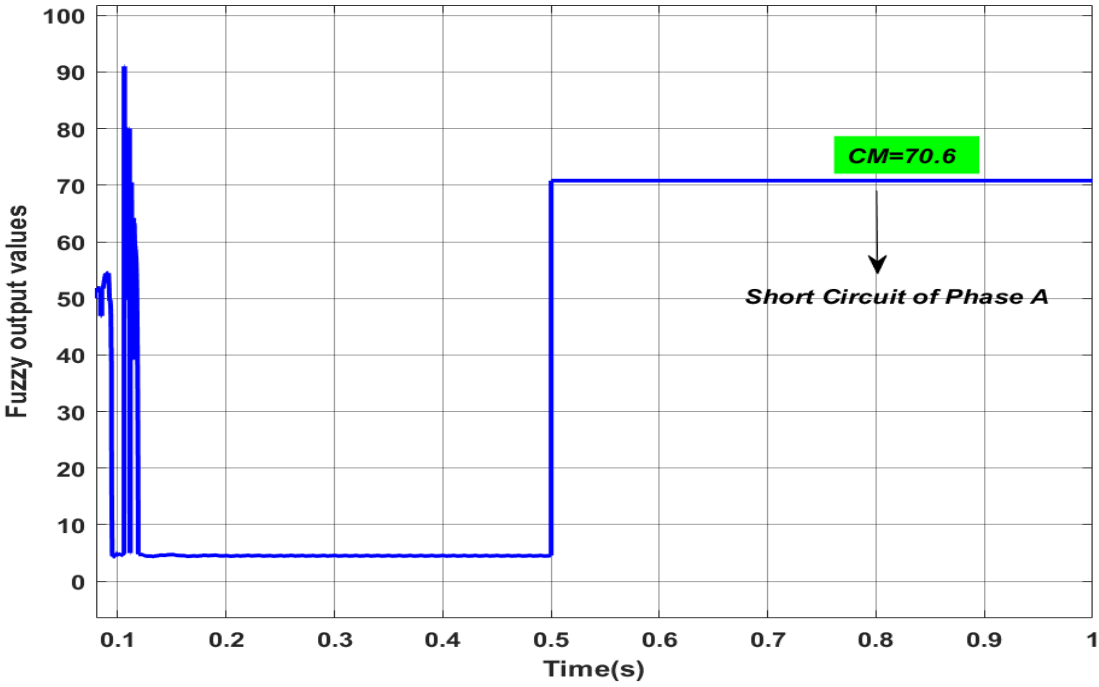

Figure III. 22 Fuzzy output values (Detection and Localization Cas).

C.Case of Critical Short-Circuit Fault in Stator Phase B

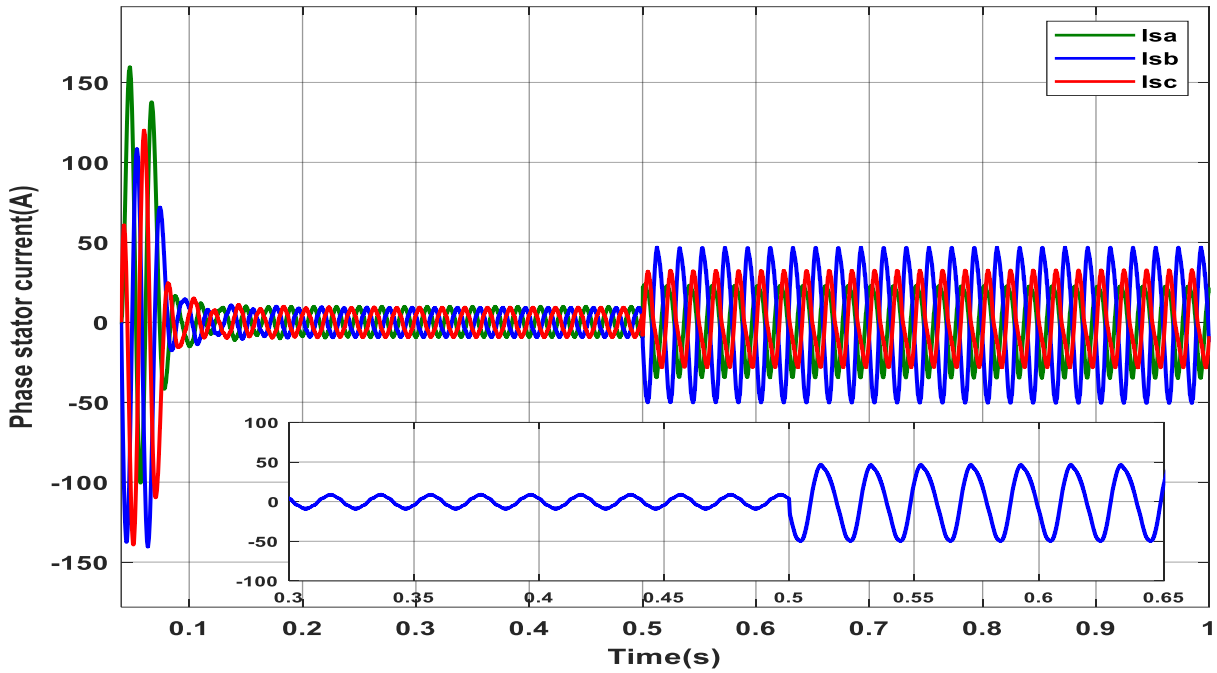

Figure III. 23 The curve of the stator current (Detection and Localization Cas).

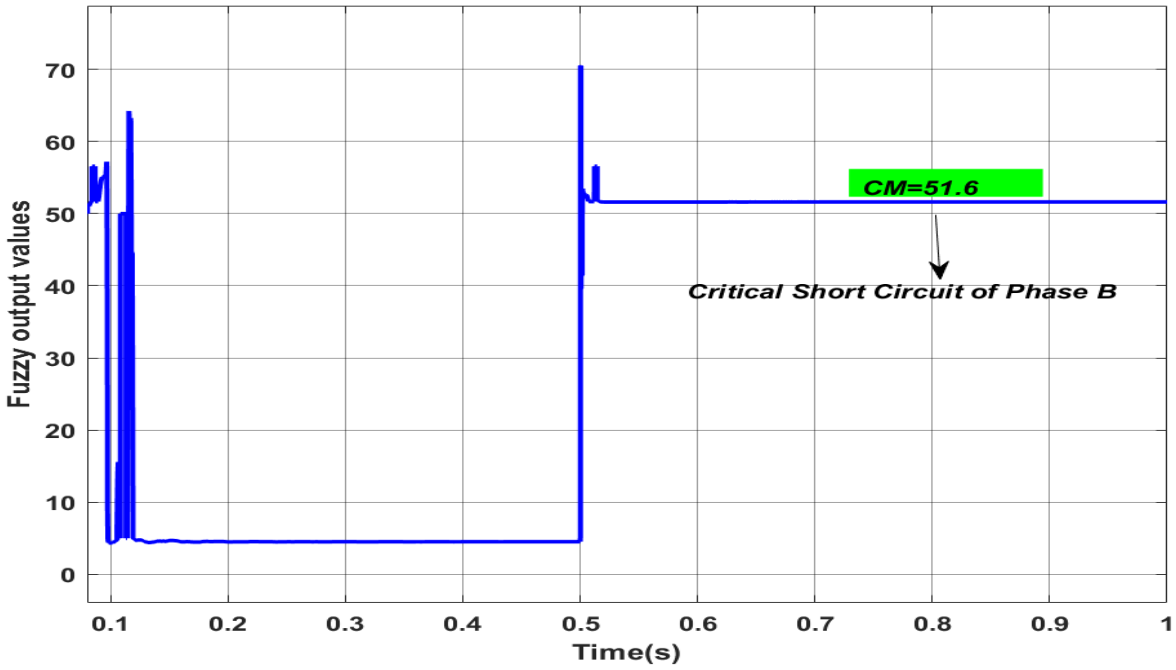

Figure III. 24 Fuzzy output values (Detection and Localization Cas).

III.7 Conclusion

This chapter introduces a diagnostic approach based on fuzzy logic, which facilitates the monitoring and detection of inter-turn short circuits and open-phase circuits in the stator windings of DFIG used in wind turbines. By capturing stator currents and computing their average absolute values, this proposed method depends exclusively on phase currents to promptly identify and pinpoint faults in real-time for systems employing the DFIG. Simulation results have shown that this approach can provide valuable information about the DFIG's status, enabling the anticipation of potential failures' severity.

CHAPTER IV

Wind Power Converter Fault Diagnosis

IV.1 Introduction

Power converter faults are a major cause of wind turbine failures. Research on fault diagnosis methods, including model-based and data-driven approaches, is essential to ensure efficient operation and maintenance. This chapter focuses on fault detection techniques for a PWM inverter used in a wind energy conversion system based on a doubly-fed induction generator. It specifically addresses short-circuit and open-circuit faults that can occur in the power switch.

The chapter begins by examining the current state of research on fault diagnosis of wind energy converters to update the relevant literature. It highlights the main types of faults faced by these converters. In particular, it explores the common faults that can affect the inverter of variable-speed wind turbine (DFIG) systems, focusing on short-circuit (SC) and open-circuit (OC) faults that impact the power switches of the inverter.

A comprehensive overview of fault diagnosis methods for wind energy converters is presented. The three main categories of diagnosis methods are discussed: model-based, signal-based, and data-driven. Each method is detailed, highlighting its advantages and specific requirements. The importance of performance metrics to evaluate the effectiveness of fault diagnosis methods is emphasized.

A methodology is proposed to diagnose open-circuit and short-circuit switch failures by combining fuzzy logic and advanced intelligence approaches based on artificial neural networks. Finally, the last section evaluates the simulation results under normal operating conditions and in the presence of open-circuit and short-circuit faults, using the Matlab/Simulink software.

IV.2 Background

Although there are numerous surveys on the condition monitoring and fault diagnosis of wind turbines [89][90][91][73], they mainly focus on the examination of the entire wind turbine system, with limited emphasis on wind power converters. The exploration of fault diagnosis in wind power converters is not comprehensive, with more attention paid to fault modes and signals than fault diagnosis methods. A detailed review of signals and signal processing techniques used for condition monitoring and fault diagnosis in wind turbines is presented in the survey by [73].

There have been various surveys conducted on fault diagnosis methods for converters, such as those by [25][26] and [92], which provide insights into model-based, signal-based, knowledge-based, and hybrid fault diagnosis methods, focusing on introducing various techniques. However, a more comprehensive qualitative and quantitative analysis of these methods is required.

[93] reviewed fault diagnosis methods for insulated gate bipolar transistors (IGBT) in three-phase power inverters with T-type or traditional two-level topologies, which included methods like Park's vector method, normalized current method, and neural networks. However, concerns regarding reliability and robustness were not addressed, and these methods may not be directly applicable to fault diagnosis of modular multilevel converters (MMC) due to the detection of faulty arms instead of faulty cells.

Studies by [94] and [95] evaluated and summarized fault diagnosis methods based on signal processing, mechanism-based, and artificial intelligence for switching devices. However, a more in-depth analysis and comparison of these methods are necessary to determine their effectiveness and applicability in fault diagnosis of wind power converters.

IV.3 Common Faults in Wind Power Converters

Wind power converters are often subject to typical faults associated with specific converter topologies used in wind turbine systems. These include diode rectifier-based converters, 2-level back-to-back (2L-BTB) converters for systems with 1-3MW power, 3-level neutral-point-clamped back-to-back (3L-NPC BTB) converters for systems with 5-8MW power, and modular multilevel converters (MMC) for high-power applications. Research indicates that the primary components susceptible to faults in wind power converters are power semiconductor devices, such as IGBTs, printed circuit boards (PCBs), and capacitors. Power semiconductor device faults, influenced by factors like PCB faults, can result in power switch faults, a common cause of converter failures. These faults, including Short-Circuit (SC) and Open-Circuit (OC) faults, can cause irreversible damage to wind power converters due to excessive current or voltage during turbine start-up, degradation of heat dissipation performance over time, and environmental factors like dust, corrosive gases, and moisture in wind farms [96].

IV.4 Inverter Faults

The two-level inverter (2L-BTB) used in DFIG is composed of six power switches, which can convert DC voltage to AC voltage, making it a crucial component in WECS [96].

Among all the faults occurring in the inverter, the most common ones relate to open circuits and short circuits in the power switches.

IV.4.1 Short-circuit fault (SC)

A short-circuit fault in a switch can occur when one of the two switches remains constantly turned on, and a subsequent short-circuit happens when the second switch is instructed to close.

This fault is typically caused by a malfunction in the control of the transistors or a physical failure of the silicon chip due to overheating, which is the most common mode of failure. Short-circuit faults are highly severe and can cause significant damage to the converter and other components within a short time due to the resulting abnormal overcurrent. Therefore, most current Fault Diagnosis methods for short-circuit faults rely on hardware circuits to minimize the response time and prevent further damage.

IV.4.2 Open circuit fault (OC)

An open circuit fault typically arises from a gate malfunction or a break in a jumper wire within the transistor, often caused by thermal cycling or as a consequence of a previous short circuit fault [97]. This fault commonly leads to a complete or partial loss of operation in one of the IGBTs that make up the static converter. When an open circuit fault occurs, it manifests as high harmonic distortion in currents. The currents in the faulty phase and the unaffected phase become out of sync, resulting in fluctuations in generator torque and a reduction in the grid power factor. Unlike a short circuit fault, an open circuit fault has a slower response time and does not typically cause significant damage to the entire system in a short timeframe [96].

IV.5 Comprehensive Overview of Fault Diagnosis Methods for Wind Power Converters

The fault diagnosis framework for wind power converters encompasses three main categories of methods: model-based, signal-based, and data-driven [26].

IV.5.1 Model-based Method

- This approach involves creating a precise mathematical or analytical model of the wind power converter system, taking into account the known physical characteristics and dynamics of the system [26][96].
- By comparing the estimated values from the model with the actual measured values, fault results are obtained through residual analysis [26][96].
- The accuracy of the system model is crucial for providing reliable diagnostic results.

IV.5.2 Signal-based Method

- This method involves studying the behavior of the wind power converter system under different component failures [26][96].

- Diagnostic variables and thresholds are generated based on the measured signals to identify the fault state of the converter through symptom analysis [26][96].
- Prior knowledge of the system is necessary for effective fault diagnosis, but a precise system model is not required.

IV.5.3 Data-driven Method

- This approach utilizes the available historical operational data to determine the system states.
- Mathematical techniques are applied to process and extract features from the measured signals, followed by the use of artificial intelligence algorithms for fault pattern training and recognition [26][96].
- While this method does not rely on a precise system model or prior knowledge of the system, it requires a significant amount of historical data for training, making it computationally intensive and time-consuming.

Different performance metrics are employed to assess the efficacy of fault diagnosis methods for wind power converters. These metrics encompass factors such as the number of faults, diagnosis duration, accuracy, precision, recall, F1-score, false detection rate, missed detection rate, and robustness [96]. By utilizing these metrics, it becomes possible to evaluate the strengths and limitations of various fault diagnosis approaches, playing a vital role in guaranteeing the dependability and effectiveness of wind power converter systems.

IV.6 Diagnostic Methodology

This section focuses on the techniques we have studied and utilized for diagnosing PWM inverter faults. The latter pertains to a wind energy conversion system employing a double-fed induction generator. More specifically, it addresses both short-circuit faults and open-circuit faults occurring in the power switch.

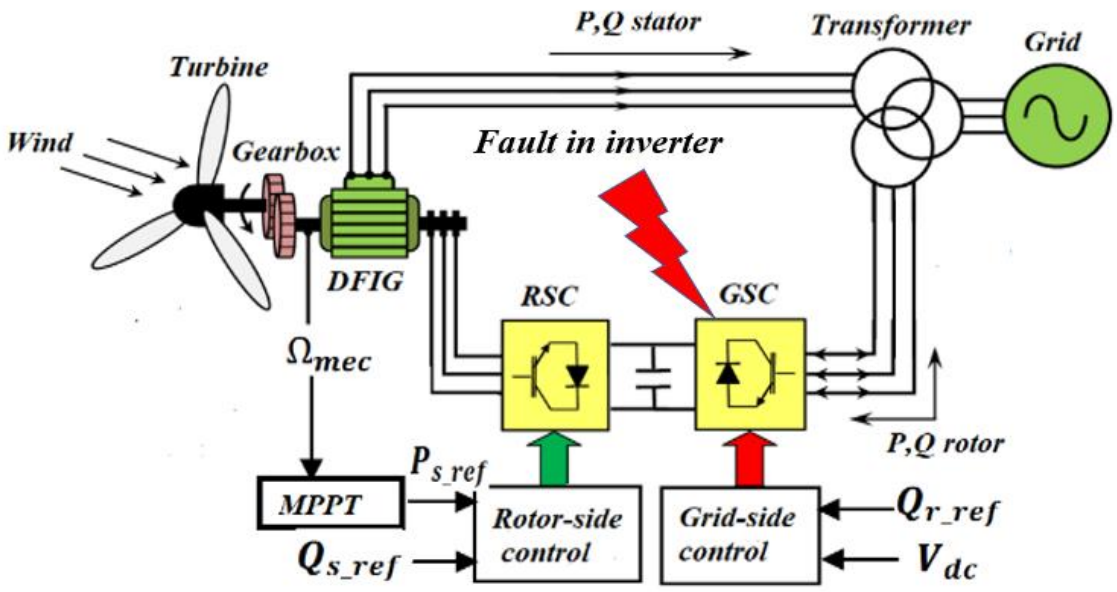

Figure IV. 1 WECS with fault in inverter.

Among the methods studied for fault diagnosis and protection of IGBT transistors, based on their performance, and implementation efforts:

IV.6.1 Spectral Analysis Method

Signal processing has a rich history of application in detecting electrical faults, with spectral analysis emerging as a prominent and efficient diagnostic method. Spectral analysis, at its essence, relies on the Fast Fourier Transform (FFT) spectrum. As per Fourier's theorem, any waveform in the time domain can be represented as a combination of weighted sines and cosines. The FFT algorithm facilitates the conversion of sampled data from the time domain to the frequency domain. In a signal sampled at a rate of fs Hz, the time interval between samples is Δt (where Δt = 1/fs). The Fast Fourier Transform computation is represented by [98]:

$$X_k = \sum_{t=0}^{N-1} x_t e^{-j2\pi i \frac{k}{N}} \ , \ \ k = 0, 1, 2, \dots, N-1 \qquad \text{(IV. 1)}$$

IV.6.2 Park Contour Trajectory Analysis Method

This method is tailored for the configuration of the three-phase two-level inverter. This approach involves detecting and pinpointing the faulty IGBT transistor within the system by analyzing the magnitude and angle of the Park vector. The Park vector is derived using the Concordia transformation. By evaluating the modulus and angle of the Park vector, this method

enables the identification of the failed IGBT transistor in the inverter system. The two-phase currents and voltages are expressed as follows:

$$\begin{bmatrix} i_\alpha \\ i_\beta \end{bmatrix} = \sqrt{\frac{2}{3}} \begin{bmatrix} 1 & -\frac{1}{2} & -\frac{1}{2} \\ 0 & \frac{\sqrt{3}}{2} & -\frac{\sqrt{3}}{2} \end{bmatrix} \begin{bmatrix} I_a \\ I_b \\ I_c \end{bmatrix} \quad \text{(IV. 2)}$$

Assuming the system is in balance, $I_a + I_b + I_c = 0$,we then implement the Concordia transformation:

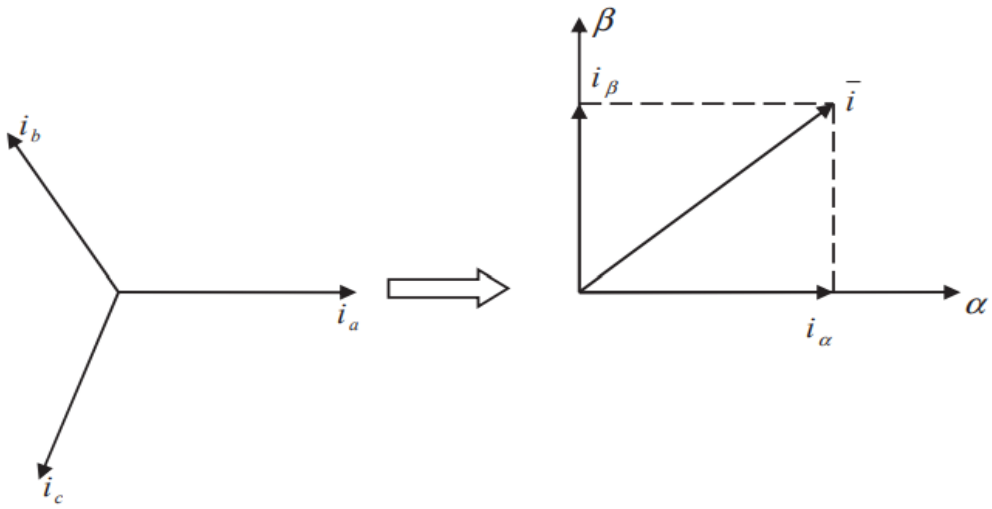

Figure IV. 2 Transformation of Concordia.

In the complex domain: $\bar{\imath} = i_\alpha + i_\beta$.

Figure (IV.3) depicts the graphical representation in Polar coordinates showing the precise fault angles associated with the open-circuit faults of the IGBT switches in the inverter.

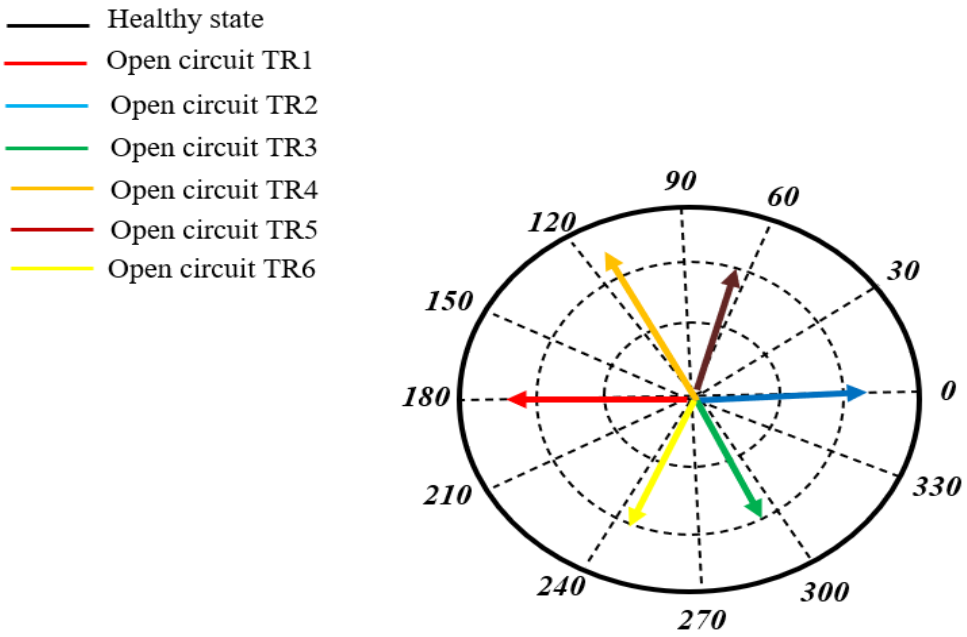

Figure IV. 3 Graphical representation of the fault angles linked to open-circuit faults of IGBT switches in the inverter, utilizing polar coordinates.

IV.6.3 Fault Detection Method Based on Fuzzy Logic

The fuzzy logic methodology is structured to calculate the average absolute current values (AAVC) through the acquisition of stator currents. This enables the instantaneous identification and localization of open-circuit or short-circuit faults in the inverter's IGBT by utilizing the basic phase currents of the generator.

IV.6.3.1 Fuzzy Monitoring Approach

Figure IV.4 illustrates a comprehensive schematic of the proposed methodology [99].

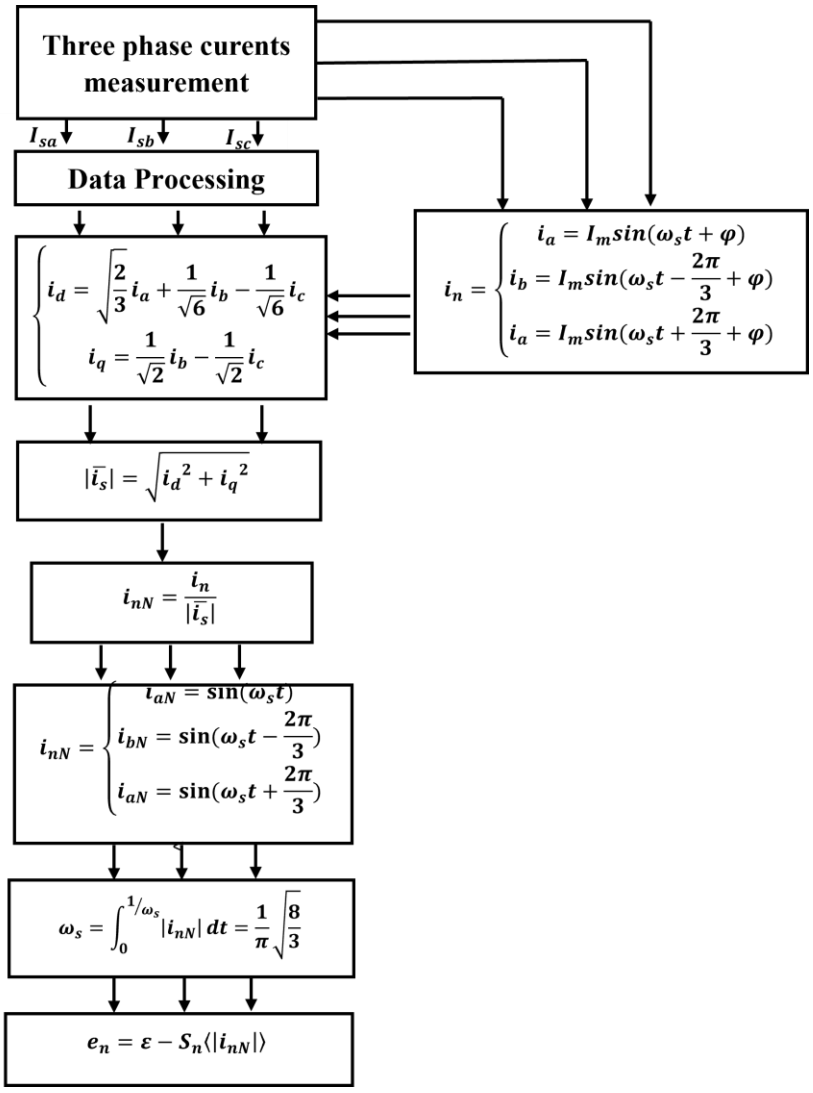

Figure IV. 4 Schematic of the proposed diagnostic approach utilizing fuzzy logic.

The measured generator phase currents are normalized by the modulus of the Park's Vector, as indicated in reference [99].

$$\begin{cases} i_d = \sqrt{\frac{2}{3}} i_a + \frac{1}{\sqrt{6}} i_b - \frac{1}{\sqrt{6}} i_c \\ i_q = \frac{1}{\sqrt{2}} i_b - \frac{1}{\sqrt{2}} i_c \end{cases} \quad \text{(IV. 3)}$$

Where; i_a, i_b and i_c represents the stator currents of the induction generator, while i_d and $i_q$denotes the components of the Park's vectors.

The modulus of the Park's vector, represented as $\bar{i_s}$, can be formulated as follows:

$$|\overline{i_s}| = \sqrt{{i_d}^2 + {i_q}^2} \tag{IV. 4}$$

The provided equation signifies the normalized stator phase currents of the induction generator [100].

$$i_{nN} = \frac{i_n}{|\overline{i_s}|} \tag{IV. 5}$$

Where: $n = a, b$ and c;

If we assume that the induction generator is powered by a reliable inverter generating a precisely balanced three-phase sinusoidal current system, it can be expressed as follows [101]:

$$i_n = \begin{cases} i_a = I_m \sin(\omega_s t + \varphi) \\ i_b = I_m \, sin\left(\omega_s t - \frac{2\pi}{3} + \varphi\right) \\ i_a = I_m \sin\left(\omega_s t + \frac{2\pi}{3} + \varphi\right) \end{cases} \tag{IV. 6}$$

Where; $I_m$stands for the maximum current amplitude, ω_s represents the generator current frequency, and φ denotes the initial phase angle.

Following this, the revised expression for the Park's Vector modulus can be defined as follows [102]:

$$|\overline{i_s}| = I_m \sqrt{\frac{3}{2}} \tag{IV. 7}$$

Irrespective of the measured generator phase currents' amplitudes, the normalized stator currents will consistently lie within the range of $\mp\sqrt{2/3}$, as [103]:

$$i_{nN} = \begin{cases} i_{aN} = \sin(\omega_s t) \\ i_{bN} = \sin\left(\omega_s t - \frac{2\pi}{3}\right) \\ i_{aN} = \sin\left(\omega_s t + \frac{2\pi}{3}\right) \end{cases} \tag{IV. 8}$$

The average absolute values of the three normalized generator phase currents, denoted as i_{nN}, can be represented as follows:

$$\int_0^{1/\omega_s} |i_{nN}| \, dt = \frac{1}{\pi} \sqrt{\frac{8}{3}} \tag{IV. 9}$$

Ultimately, the three input monitoring variables $e_n(e_a, e_b, e_c)$ in the fuzzy system inference are derived from the errors in the average absolute values of the normalized currents, as indicated by the equation following [101]:

$$e_n = \varepsilon - S_n\langle|i_{nN}|\rangle \quad \text{(IV. 10)}$$

The constant value ε, equal to the average absolute value, can be represented as follows:

$$\varepsilon = \frac{1}{\pi}\sqrt{\frac{8}{3}} \approx 0.5198 \quad \text{(IV. 11)}$$

The values of E_n and $S_n$allow for the creation of a distinct fault signature, as demonstrated by the following equations:

$$E_n = \begin{cases} N\ for\ e_n < 0 \\ P\ for\ e_n > 0 \end{cases} \quad \text{(IV. 12)}$$

$$S_n = \begin{cases} N\ for\ i_{nN} < 0 \\ P\ for\ i_{nN} > 0 \end{cases} \quad \text{(IV. 13)}$$

IV.6.3.2 Input and output variables

The input variables of the fuzzy system are determined by choosing the values of(E_a, E_b, and E_s) and (S_a, S_b, and S_c) .These input variables (E_a, E_b, and E_s) and (S_a, S_b, and S_c) are considered linguistic variables and are denoted as t(Q) = {Zero (Z), Positive (P), Negative (N)}, as illustrated in Figure IV.5.

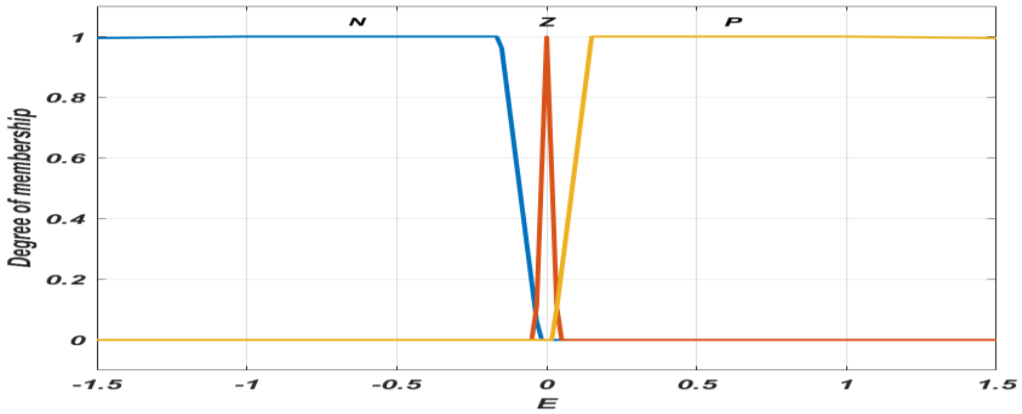

Figure IV. 5 Membership functions for input.

Figure IV.6 shows CM-SC representing the inverter state (Short circuit switch) as a linguistic variable, labeled as T(CM-CC) = {sc-TR1, sc-TR2, sc-TR3, sc-TR4, sc-TR5, sc-TR6, Healthy}.

In Figure IV.7, CM_O illustrates the inverter state (Open circuit switch) as a linguistic variable, denoted as T(CM-OC) = {op-TR1, op-TR2, op-TR3, op-TR4, op-TR5, op-TR6, Healthy}.

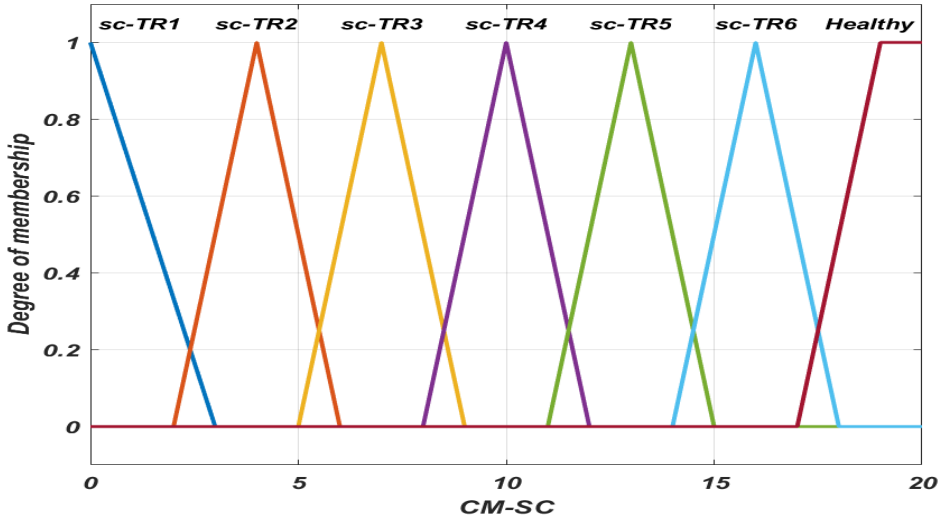

Figure IV. 6 Membership functions for output variables (SC switch fault).

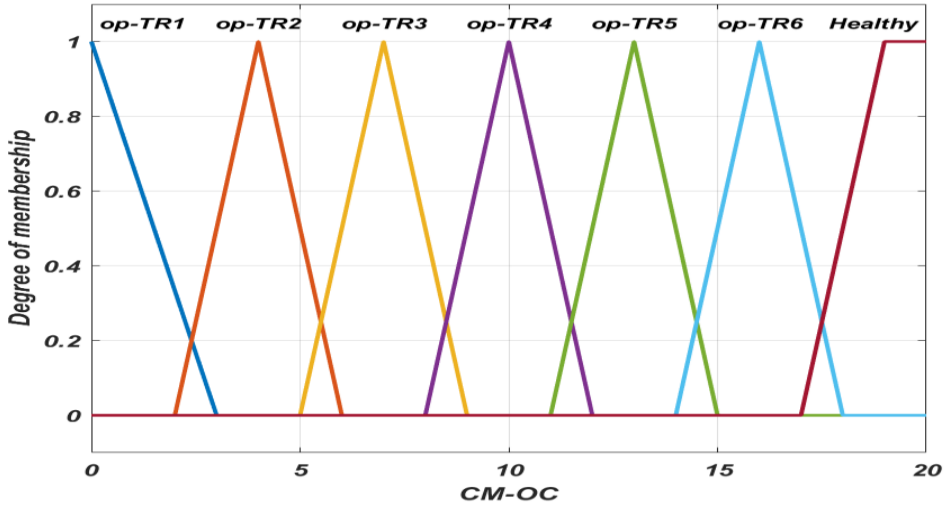

Figure IV. 7 Membership functions for output variables (OC switch fault).

The fuzzy rules are specified as follows:

Table IV. 1 Fuzzy rules membership function.

Short circuit switch fault of inverter									
Rules	**if** Ea	**and** Eb	**and** Ec		**if** Sa	**and** Sb	**and** Sc		**is**
Rule01	N	P	P		P	N	N		SC-TR1
Rule02	N	P	P		N	P	P		SC-TR2
Rule03	P	N	P		N	P	N		SC-TR3
Rule04	P	N	P		P	N	P		SC-TR4
Rule05	P	P	N		N	N	P		SC-TR5
Rule06	P	P	N		P	P	N		SC-TR6
Rule07	Z	Z	Z		Z	Z	Z		Healthy
Open circuit switch fault of inverter									
Rule01	P	N	N		N	P	P		OC-TR1
Rule02	P	N	N		P	N	N		OC-TR2
Rule03	N	P	N		P	N	P		OC-TR3
Rule04	N	P	N		N	P	N		OC-TR4
Rule05	N	N	P		P	P	N		OC-TR5
Rule06	N	N	P		N	N	P		OC-TR6

IV.6.4 Neural Network-Based Fault Detection Method

Neural network diagnosis is a computational model inspired by the operation of human neurons, designed in a schematic manner. It is based on the principles of biological neurons and is utilized to detect faults within a system. For successful fault identification, neural network diagnosis necessitates an adequate number of examples illustrating both normal operation and anomalies [104]. During the training phase, the input network processes the features, while the output network provides the required diagnosis [105].

The diagram shown in Figure 8 illustrates the use of three-phase stator currents for extracting features. Under normal or healthy conditions, these current values come together to create a three-dimensional (3D) circle.

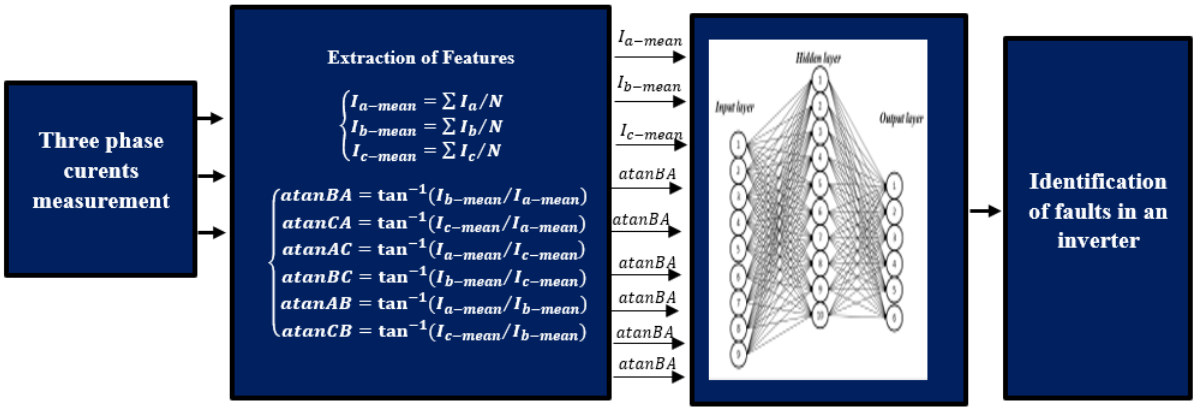

Figure IV. 8 Schematic of the proposed diagnostic method employing NN.

The creation of the three-dimensional circle is explained by equation (IV.14) [106].

$$R^2 = I_a^2 + I_b^2 + I_c^2 \tag{IV.14}$$

In each fault scenario, the 3D circle experiences a specific pattern change. Each single and multiple fault scenario displays its own distinctive 3D pattern. Equations are employed to clarify the different extracted features derived from the examination of three-phase currents.

Equation (IV.15) is utilized to compute the average value of each phase [106].

$$\begin{cases} I_{a-mean} = \sum I_a/N \\ I_{b-mean} = \sum I_b/N \\ I_{c-mean} = \sum I_c/N \end{cases} \tag{IV.15}$$

With; N number of samples.

In this method, the subsequent feature extraction step includes determining angles for the mean points acquired from the earlier process. Angles are computed for every mean point of the plotted 3D currents. As alterations or the lack of a phase can influence the mean point's location in the three-dimensional space, distinct angles can be extracted for each fault situation. Two angles are computed for each mean value in both axis directions, leading to a total of six angles. These six angles are derived using Equation (IV.16) [106].

$$\begin{cases} atanBA = \tan^{-1}(I_{b-mean}/I_{a-mean}) \\ atanCA = \tan^{-1}(I_{c-mean}/I_{a-mean}) \\ atanAC = \tan^{-1}(I_{a-mean}/I_{c-mean}) \\ atanBC = \tan^{-1}(I_{b-mean}/I_{c-mean}) \\ atanAB = \tan^{-1}(I_{a-mean}/I_{b-mean}) \\ atanCB = \tan^{-1}(I_{c-mean}/I_{b-mean}) \end{cases} \quad (IV.16)$$

IV.6.4.1 Architecture of The Employed ANN

The ANN system is designed with neurons that share uniform structures and are interconnected similar to those found in the human nervous system. It is organized into layers where each neuron receives inputs from the outputs of preceding neurons. Specifically, neurons in the input layer are exclusively connected to the subsequent layer, while neurons in the hidden layer possess the distinctive property of being interconnected with all neurons in both the preceding and succeeding layers [107]. In our NN setup, the input layer comprises nine neurons responsible for transmitting input values to the hidden layer. For a short circuit switch fault (Figure IV.9), the hidden layer consists of 20 neurons, and for an open circuit switch fault (Figure IV.10), it has 10 neurons. The output layer is composed of six neurons, with the system's desired output being binary, represented as either (1 or 0).

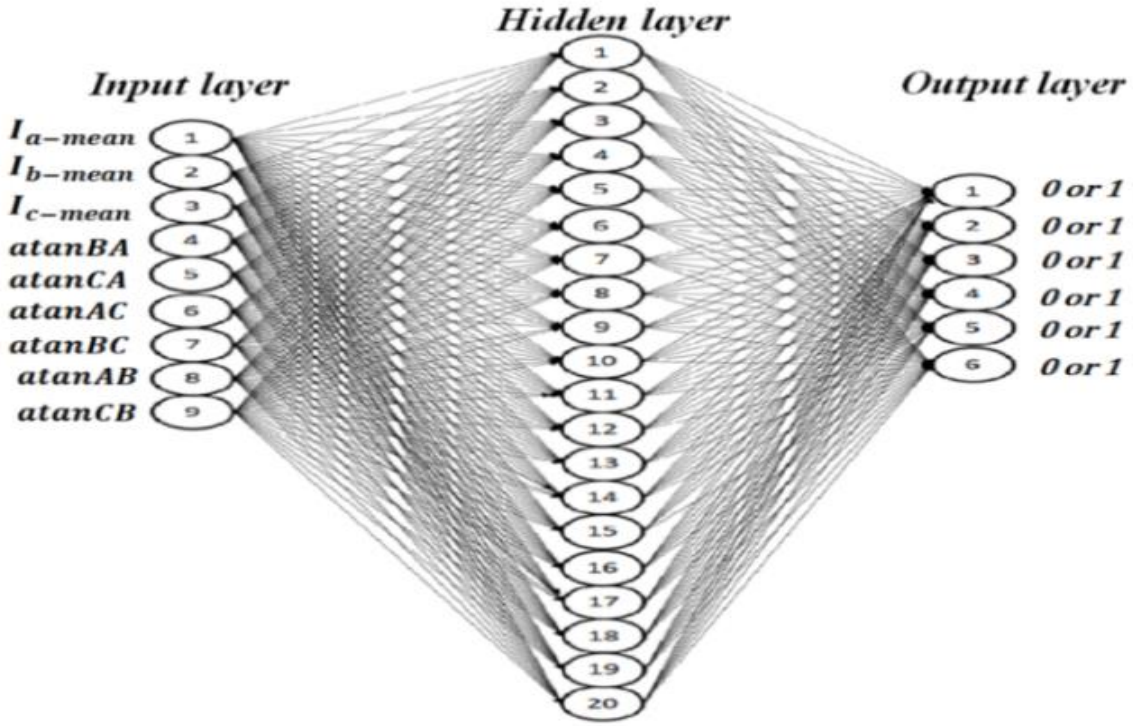

Figure IV. 9 NN structure (SC switch fault).

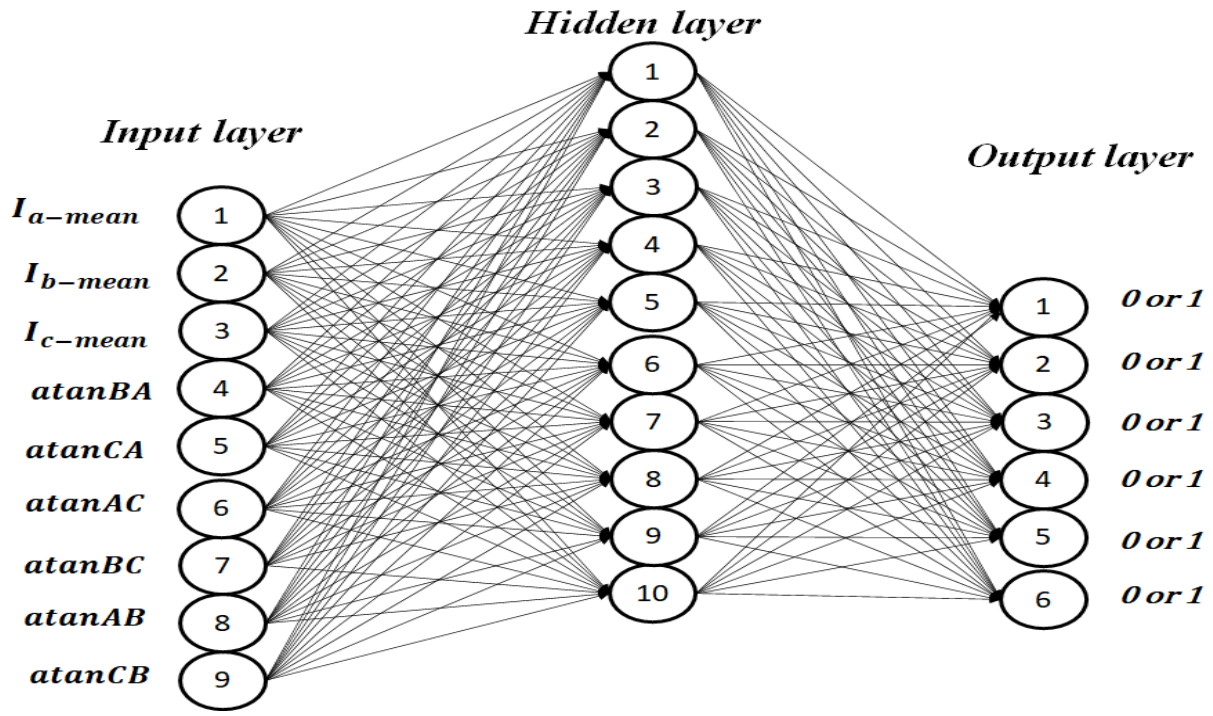

Figure IV. 10 NN structure (OC switch fault).

IV.7 Study of Results

In our thesis, the Matlab/Simulink software is utilized to investigate the impacts of short-circuit and open-circuit faults in the inverter. A fault is intentionally introduced at 1.5s for analysis purposes. This section evaluates the simulation results under normal operating conditions and when an open circuit fault and a short circuit fault are present. Table IV.2 summarizes the data used for Neural Network training. It is divided into two parts: one for short-circuit faults and the other for open-circuit faults. Each fault scenario is presented alongside the healthy state. The "**Faulty switch**" rows identify the specific inverter switches affected under each fault condition. For every scenario, a **feature vector** is constructed ***V***. These features serve as inputs for the NN, enabling it to detect and classify faults. The "**Output code of NN**" row assigns a unique binary code to each scenario.

Figures (IV.11, IV.12, IV.13, IV.14, IV.15, and IV.16) depict the simulation outcomes in the normal state and when open circuit and short circuit faults occur in various switches of an inverter within a wind energy conversion chain based on the DFIG. These results include phase stator currents, stator current spectrum, Park contour analysis, output fuzzy value, and NN test.

Table IV. 2 Feature data for NN training.

Short circuit fault																				
Training data: ***Feature vector: V = [I_{a-mean}, I_{b-mean}, I_{c-mean}, θ_{ba}, θ_{ca}, θ_{ac}, θ_{bc}, θ_{ab}, θ_{cb}]***																				
Faulty switch (short-circuit)	***Healthy***	***TR1***	***TR2***	***TR3***	***TR4***	***TR5***	***TR6***	***TR1 & TR3***	***TR1 & TR4***	***TR1 & TR5***	***TR1 & TR6***	***TR2 & TR3***	***TR2 & TR4***	***TR2 & TR5***	***TR2 & TR6***	***TR3 & TR5***	***TR3 & TR6***	***TR4 & TR5***	***TR4 & TR6***	***TR1 & TR4 & TR5***	***TR2 & TR3 & TR6***
Output code of neural network	0	1	0	0	0	0	0	1	1	1	1	0	0	0	0	0	0	0	0	1	0
	0	0	1	0	0	0	0	0	0	0	0	1	1	1	1	0	0	0	0	0	1
	0	0	0	1	0	0	0	1	0	0	0	1	0	0	0	1	1	0	0	0	1
	0	0	0	0	1	0	0	0	1	0	0	0	1	0	0	0	0	1	1	1	0
	0	0	0	0	0	1	0	0	0	1	0	0	0	1	0	1	0	1	0	1	0
	0	0	0	0	0	0	1	0	0	0	1	0	0	0	1	0	1	0	1	0	1
Open circuit fault																				
Training data: ***Feature vector: V = [I_{a-mean}, I_{b-mean}, I_{c-mean}, θ_{ba}, θ_{ca}, θ_{ac}, θ_{bc}, θ_{ab}, θ_{cb}]***																				
Faulty switch (Open-circuit)	***TR1***	***TR2***	***TR3***	***TR4***	***TR5***	***TR6***	***TR1 & TR3***	***TR1 & TR4***	***TR1 & TR5***	***TR1 & TR6***	***TR2 & TR3***	***TR2 & TR4***	***TR2 & TR5***	***TR2 & TR6***	***TR3 & TR5***	***TR3 & TR6***	***TR4 & TR5***	***TR4 & TR6***	***All***		
Output code of NN	1	0	0	0	0	0	1	1	1	1	0	0	0	0	0	0	0	0	1		
	0	1	0	0	0	0	0	0	0	0	1	1	1	1	0	0	0	0	1		
	0	0	1	0	0	0	1	0	0	0	1	0	0	0	1	1	0	0	1		
	0	0	0	1	0	0	0	1	0	0	0	1	0	0	0	0	1	1	1		
	0	0	0	0	1	0	0	0	1	0	0	0	1	0	1	0	1	0	1		
	0	0	0	0	0	1	0	0	0	1	0	0	0	1	0	1	0	1	1		

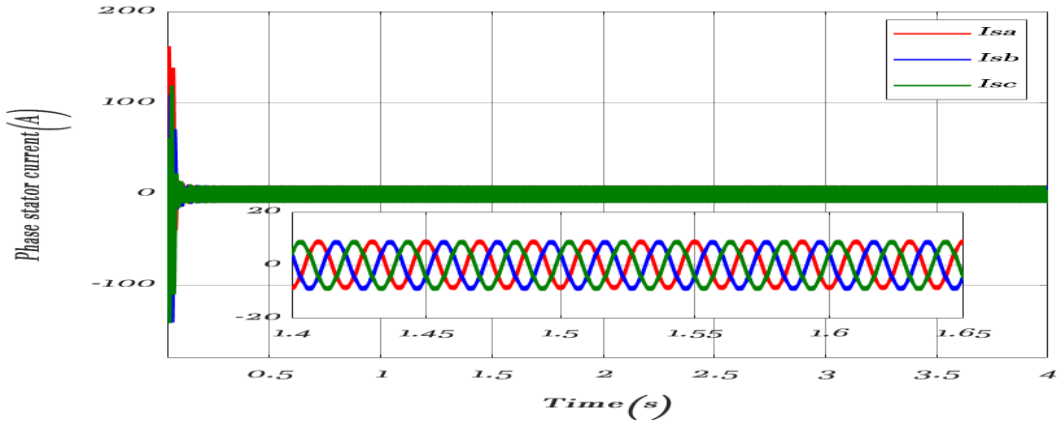

Figure IV.11. a. Phase stator current in the healthy case.

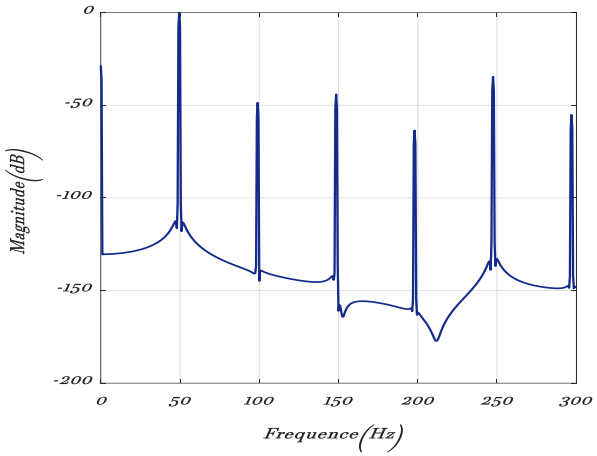

Figure IV.11. b. Stator current spectrum in the healthy case.

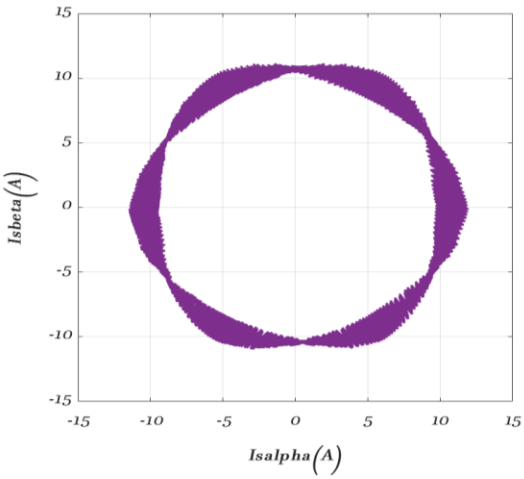

Figure IV.11. c. Analysis of the Park contour in the healthy case.

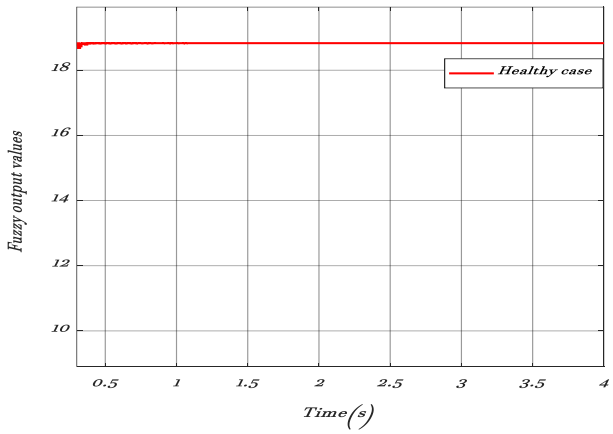

Figure IV.11. d Output fuzzy values in the healthy case.

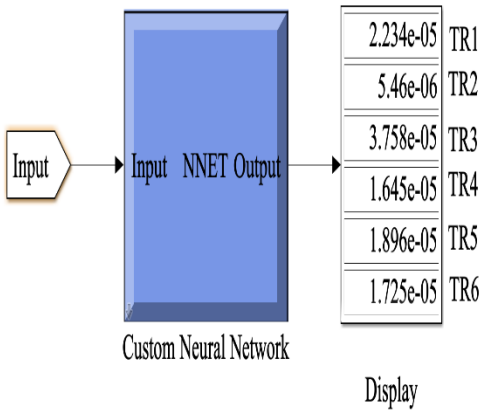

Figure IV.11. d.NN testing.

Figure IV. 11 Simulation results in the healthy case.

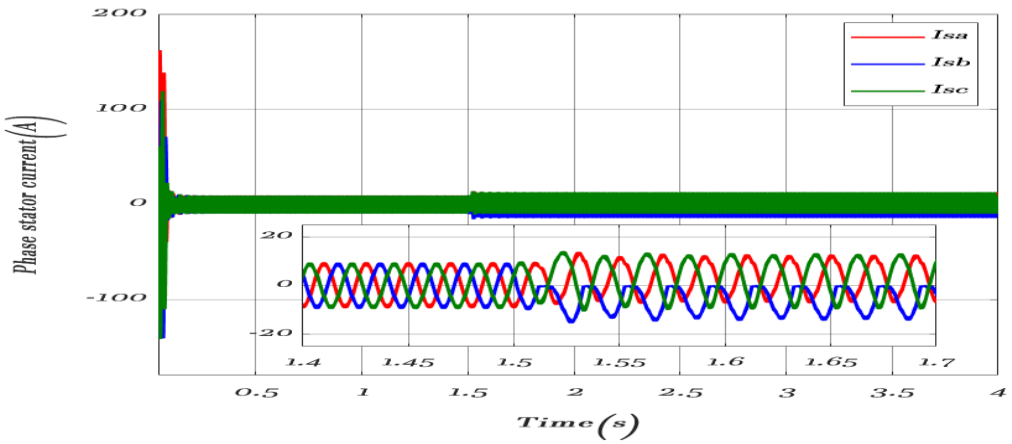

Figure IV.12. a. Phase stator current in the case of OC switch fault in TR3.

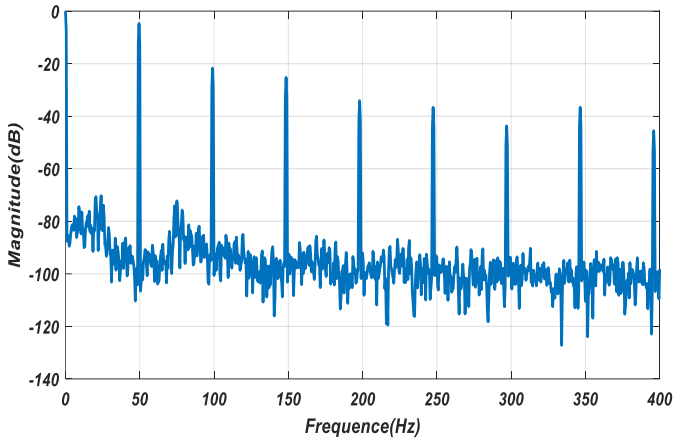

Figure IV.12. b. Stator current spectrum in the case of OC switch fault in TR3.

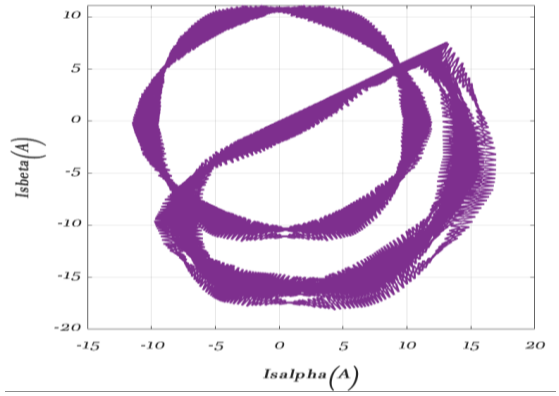

Figure IV.12. c. Analysis of the Park contour in the case of OC switch fault in TR3.

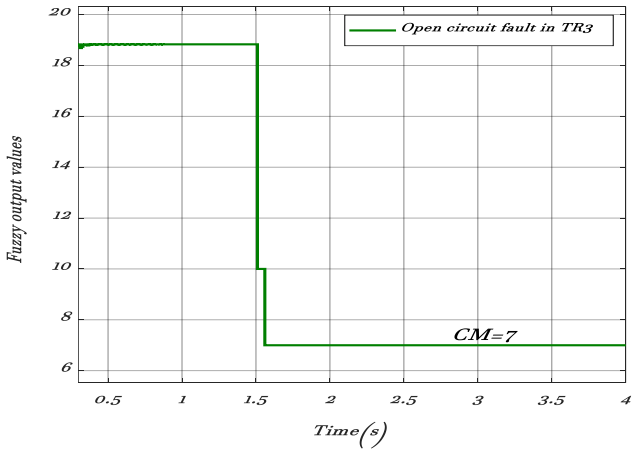

Figure IV.12. d. Output fuzzy values in the case of OC switch fault in TR3.

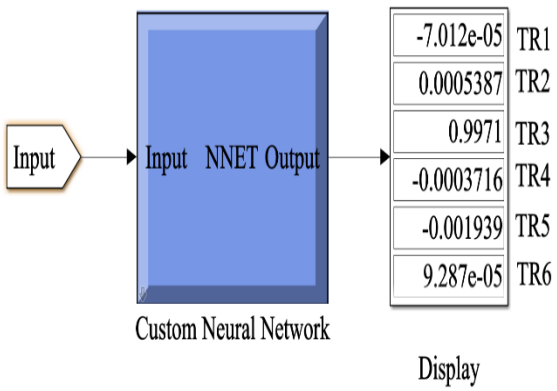

Figure IV.12. d. NN testing.

Figure IV. 12 Simulation results in the case of OC switch fault in TR3.

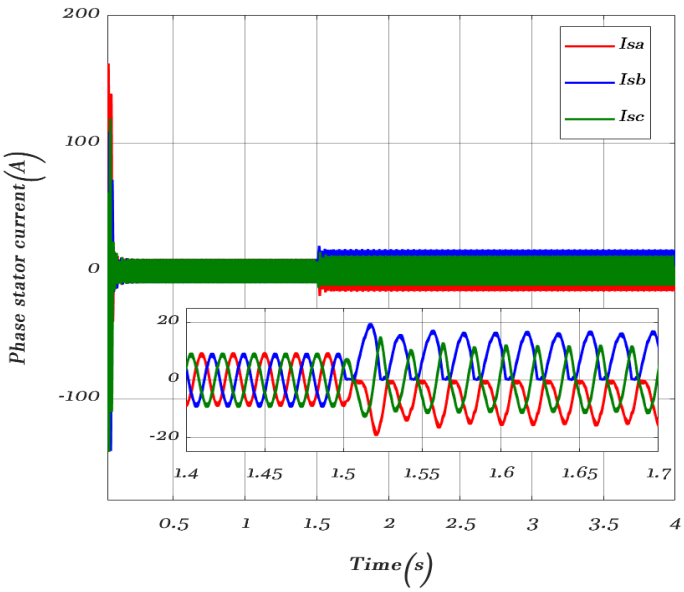

Figure IV.13. a. Phase stator current in the case of OC switch fault in TR1&TR4.

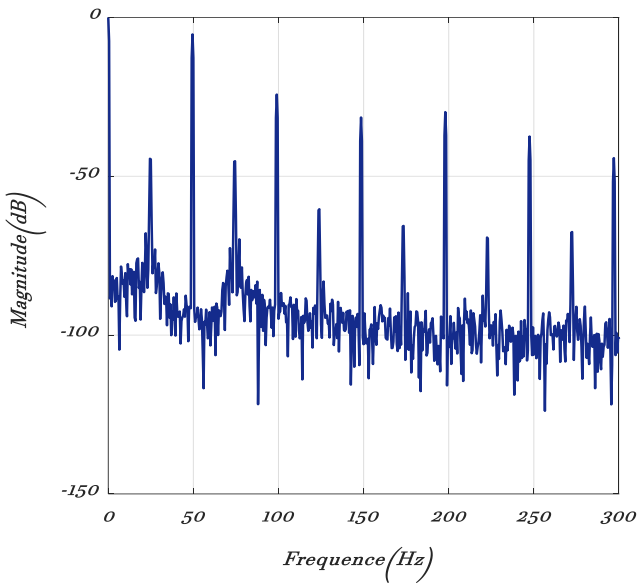

Figure IV.13. b. Stator current spectrum in the case of OC switch fault in TR1&TR4.

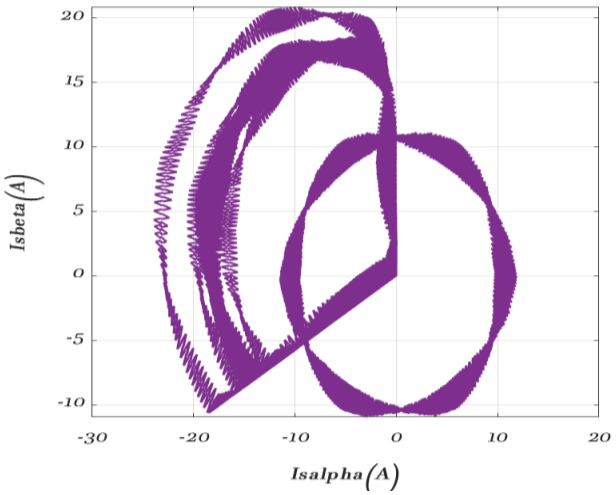

Figure IV.13. c. Analysis of the Park contour in the case of OC switch fault in TR1 &TR4.

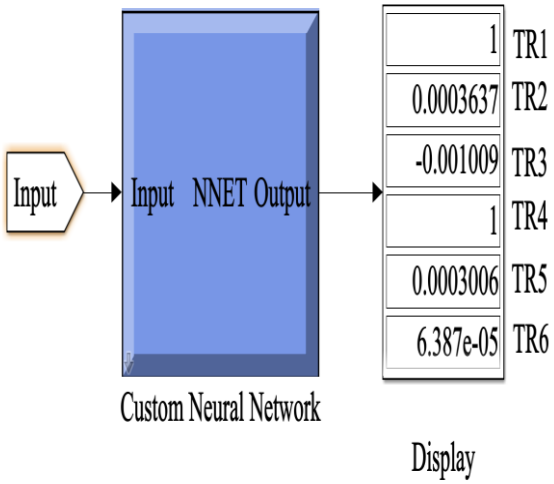

Figure IV.13. d. NN testing.

Figure IV. 13 Simulation results in the case of OC switch fault in TR1&TR4.

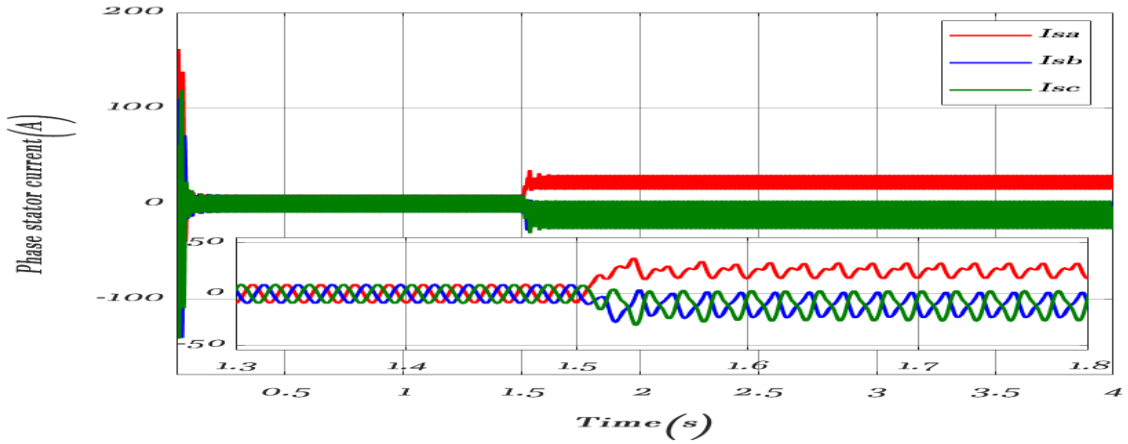

Figure IV.14. a. Phase stator current in the case of SC switch fault in TR1.

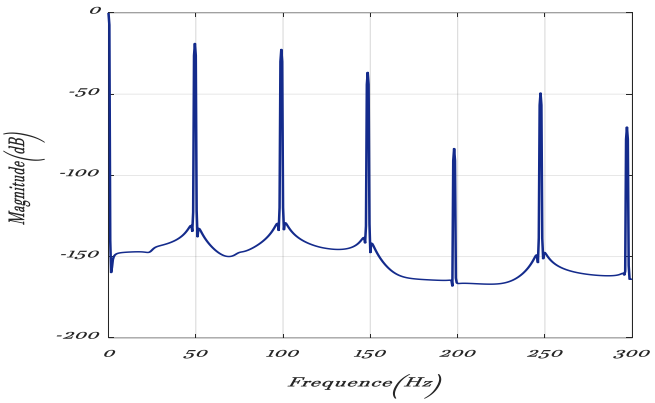

Figure IV.14. b. Stator current spectrum in the case of SC switch fault in TR1.

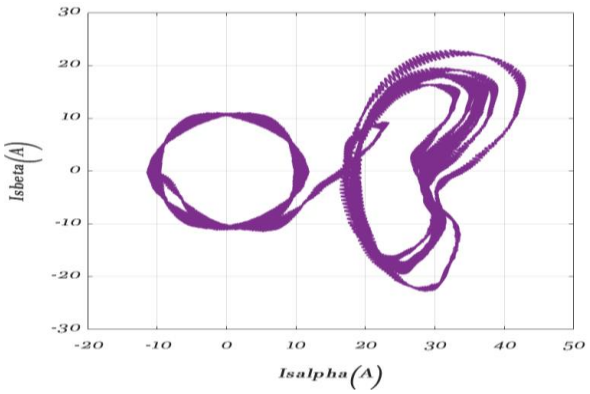

Figure IV.14. c. Analysis of the Park contour in the case of SC switch fault in TR1.

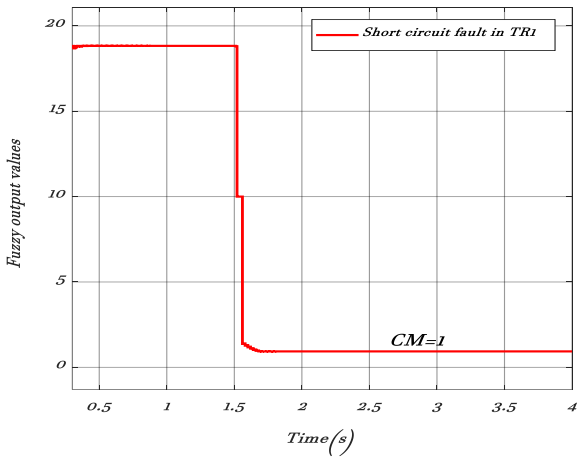

Figure.14. d. Output fuzzy values in the case of SC switch fault in TR1.

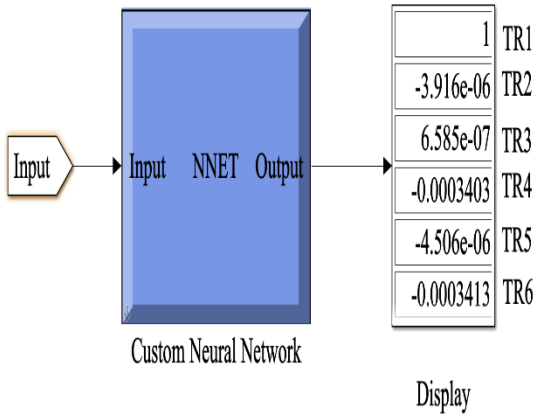

Figure.14. d. NN testing.

Figure IV. 14 Simulation results in the case of short-circuit switch fault in TR1.

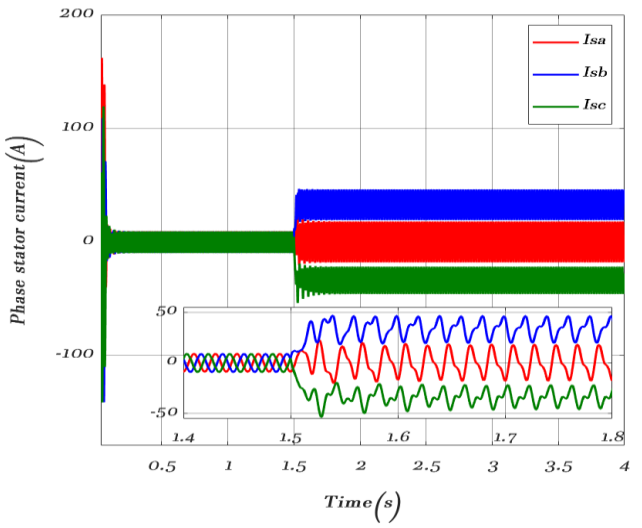

Figure IV.15. a. Phase stator current in the case of SC switch fault in TR3 and TR6.

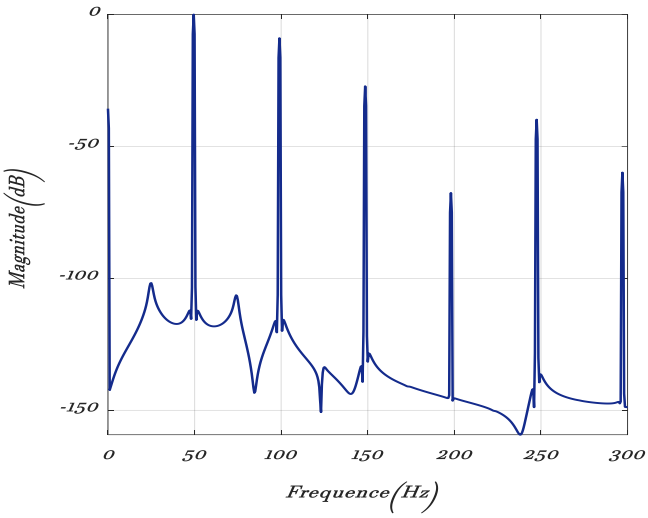

Figure IV.15. b. Stator current spectrum in the case of SC switch fault in TR3 and TR6.

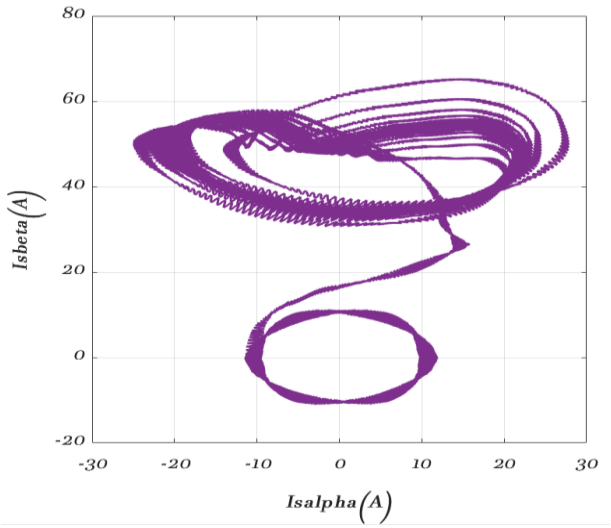

Figure IV.15. c. Analysis of the Park contour in the case of SC switch fault in TR3 and TR6.

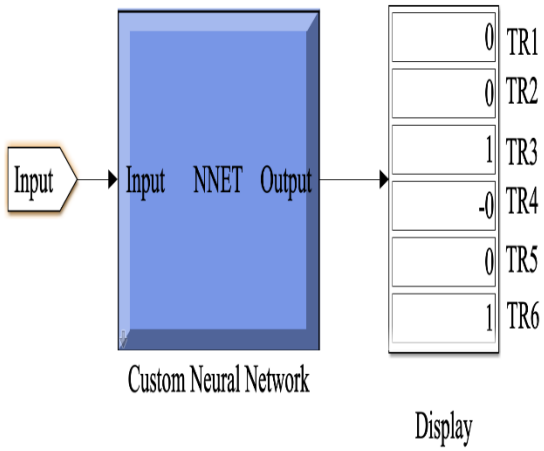

Figure.15. d. NN testing.

Figure IV. 15 Simulation results in the case of SC switch fault in TR3 and TR6.

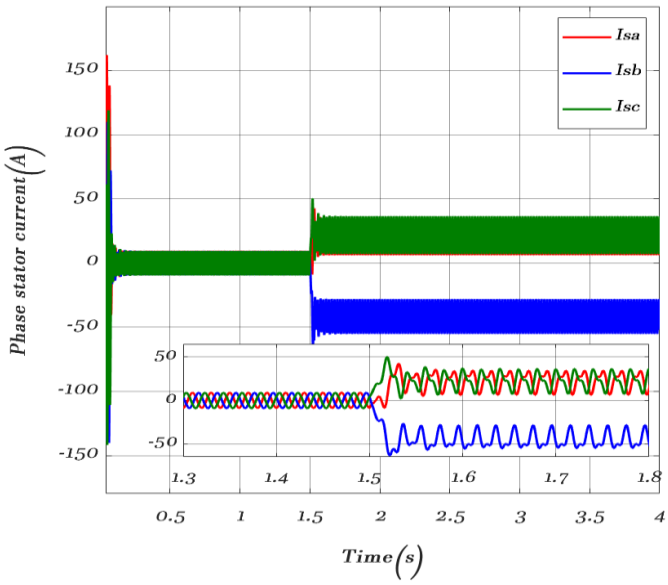

Figure IV.16. a. Phase stator current in the case of SC switch fault in TR1&TR4&TR5.

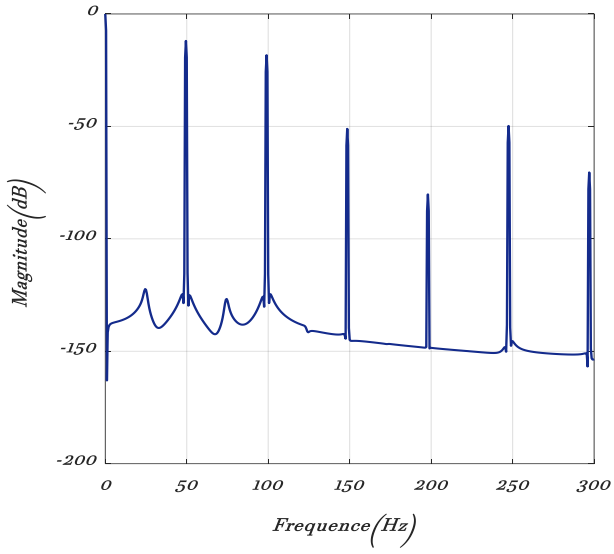

Figure IV.16. b. Stator current spectrum in the case of SC switch fault in TR1&TR4&TR5.

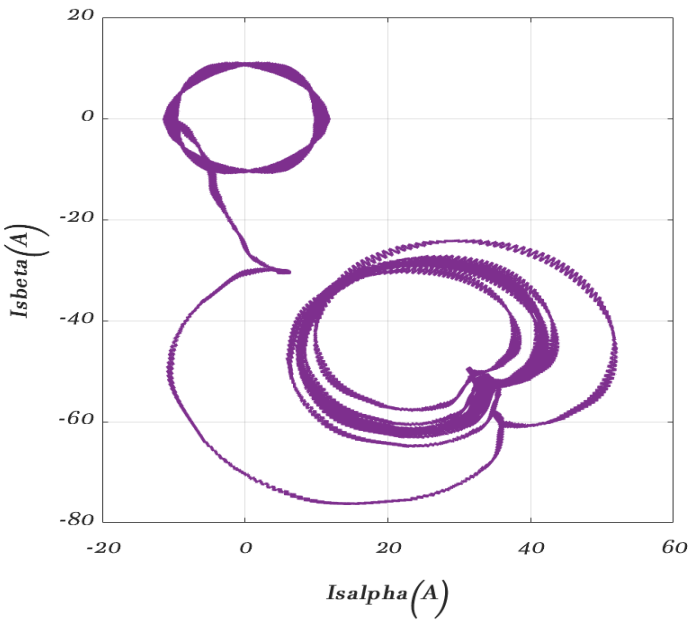

Figure IV.16. c. Analysis of the Park contour in the case of SC switch fault in TR1&TR4&TR5.

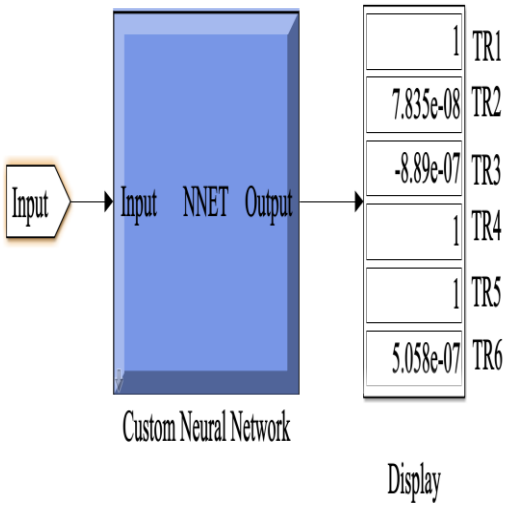

Figure IV.16. d. NN testing.

Figure IV. 16 Simulation results in the case of SC switch fault in TR1 andTR4 and TR5.

- An open circuit fault on switch TR3 results in the absence of the positive phase B current alternation starting at 1.5 seconds (Figure IV.12. a). Additionally, an open circuit fault on switches TR1 and TR4 leads to the loss of the positive phase A current alternation and the absence of the negative phase B current alternation (Figure IV.13. a).

- Spectral analysis reveals a spectrum with similar spectral lines but higher amplitudes when an open circuit fault is present (Figure IV.12.b and Figure IV.13.b). Open circuit faults in single or multiple switches cause changes in the envelope repetition and distort the elliptical shape of the Park transform graph (Figure IV.12.c and Figure IV.13.c).
- In Figure IV.12.d, the output fuzzy value signifies the fault detection. In the case of an open circuit fault in switch TR3, the decision reflects CM = 7 within the range {op-TR3 [5 9]}.
- In the scenario of a short-circuit fault involving a single switch, double switches, and three switches, the three-phase stator currents Isa, Isb, and Isc exhibit imbalance at the time of failure (t=1.5 s), with a shift in the sequence of the three-phase current (Figures IV.14.a, IV.15.a, and IV.16.a). A short-circuit fault in the inverter leads to a sudden surge in the electrical current within the phase containing the faulty switch.
- Figures IV.13.b, IV.13.c, IV.14.b, IV.14.c, IV.15.b, IV.15.c, IV.16.b, and IV.16.c illustrate the stator current spectrum and the analysis of the park contour in various scenarios of open circuit faults (double switches) and short circuit faults (single, double, or triple switches). The detection of faults is identified by the amplified amplitudes of the spectral lines and the distortion of the elliptical shapes in the Park transform graphs.
- In the case of a short-circuit fault occurring in switch TR1, the assessment shows CM=1 within the range {Sc-TR1 [0 3]} (Figure IV.14.d).
- The outcomes of the diagnostic system based on neural networks are presented in figures IV.11.e, IV.12.e, IV.13.d, IV.14.e, IV.15.d, and IV.16.d. These visual representations showcase the results of the neural network training under normal operational circumstances as well as instances of single, double, or triple open and short circuit faults. The figures offer a visual insight into the learning process.
- The MATLAB software was utilized for machine learning until reaching a significantly low mean squared error. The results indicate that the neural network-based diagnostic approach outperforms the fuzzy logic-based method in detecting single, double, and triple faults, showcasing an accuracy rate of around 100% for single faults, 95% for double faults, and 95% for triple faults. Moreover, it demonstrates rapid fault detection under consistent environmental conditions.

IV.8 Conclusion

In conclusion, this chapter has introduced an efficient approach for monitoring, diagnosing, and pinpointing short-circuit and open-circuit faults in wind turbine inverter switches by employing fuzzy logic to monitor the phase of stator currents. Additionally, it suggests utilizing artificial neural networks for fault classification in the IGBTs of wind power converters, featuring a straightforward design. The simulation outcomes using MATLAB software demonstrate that the neural network-based technique can identify single, double, and triple faults more accurately than the fuzzy logic-based method, with a rapid response time. This method could prove highly beneficial for promptly detecting faults in wind turbine inverters, facilitating swift repairs and reducing downtime.

GENERAL CONCLUSION

General Conclusion

The thesis proposes innovative solutions to enhance the reliability and efficiency of wind turbines through advanced approaches in modeling, control, and diagnostics.

Our research underscores innovative approaches to monitor, diagnose, and detect faults in wind systems, emphasizing the pivotal role of artificial intelligence and advanced control techniques in enhancing the reliability and efficiency of wind turbines. The initial chapter introduces the fundamentals of wind turbines, the various types utilized, and the essential components of wind systems. The subsequent chapter addresses the modeling and control of variable-speed wind turbines based on DFIG technology, highlighting control strategies aimed at optimizing performance. Moving forward, the third chapter investigates methods for diagnosing electrical faults in DFIGs, with a specific focus on leveraging artificial intelligence for precise detection. Finally, the fourth chapter concentrates on failures in power converters within wind conversion systems, proposing data-driven diagnostic methods complemented by AI.

The simulation results show that the proposed diagnostic framework effectively detects electrical faults in machines and power converters, bolstered by logical and objective discussions.

Despite the progress made, challenges remain, particularly in terms of experimentally validating the proposed methods and practically integrating diagnostic systems in the wind industry. To overcome these challenges, it is recommended to continue research to optimize artificial intelligence algorithms and conduct field experiments to confirm the results obtained.

Future perspectives include:

- Extending the application of these methods to other systems.
- Exploring new diagnostic approaches based on machine learning and enhancing the integration of artificial intelligence technologies in wind systems.
- Testing and comparing other fault scenarios and types by adopting new diagnostic approaches.

REFERENCES

BIBLIOGRAPHICS

References Bibliographics

[1] Odgaard, P. F., & Stoustrup, J. (2015). A benchmark evaluation of fault tolerant wind turbine control concepts. *IEEE Transactions on Control Systems Technology, 23*(3), 1221-1228. https://doi.org/10.1109/TCST.2014.2361291

[2] Abu-Rub, H., Malinowski, M., & Al-Haddad, K. (2014). Power Electronics for Renewable Energy Systems, Transportation and Industrial Applications. In *Power Electronics for Renewable Energy Systems, Transportation and Industrial Applications* (Vol. 9781118634, pp. 1–795). https://doi.org/10.1002/9781118755525

[3] Mouchaweh, M. S. (n.d.). *Systèmes de surveillance de défauts pour la maintenance prévisionnelle de parcs de turbines éoliennes*. Techniques de l'Ingénieur. Retrieved 28 October 2024, from https://www.techniques-ingenieur.fr/base-documentaire/genie-industriel-th6/mise-en-uvre-de-la-maintenance-42136210/systemes-de-surveillance-de-defauts-pour-la-maintenance-previsionnelle-de-parcs-de-turbines-eoliennes-mt9286/

[4] Fanjason, J. R. (2013). *Diagnostic des systèmes à énergies renouvelables de type éolien* [PhD thesis, Université Pascal Paoli; École supérieure polytechnique d'Antsiranana (Madagascar)]. https://theses.hal.science/tel-01022178

[5] Hafner, M., & Luciani, G. (Eds.). (2022). *The Palgrave handbook of international energy economics*. Springer International Publishing. https://doi.org/10.1007/978-3-030-86884-0

[6] Vukosavic, S. N. (2018). *Grid-Side Converters Control and Design: Interfacing Between the AC Grid and Renewable Power Sources* (1st ed.). Springer Cham. DOI: https://doi.org/10.1007/978-3-319-73278-7

[7] Idrissi, I. (2019). *Contribution au diagnostic des défauts de la machine asynchrone doublement alimentée de l'éolienne à vitesse variable* [PhD thesis, Normandie Université; Université Sidi Mohamed ben Abdellah (Fès, Maroc)]. https://theses.hal.science/tel-02307160

[8] Saci, A. (2022). *Fault diagnosis in a wind turbine using intelligent techniques* [PhD thesis, Ziane Achour University of Djelfa (Djelfa, Algeria)]. https://www.theses-algerie.com

[9] Said, C. (2017). *Contribution to the optimization of predictive control of integrated static converters in wind energy conversion chains* [PhD thesis, Larbi Ben M'hidi University, Oum El Bouaghi, Algeria]. https://doi.org/10.13140/RG.2.2.14512.25600

[10] Saci, A., Cherroun, L., & Boudiaf, M. (2022). Investigation of modeling and control of a grid side system based on DFIG for a wind turbine machine. *In 2022 19th International Multi-Conference on Systems, Signals & Devices (SSD)* (pp. 315–320). https://doi.org/10.1109/SSD54932.2022.9955842

[11] García-Sánchez, T., Muñoz-Benavente, I., Gómez-Lázaro, E., & Fernández-Guillamón, A. (2020). Modelling types 1 and 2 wind turbines based on IEC 61400-27-1: Transient response under voltage dips. *Energies*, *13*(16), 4078. https://doi.org/10.3390/en13164078

[12] Abdelkhalek, Noha. M., Abdelsalam, I., & Marei, M. I. (2018). A reduced cost wind energy conversion system based on permanent magnet synchronous generator with a parallel connected ac-dc buck-boost converter. *2018 IEEE International Conference on Environment and Electrical Engineering and 2018 IEEE Industrial and Commercial Power Systems Europe (EEEIC / I&CPS Europe)*, 1–5. https://doi.org/10.1109/EEEIC.2018.8494627

[13] Gao, Z., & Liu, X. (2021). An overview on fault diagnosis, prognosis and resilient control for wind turbine systems. *Processes*, *9*(2), 300. https://doi.org/10.3390/pr9020300

[14] Bourdium, S. (2015). *Contribution au diagnostic des générateurs utilisés dans les systèmes éoliens* [PhD thesis, Université de Batna 2, (Batna, Algeria)]. http://eprints.univ-batna2.dz/1238/

[15] Ghennam, T. (2011). *Supervision d'une ferme éolienne pour son intégration dans la gestion d'un réseau électrique, Apports des convertisseurs multi niveaux au réglage des éoliennes à base de machine asynchrone à double alimentation* [Phdthesis, Ecole Centrale de Lille ; École Militaire Polytechnique (Alger)]. https://theses.hal.science/tel-00708171

[16] Attoui,I . (2015). *Contribution Au Diagnostic De Defauts D'une Generatrice Asynchrone Dans Une Chaine De Conversion D'energie Eolienne* [PhD thesis, Badji Mokhtar University - Annaba (BMUA), (Algeria)]. https://www.theses-algerie.com

[17] Azzouz.S. (2019). *Amelioration de la commande d'un systeme eolien a base d'une machine mada utilisant les techniques intelligentes* [PhD thesis, Mohamed Boudiaf University - M'sila (Algeria)]. http://dspace.univ-msila.dz:8080//xmlui/handle/123456789/18761

[18] Eoliennes. (n.d.). *Energie Plus Le Site*. Retrieved 28 October 2024, from https://energieplus-lesite.be/techniques/eolien6/eoliennes/

[19] Fadda Mohamed, L. (2017). *Contribution à la modélisation et au diagnostic intelligent des systèmes de production d'énergie électrique à base d'énergies renouvelables* [PhD thesis, University May 8, 1945 Guelma (Algeria)]. http://dspace.univ-guelma.dz/jspui/handle/123456789/6179

[20] Toscano, R. (2011). *Commande et diagnostic des systèmes dynamiques—Modélisation, analyse, commande par PID et par retour d'état, diagnostic*. https://www.abebooks.fr/9782729863364/Commande-diagnostic-syst%C3%A8mes-dynamiques-Mod%C3%A9lisation-2729863362/plp

[21] Mayouf, M., & Bakhti, H. (2021). Monitoring and control of a permanent magnet synchronous generator-based wind turbine applied to battery charging. *Energy Sources, Part A: Recovery, Utilization, and Environmental Effects*, *43*(18), 2281–2296. https://doi.org/10.1080/15567036.2019.1666934

[22] Doraiswami, R., & Cheded, L. (2017). *Fault Detection and Isolation*. InTech. doi:10.5772/67870

[23] Laouti, N., Othman, S., Alamir, M., & Sheibat-Othman, N. (2014). Combination of model-based observer and support vector machines for fault detection of wind turbines. *International Journal of Automation and Computing*, *11*(3), 274–287. https://doi.org/10.1007/s11633-014-0790-9

[24] Khan, S., & Yairi, T. (2018). A review on the application of deep learning in system health management. *Mechanical Systems and Signal Processing*, *107*, 241–265. https://doi.org/10.1016/j.ymssp.2017.11.024

[25] Gao, Z., Cecati, C., & Ding, S. X. (2015). A survey of fault diagnosis and fault-tolerant techniques—part i: Fault diagnosis with model-based and signal-based approaches. *IEEE Transactions on Industrial Electronics*, *62*(6), 3757–3767. https://doi.org/10.1109/TIE.2015.2417501

[26] Gao, Z., Cecati, C., & Ding, S. X. (2015). A survey of fault diagnosis and fault-tolerant techniques—part ii: Fault diagnosis with knowledge-based and hybrid/active approaches. *IEEE Transactions on Industrial Electronics*, *62*(6), 3768–3774. https://doi.org/10.1109/TIE.2015.2419013

[27] Jung, M., Niculita, O., & Skaf, Z. (2018). Comparison of different classification algorithms for fault detection and fault isolation in complex systems. *Procedia Manufacturing*, *19*, 111–118. https://doi.org/10.1016/j.promfg.2018.01.016

[28] Mouzakitis, A. (2013). Classification of fault diagnosis methods for control systems. *Measurement and Control*, *46*(10), 303–308. https://doi.org/10.1177/0020294013510471

[29] BİÇEN, Y., & ARAS, F. (2015). A robust algorithm based on a failure-sensitive matrix for fault diagnosis of power systems: An application on power transformers. *Turkish Journal of*

Electrical Engineering and Computer Sciences, *23*(1), 298–315. https://doi.org/10.3906/elk-1301-24

[30] Odgaard, P. F., & Johnson, K. E. (2013). Wind turbine fault detection and fault tolerant control—An enhanced benchmark challenge. *2013 American Control Conference*, 4447–4452. https://doi.org/10.1109/ACC.2013.6580525

[31] Wu, K., An, S., Ma, G., & Tao, Y. (2012). Research and application of fuzzy expert system on transformer fault diagnosis. *2012 International Conference on Computer Science and Electronics Engineering*, *1*, 378–382. https://doi.org/10.1109/ICCSEE.2012.308

[32] Villez, K., & Rengaswamy, R. (2013). A generative approach to qualitative trend analysis for batch process fault diagnosis. *2013 European Control Conference (ECC)*, 1958–1963. https://doi.org/10.23919/ECC.2013.6669494

[33] Maurya, M. R., Rengaswamy, R., & Venkatasubramanian, V. (2005). Fault diagnosis by qualitative trend analysis of the principal components. *Chemical Engineering Research and Design*, *83*(9), 1122–1132. https://doi.org/10.1205/cherd.04280

[34] Thürlimann, C. M., Dürrenmatt, D. J., & Villez, K. (2015). Evaluation of qualitative trend analysis as a tool for automation. In *Computer Aided Chemical Engineering* (Vol. 37, pp. 2531–2536). Elsevier. https://doi.org/10.1016/B978-0-444-63576-1.50116-3

[35] Maurya, M. R., Rengaswamy, R., & Venkatasubramanian, V. (2003). Qualitative trend analysis of the principal components: Application to fault diagnosis. In *Computer Aided Chemical Engineering* (Vol. 15, pp. 968–973). Elsevier. https://doi.org/10.1016/S1570-7946(03)80433-9

[36] Chen, A., Zhou, H., An, Y., & Sun, W. (2016). PCA and PLS monitoring approaches for fault detection of wastewater treatment process. *2016 IEEE 25th International Symposium on Industrial Electronics (ISIE)*, 1022–1027. https://doi.org/10.1109/ISIE.2016.7745032

[37] Venkatasubramanian, V., Rengaswamy, R., Kavuri, S. N., & Yin, K. (2003). A review of process fault detection and diagnosis. *Computers & Chemical Engineering*, *27*(3), 327–346. https://doi.org/10.1016/S0098-1354(02)00162-X

[38] Jo, H., Park, C., Lee, E., Choi, H. K., & Park, J. (2020). Path Loss Prediction Based on Machine Learning Techniques: Principal Component Analysis, Artificial Neural Network, and Gaussian Process. *Sensors*, *20*(7), 1927. https://doi.org/10.3390/s20071927

[39] Kumar, P., Ambekar, S., Kumar, M., & Roy, S. (2020). Analytical statistics techniques of classification and regression in machine learning. In *Data Mining—Methods, Applications and Systems*. IntechOpen. https://doi.org/10.5772/intechopen.84922

[40] Dion, G., Mejaouri, S., & Sylvestre, J. (2018). Reservoir computing with a single delay-coupled non-linear mechanical oscillator. *Journal of Applied Physics*, *124*(15), 152132. https://doi.org/10.1063/1.5038038

[41] Sun, J., Yan, C., & Wen, J. (2018). Intelligent bearing fault diagnosis method combining compressed data acquisition and deep learning. *IEEE Transactions on Instrumentation and Measurement*, *67*(1), 185–195. https://doi.org/10.1109/TIM.2017.2759418

[42] Haman, A. (2023). *Classification de signaux temporels avec un capteur neuromorphique: Application au diagnostic de fautes automobiles* [Mémoire de maîtrise, Université de Sherbrooke (Canada)]. https://savoirs.usherbrooke.ca/handle/11143/21238

[43] Dai, J., Tang, J., Huang, S., & Wang, Y. (2019). Signal-Based Intelligent Hydraulic Fault Diagnosis Methods: Review and Prospects. *Chinese Journal of Mechanical Engineering*, *32*(1), 1-22. https://doi.org/10.1186/s10033-019-0388-9

[44] Harihara, P. P., Kim, K., & Parlos, A. G. (2003). Signal-based versus model-based fault diagnosis-a trade-off in complexity and performance. *4th IEEE International Symposium on Diagnostics for Electric Machines, Power Electronics and Drives, 2003. SDEMPED 2003.*, 277–282. https://doi.org/10.1109/DEMPED.2003.1234586

[45] Gaillard, A. (2010). *Système éolien basé sur une MADA: Contribution à l'étude de la qualité de l'énergie électrique et de la continuité de service* [PhD thesis, Université Henri Poincaré - Nancy 1]. https://hal.univ-lorraine.fr/tel-01748204

[46] Semmache, H., Bounoua, A., Bausière, R., & Benramdane, N. (1999). Développement des performances des systèmes énergétiques dans la production d'énergie éolienne. *Revue des Energies Renouvelables Valorisation*.

[47] Bouderbala, M., Bossoufi, B., Lagrioui, A., Taoussi, M., Aroussi, H. A., & Ihedrane, Y. (2019). Direct and indirect vector control of a doubly fed induction generator based in a wind energy conversion system. *International Journal of Electrical and Computer Engineering (IJECE)*, *9*(3), 1531. https://doi.org/10.11591/ijece.v9i3.pp1531-1540

[48] Heier, S. (2014). *Grid integration of wind energy: Onshore and offshore conversion systems* (Third edition). Wiley.https://doi.org/10.1002/9781118703274

[49] Cherfia, N. (2018). *Etude d'une Chaine de Conversion de l'Energie Eolienne* [PhD thesis, Mentouri Brothers University Constantine 1 (Algeria)]. https://www.researchgate.net/publication/330225602_Etude_d%27une_Chaine_de_Conversion_de_l%27Energie_Eolienne

[50] Petersson, A. (2005). *Analysis, modeling and control of doubly-fed induction generators for wind turbines* (Technical Report No. 464L). School of Electrical Engineering, Chalmers University of Technology.

[51] Djeriri, Y. (2015). *Commande directe du couple et des puissances d'une MADA associée à un système éolien par les techniques de l'intelligence artificielle* [PhD thesis, Djilali Liabes University of Sidi Bel Abbes (Algeria)]. https://dspace.univ-sba.dz/handle/123456789/1526

[52] Frédéric Poitiers. (2003). *Étude et commande de génératrices asynchrones pour l'utilisation de l'énergie éolienne: Machine asynchrone à cage autonome: Machine asynchrone à double alimentation reliée au réseau* [These de doctorat, École doctorale sciences et technologies de l'information et des matériaux (Nantes)]. https://theses.fr/2003NANT2078

[53] Abad, G. (Ed.). (2016). *Power electronics and electric drives for traction applications*. Wiley. https://doi.org/10.1002/9781118954454

[54] Phankong, N., Manmai, S., Bhumkittipich, K., & Nakawiwat, P. (2013). Modeling of grid-connected with permanent magnet synchronous generator (Pmsg) using voltage vector control. *Energy Procedia*, *34*, 262–272. https://doi.org/10.1016/j.egypro.2013.06.754

[55] Zhang, Y., Liu, H., & Mantooth, H. A. (2016). Control strategy of high power converters with synchronous generator characteristics for PMSG-based wind power application. *2016 IEEE Applied Power Electronics Conference and Exposition (APEC)*, 3180–3184. https://doi.org/10.1109/APEC.2016.7468319

[56] Rahimi, M. (2017). Modeling, control and stability analysis of grid connected PMSG based wind turbine assisted with diode rectifier and boost converter. *International Journal of Electrical Power & Energy Systems*, *93*, 84–96. https://doi.org/10.1016/j.ijepes.2017.05.019

[57] Song, S.-H., Kang, S., & Hahm, N. (2003). Implementation and control of grid connected AC-DC-AC power converter for variable speed wind energy conversion system. *Eighteenth Annual IEEE Applied Power Electronics Conference and Exposition, 2003. APEC '03.*, *1*, 154–158 vol.1. https://doi.org/10.1109/APEC.2003.1179207

[58] Chojaa, H., Derouich, A., Chehaidia, S. E., Zamzoum, O., Taoussi, M., & Elouatouat, H. (2021). Integral sliding mode control for DFIG based WECS with MPPT based on artificial neural network under a real wind profile. *Energy Reports*, *7*, 4809–4824. https://doi.org/10.1016/j.egyr.2021.07.066

[59] Soomro, M. A., Memon, Z. A., Kumar, M., & Baloch, M. H. (2021). Wind energy integration: Dynamic modeling and control of DFIG based on super twisting fractional order terminal sliding mode controller. *Energy Reports*, *7*, 6031–6043. https://doi.org/10.1016/j.egyr.2021.09.022

[60] Zouheyr, D., Lotfi, B., Thierry, L., & Abdelmadjid, B. (2021). Grid Side Inverter Control for a Grid Connected Synchronous Generator Based Wind Turbine Experimental Emulator. *European Journal of Electrical Engineering*, *23*(1), 1–7. https://doi.org/10.18280/ejee.230101

[61] Youness, E. M., Aziz, D., Abdelaziz, E. G., Jamal, B., Najib, E. O., Othmane, Z., Khalid, M., & Bossoufi, B. (2019). Implementation and validation of backstepping control for PMSG wind turbine using dSPACE controller board. *Energy Reports*, *5*, 807–821. https://doi.org/10.1016/j.egyr.2019.06.015

[62] Moreira, A. B., Barros, T. A. S., Teixeira, V. S. C., & Ruppert, E. (2017). Power control for wind power generation and current harmonic filtering with doubly fed induction generator. *Renewable Energy*, *107*, 181–193. https://doi.org/10.1016/j.renene.2017.01.059

[63] Wickramasinghe, A., Perera, S., Agalgaonkar, A. P., & Meegahapola, L. (2016). Synchronous mode operation of DFIG based wind turbines for improvement of power system inertia. *Renewable Energy*, *95*, 152–161. https://doi.org/10.1016/j.renene.2016.04.010

[64] Boutoubat, M., Mokrani, L., & Machmoum, M. (2013). Control of a wind energy conversion system equipped by a DFIG for active power generation and power quality improvement. *Renewable Energy*, *50*, 378–386. https://doi.org/10.1016/j.renene.2012.06.058

[65] Gayen, P. K., Chatterjee, D., & Goswami, S. K. (2015). Stator side active and reactive power control with improved rotor position and speed estimator of a grid connected DFIG (Doubly-fed induction generator). *Energy*, *89*, 461–472. https://doi.org/10.1016/j.energy.2015.05.111

[66] Chetouani, E., Errami, Y., Obbadi, A., & Sahnoun, S. (2023). Self-adapting PI controller for grid-connected DFIG wind turbines based on recurrent neural network optimization control under unbalanced grid faults. *Electric Power Systems Research*, *214*, 108829. https://doi.org/10.1016/j.epsr.2022.108829

[67] Abdeddaim, S., & Betka, A. (2013). Optimal tracking and robust power control of the DFIG wind turbine. *International Journal of Electrical Power & Energy Systems*, *49*, 234-242. https://doi.org/10.1016/j.ijepes.2012.12.014

[68] S. Mensou, A. Essadki, T. Nasser, & B. B. Idrissi. (2017). An efficient nonlinear backstepping controller approach of a wind energy conversion system based on a dfig. *International Journal of Renewable Energy Research-IJRER, v7i4*. https://doi.org/10.20508/ijrer.v7i4.6112.g7192

[69] Mesai, A. H., Bentaallah, A., Djeriri, Y., & Mahmoudi, A. (2020). Comparative study between pi and fuzzy pi controllers for DFIG integrated in variable speed wind turbine. *International Journal of Energetica*, *4*(2), 8–13. https://doi.org/10.47238/ijeca.v4i2.102

[70] Daneshi-Far, Z., Capolino, G. A., & Henao, H. (2010). Review of failures and condition monitoring in wind turbine generators. *The XIX International Conference on Electrical Machines - ICEM 2010*, 1–6. https://doi.org/10.1109/ICELMACH.2010.5608150

[71] Ribrant, J., & Bertling, L. M. (2007). Survey of failures in wind power systems with focus on swedish wind power plants during 1997–2005. *IEEE Transactions on Energy Conversion*, *22*(1), 167–173. https://doi.org/10.1109/TEC.2006.889614

[72] Verbruggen, T.W. (2003). *Wind turbine operation & maintenance based on condition monitoring wt-ω*. http://www.ecn.nl/docs/library/report/2003/c03047.pdf

[73] Qiao, W., & Lu, D. (2015). A survey on wind turbine condition monitoring and fault diagnosis—part i: Components and subsystems. *IEEE Transactions on Industrial Electronics*, *62*(10), 6536–6545. https://doi.org/10.1109/TIE.2015.2422112

[74] Lau, B. C. P., Ma, E. W. M., & Pecht, M. (2012). Review of offshore wind turbine failures and fault prognostic methods. *Proceedings of the IEEE 2012 Prognostics and System Health Management Conference (PHM-2012 Beijing)*, 1–5. https://doi.org/10.1109/PHM.2012.6228954

[75] Odgaard, P. F., & Stoustrup, J. (2010). Unknown input observer based detection of sensor faults in a wind turbine. *2010 IEEE International Conference on Control Applications*, 310–315. https://doi.org/10.1109/CCA.2010.5611266

[76] Şabanoviç, A. (2007). SMC framework in motion control systems. *International Journal of Adaptive Control and Signal Processing*, *21*(8-9), 731-744. https://doi.org/10.1002/acs.968

[77] Schlechtingen, M., & Ferreira Santos, I. (2011). Comparative analysis of neural network and regression based condition monitoring approaches for wind turbine fault detection. *Mechanical Systems and Signal Processing*, *25*(5), 1849-1875. https://doi.org/10.1016/j.ymssp.2010.12.007

[78] Brandão, R. F. M., Carvalho, J. A. B., & Barbosa, F. P. M. (2010). Neural networks for condition monitoring of wind turbines. *2010 Modern Electric Power Systems*, 1–4. https://ieeexplore.ieee.org/abstract/document/6007206

[79] Elhor, N., Bertrand, R., Postaire, J. G., & Hamad, D. (1999). Neural networks for wind turbine supervision. *E&i Elektrotechnik Und Informationstechnik*, *116*(6), 366–369. https://doi.org/10.1007/BF03159197

[80] Simani, S., Castaldi, P., & Bonfè, M. (2011). Hybrid model–based fault detection of wind turbine sensors. *IFAC Proceedings Volumes*, *44*(1), 7061–7066. https://doi.org/10.3182/20110828-6-IT-1002.01311

[81] Lu, Y., Tang, J., & Luo, H. (2011). Wind turbine gearbox fault detection using multiple sensors with feature level data fusion. *Volume 1: Aircraft Engine; Ceramics; Coal, Biomass and Alternative Fuels; Wind Turbine Technology*, 907–914. https://doi.org/10.1115/GT2011-46538

[82] Odgaard, P. F., & Stoustrup, J. (2013). Fault tolerant wind farm control—A benchmark model. *2013 IEEE International Conference on Control Applications (CCA)*, 412–417. https://doi.org/10.1109/CCA.2013.6662784

[83] Yang, W., Tavner, P. J., & Wilkinson, M. (2008). Condition monitoring and fault diagnosis of a wind turbine with a synchronous generator using wavelet transforms. *2008 4th IET Conference on Power Electronics, Machines and Drives*, 6–10. https://doi.org/10.1049/cp:20080473

[84] Merabet, H. (2015). *Diagnostic des defauts mecaniques et electromagnetiques sur les aerogenerateurs a base de machine asynchrone a double alimentation.* [PhD thesis, Badji Mokhtar University-Annaba (Algeria)]. https://library.crti.dz/dc295

[85] Mellah, H., Arslan, S., Sahraoui, H., Hemsas, K. E., & Kamel, S. (2022). The Effect of Stator Inter-Turn Short-Circuit Fault on DFIG Performance Using FEM. *Engineering, Technology & Applied Science Research*, *12*(3), 8688–8693. https://doi.org/10.48084/etasr.4923

[86] Hoang, K. D., Zhu, Q., & Foster, M. (2013). Direct torque control of permanent magnet brushless AC drive with single-phase open-circuit fault accounting for influence of inverter voltage drop. *IET Electric Power Applications*, *7*(5), 369-380. https://doi.org/10.1049/iet-epa.2012.0290

[87] AKAR, M., & ÇANKAYA, İ. (2012). Broken rotor bar fault detection in inverter-fed squirrel cage induction motors using stator current analysis and fuzzy logic. *Turkish Journal of Electrical Engineering and Computer Sciences*, *20*(7), 1077–1089. https://doi.org/10.3906/elk-1102-1050

[88] Vijay P. Pandey & P. Choudhary. (2013). Induction Motor Condition Monitoring Using Fuzzy Logic. *Advance in Electronic and Electric Engineering, Volume 3, Number 6 (2013), pp. 755–764*(2231-1297,). http://www.ripublication.com/aeee/015_pp%20%20%20%20755-764.pdf

[89] Artigao, E., Martín-Martínez, S., Honrubia-Escribano, A., & Gómez-Lázaro, E. (2018). Wind turbine reliability: A comprehensive review towards effective condition monitoring development. *Applied Energy*, *228*, 1569-1583. https://doi.org/10.1016/j.apenergy.2018.07.037

[90] Zhang, P., & Lu, D. (2019). A Survey of Condition Monitoring and Fault Diagnosis toward Integrated O&M for Wind Turbines. *Energies*, *12*(14), 2801. https://doi.org/10.3390/en12142801

[91] Qiao, W., Zhang, P., & Chow, M.-Y. (2015). Condition monitoring, diagnosis, prognosis, and health management for wind energy conversion systems. *IEEE Transactions on Industrial Electronics*, *62*(10), 6533–6535. https://doi.org/10.1109/TIE.2015.2464785

[92] Wan, Z., Lin, Q., Qiao, F., Zhang, Z., Zong, Y., & Su, X. (2019). A review of power electronic parametric fault diagnosis methods. *2019 4th International Conference on Intelligent Green Building and Smart Grid (IGBSG)*, 448–451. https://doi.org/10.1109/IGBSG.2019.8886330

[93] Lu, B., & Sharma, S. K. (2009). A literature review of igbt fault diagnostic and protection methods for power inverters. *IEEE Transactions on Industry Applications*, *45*(5), 1770–1777. https://doi.org/10.1109/TIA.2009.2027535

[94] Liu, H., Ma, K., Wang, C., & Blaabjerg, F. (2016). Fault diagnosis and fault-tolerant control of modular multi-level converter high-voltage dc system: A review. *Electric Power Components and Systems*, *44*(16), 1759–1785. https://doi.org/10.1080/15325008.2016.1198439

[95] Wang, C., Zhou, L., & Li, Z. (2019). Survey of switch fault diagnosis for modular multilevel converter. *IET Circuits, Devices & Systems*, *13*(2), 117-124. https://doi.org/10.1049/iet-cds.2018.5136

[96] Liang, J., Zhang, K., Al-Durra, A., Muyeen, S., & Zhou, D. (2022). A state-of-the-art review on wind power converter fault diagnosis. *Energy Reports*, *8*, 5341-5369. https://doi.org/10.1016/j.egyr.2022.03.178

[97] Orłowska-Kowalska, T., Blaabjerg, F., & Rodríguez, J. (Eds.). (2014). *Advanced and intelligent control in power electronics and drives* (Vol. 531). Springer International Publishing. https://doi.org/10.1007/978-3-319-03401-0

[98] Manoj, J, Kulkarni, A. G, & Qureshi, M. F. (2014). Diagnostics of Induction Motor Based on Spectral Analysis of Stator Current Signal Using Fast Fourier Transform and Genetically Tuned Interval Type-2 Fuzzy Classifier Methods. *Advances in Modelling and Analysis*, *57(1), 47–67*.

[99] Mei, Y., & Yuan, H. (2018). A novel open-circuit fault diagnosis method for voltage source inverter. *2018 IEEE International Power Electronics and Application Conference and Exposition (PEAC)*, 1–6. https://doi.org/10.1109/PEAC.2018.8590418

[100] Mohamed, A.S., Azazy, H.Z, & Din, A.S. (2013). Open-circuit Fault Diagnosis of Three-phase Induction Motor Drive Systems. *Journal of Electrical Engineering*, *13(3):60–68*.

[101] Merabet, H., Bahi, T., Bedoud, K., & Drici, D. (2019). Real-time switches fault diagnosis for voltage source inverter driven induction motor drive. *International Journal of Electrical and Electronic Engineering & Telecommunications*, 103–107. https://doi.org/10.18178/ijeetc.8.2.103-107

[102] Hichem, M., Tahar, B., Kholoud, B., Youcef, S., Djalel, D., & Ghania, B. (2019). Diagnosis and localization of fault pwm inverter in energy conversion system using fuzzy logic. *2019 1st International Conference on Sustainable Renewable Energy Systems and Applications (ICSRESA)*, 1–5. https://doi.org/10.1109/ICSRESA49121.2019.9182311

[103] Mala Ratan Ubale & R. B. Dhumale. (2013). Open switch fault diagnosis in three phase inverter using diagnostic variable method. *International Journal of Research in Engineering and Technology*, *02*(12), 636–640. https://doi.org/10.15623/ijret.2013.0212108

[104] Abid, M., Laribi, S., Larbi, M., & Allaoui, T. (2022). Diagnosis and localization of fault for a neutral point clamped inverter in wind energy conversion system using artificial neural

network technique. *Electrical Engineering & Electromechanics, 5*, 55–59. https://doi.org/10.20998/2074-272X.2022.5.09

[105] Frank, P. (1994). Application of Fuzzy Logic to Process Supervision and Fault Diagnosis. *IFAC Proceedings Volumes*, *27*(5), 507-514. https://doi.org/10.1016/S1474-6670(17)48077-3

[106] Asghar, F., Talha, M., & Kim, S. H. (2017). Comparative study of three fault diagnostic methods for three phase inverter with induction motor. *International Journal of Fuzzy Logic and Intelligent Systems, 17*(4), 245–256. https://doi.org/10.5391/IJFIS.2017.17.4.245

[107] Rohan, A., & Kim, S. H. (2016). Fault detection and diagnosis system for a three-phase inverter using a dwt-based artificial neural network. *International Journal of Fuzzy Logic and Intelligent Systems, 16*(4), 238–245. https://doi.org/10.5391/IJFIS.2016.16.4.238

SCIENTIFIC PRODUCTION

Scientific production

The research work recorded in this thesis resulted in the following international publications and communications:

I- International and national publications

1. L.YOUSFI, **S. AOUN**, M. SEDRAOUI, "Speed sensorless vector control of doubly fed induction machine using fuzzy logic control equipped with Luenberger observer", International Journal of Dynamics and Control (IJDY), 29 April, 2022. https ://doi.org/10.1007/s40435-022-00946-0
2. **S.AOUN**, A.BOUKADOUM, L,YOUSFI, "Advanced power control of a variable speed wind turbine based on a doubly fed induction generator using field-oriented control with fuzzy and neural controllers" International Journal of Dynamics and Control (IJDY) 30 November 2023. DOI: 10.1007/s40435-023-01345-9
3. S. AOUN, A. BOUKADOUM, L. YOUSFI, "Indirect Vector Control of a DFIG Based In A wind Energy Conversion System" 152-161 Algerian Journal of Engineering Architecture and Urbanism, Vol. 5 Nr. 3 2021

II- International communications

1. **S. Aoun**, A. Boukadoum, L. Yousfi, "Indirect Vector Control of A DFIG Based In A wind Energy Conversion System", an international seminar on industry and technology organized by an international indexed journal: Algerian Journal of Engineering, Architecture and Urbanism, 02/27/2021.
2. **S. Aoun**, A. Boukadoum, L. Yousfi, "Vector Control of Doubly Fed Induction Generator in Wind Power System using PI Controller", 1st International Conference on Sustainable Energy and Advanced Materials, IC-SEAM’21 April 21-22, 2021, Ouargla, ALGERIA.
3. **S.Aoun**, L.Yousfi, A.Boukadoum "Fuzzy Diagnosis of Faults for DFIG Used in a Wind Energy conversion System" Conference: First International Conference on Andvances in Electrical and Computer Engineering (ICAECE'2023) May 15-16,2023, University of Echahid Cheikh Larbi Tebessi, Tebessa,